High Resolution Laser Spectroscopy of Diatomic Scandium-containing Molecules

LIAO, Zhenwu

A Thesis Submitted in Partial Fulfillment

of the Requirements for the Degree of

Doctor of Philosophy

in

Chemistry

The Chinese University of Hong Kong

October 2013

Thesis/Assessment Committee

Professor Sik Lok LAM (Chair)

Professor Man-Chor CHAN (Thesis Supervisor)

Professor To NGAI (Committee Member)

Professor Allan Shi-Chung CHEUNG (External Examiner)

ABSTRACT

This thesis reports the spectroscopic studies of diatomic molecules formed by scandium with non-metals using the laser-ablated metal vapor reacting with jet expansion of appropriate gas mixture. These molecules provide ideal model systems for investigating the role of d electrons in chemical bonding, as scandium atom possesses only one d-electron. Electronic spectra of ScP, ScBr and ScI have been studied using laser induced fluorescence (LIF) spectroscopy. The analysis of the spectra has revealed new information on structures of these molecules.

The spectrum of ScP molecule has been observed for the first time. LIF spectrum of ten vibronic bands with v up to 4 of the $[11.9]^1\Sigma^+ - X^1\Sigma^+$ system between 775 – 900 nm has been recorded and analyzed, accurate molecular constants for the two $^1\Sigma^+$ states involved have been determined. The equilibrium bond length in the $[11.9]^1\Sigma^+$ state was found to be slightly shorter than that in the $X^1\Sigma^+$ state, suggesting a greater bond order in the excited state. Detailed analysis of the structural parameters in both states indicates that simple molecular orbital theory fails for this molecule.

LIF spectra of the $C^1\Sigma^+ - X^1\Sigma^+$, $e^3\Delta - a^3\Delta$, and $d^3\Phi - a^3\Delta$ systems of ScBr, and the $C^1\Sigma^+ - X^1\Sigma^+$ system of ScI between 775 – 900 nm were recorded. The measured line positions were fitted using a least-squares program to obtain accurate molecular constants for the $C^1\Sigma^+$ and $X^1\Sigma^+$ states of ScI, and $C^1\Sigma^+$, $X^1\Sigma^+$, $e^3\Delta$, $d^3\Phi$, and $a^3\Delta$ states

of ScBr. Molecular orbital energy level diagrams of the molecules have been constructed to explain the origin of the observed electronic states. A comparison of the molecular constants of the low-lying electronic states of scandium monohalides from similar electronic configurations indicates a weakening of chemical bonding between the scandium and the halogen atoms down the group.

中 文 摘 要

在本篇論文中，我們對含鈧的雙原子分子進行了高分辨近紅外光譜研究。作為第一個過渡態金屬元素，鈧與非金屬元素形成的雙原子分子是研究 d 軌道參與形成化學鍵的最理想的分子系統。基於激光消融，超聲射流和激光誘導螢光光譜技術，我們成功的製備了 ScP，ScBr 和 ScI 目標分子，並採集到它們在 775nm – 900nm 範圍內的高分辨電子光譜。

我們第一次在實驗上觀察到 ScP 分子的光譜：[11.9] $^1\Sigma^+ - X^1\Sigma^+$ 電子躍遷。我們對於所採集到的十個振動帶光譜的所有轉動躍遷譜線進行最小二乘法擬合得到了一組高準確度的光譜常數。通過比較 ScP 分子在這兩個電子態時的平衡分子間距（re），我們發現 ScP 分子在激發態時比基態有更強的化學鍵。我們對於分子在這兩個電子態時的結構常數進行了詳細的分析，結果表明簡單的分子軌道理論不能用於解釋 ScP 分子的電子態性質。

對於 ScBr 和 ScI 分子，我們測量到了共四個電子躍遷光譜，分別是 ScBr 分子的 $C^1\Sigma^+ - X^1\Sigma^+$，$e^3\Delta - a^3\Delta$，和 $d^3\Phi - a^3\Delta$ 系統，和 ScI 的 $C^1\Sigma^+ - X^1\Sigma^+$系統。我們也分別對於每個系統中的所有轉動躍遷譜線進行了最小二乘法擬合，得到了這些電子態的高精度的光譜常數。然後，我們構建了分子軌道能级圖來分析形成這些電子態的电子組態。並通過比較所有鈧與鹵素形成的雙原子分子在各個相同電子態上的分子常數，我們發現較重的元素與鈧形成的分子具有更弱的化學鍵。

ACKNOWLEDGEMENTS

I own the most sincere gratitude to my supervisor, Professor Man-Chor Chan, for letting me join his research group and being a wonderful advisor and teacher throughout my five years research studies. His brilliant idea, thoughtful insight, patient guidance, beneficial instruction, fruitful discussion, encouragement and criticism have been the key factor in all my achievements during the course of my studies. He is full of passion and energy, with permanent interest and enthusiasm in science. What I have learned are not only the theoretical knowledge and experimental techniques, but also the enthusiasm to the scientific research. Thank you very much!

I also appreciate so much for the supporting I have received from Prof. A. S-C. Cheung in HKU. He taught me a lot on how to analyze a complicated electronic spectrum, and discussed the results with great enthusiasm. Thanks are also given to Dr. Ye Xia in his group, who usually helped me out of the trouble during the experiments.

I am very thankful to my past and present group members for creating a cheerful and friendly workplace. My sincere thanks are given to Dr. Lei Yan and Dr. Yan Song for sharing many valuable research experiences. I also want to gratefully acknowledge Ms. Mei Yang, Mr. Biuwa Li for their assistance and many helpful discussions. Their friendship is also well appreciated.

Acknowledgement is also given to the staff of technical supporting unit for their sincere assistance and suggestions, which made my research progress much smoother.

Finally, I would like to express my deepest gratitude to my family for their forever love and trust to me, without whose support and encouragement this thesis would never have been submitted.

Table of Contents

List of Figures

List of Tables

Chapter I

Introduction

I.1. Motivation

Transition metals play a unique role in chemistry. Their involvement in organometallic chemistry [1, 2], surface science [3], catalysis [4, 5], high-temperature chemistry [6, 7], and astrochemistry and astrophysics [8, 9] are well-established. Transition metals, either as element or organometallic compounds, are known to serve as heterogeneous or homogeneous catalysts for chemical reactions. This remarkable property has been ascribed [4] to (1) the d electrons easily forming both σ and π bonds with other elements that allows transition metals to readily form linkages with almost every other element or organic molecule and (2) the variability of oxidation states of transition metal elements that allows them to readily exchange between oxidation states during the course of a chemical/catalytic reaction. Transition metal molecules are found as reaction intermediates in combustion chemistry [6, 7]. Knowledge of structures and electronic states and energies of these short-lived species are crucial in understanding reaction pathways and products. Transition metal compounds also exist in the upper atmosphere and interstellar medium. It is well known that transition metal oxide and hydride spectra are observed in the atmosphere of cool M- and S-type stars [8].

While transition metal compounds are of great interests in various fields of research. Theoretical understanding of compounds containing transition metals is still limited. Ab initio calculations have not provided reliable predictions for even the very simple systems such as diatomic molecules [10]. Because of the involvement of d electrons in the bonding, electron correlations become vital factors in determining the energies of electronic states. Experimental studies have also been limited by the challenge of their production with sufficient number density [11]. The recent application of laser ablation of transition metal followed by reaction with parent gas provides a new approach to generate simple diatomic molecules containing transition metals under mild experimental conditions [12]. Together with the supersonic expansion technique, molecules can be produced at low rotational and translational temperatures for spectroscopic studies [13, 14].

Because of the involvement of d electrons, these systems usually possess a number of low-lying electronic states and transitions between them lie within the near-infrared and visible regions [15]. Electronic spectroscopy therefore has been widely used to study the electronic states of transition metal diatomic systems. Fluorescence emission from higher electronic states has been traditionally used due to its high sensitivity as a result of zero-background detection [16]. Emission spectroscopy requires high population of the excited electronic state, a condition that is not always achieved as most molecules produced are in electronic ground state. In order to produce molecules in the higher excited states, violent reaction conditions,

that are difficult to handle, are always needed [16].

With the advancement of laser light sources, transition metal compounds are produced under much milder conditions for spectroscopic studies. The combination of laser ablation of metal, supersonic free-jet expansion of gaseous reaction mixture, and laser-induced fluorescence spectroscopy has demonstrated to be a successful tool in studying electronic spectra of metal-containing compounds without violent conditions [17, 18]. In this experimental approach, metal vapor produced by the local heating of a focused pulsed laser beam reacts with appropriate gas to form the desired products. After the expansion of the reaction mixture through a nozzle to form a supersonic gas jet, molecules are cooled rotationally and translationally for spectroscopic studies. Molecules produced using this approach are usually in the ground electronic state. Instead of recording the electronic spectrum using absorption spectroscopy, laser-induced fluorescence (LIF) spectroscopy has been widely used. In this approach, molecules in the ground electronic state are excited using a tunable laser source and the total fluorescence emitted from the excited state is then measured. Since emission is detected only after the absorption of light, by plotting the emission against excitation frequency, one can obtain a LIF spectrum similar to the corresponding absorption spectrum with the same states involved [19]. In other words, the sensitivity of zero-background detection is achieved with only requirement of population in the ground electronic state. Experimental results reported in this thesis were obtained using this approach.

In this thesis, spectroscopic studies of a number of scandium-containing diatomic molecules will be discussed. In Chapter 2, the general experimental setup will be presented. The first spectroscopic observation of ScP will be discussed in Chapter 3. In Chapter 4, electronic transitions of ScBr and ScI will be reported. A comparison of bonding in scandium monohalides will also be given. A concluding remark will be presented in Chapter 5.

I.2. Electronic spectroscopy of diatomic molecules: background knowledge

Theoretical treatment of motion and energy of molecular systems constitutes to an advanced subject in quantum mechanics [20, 21]. Since molecules are composed of charged particles such as electrons and nuclei, their motions are inevitably mutually correlated that makes the Schrödinger equation of molecular systems practically unsolvable without making approximation. The Born-Oppenheimer approximation has been widely used to separate the motions of electrons and nuclei [22]. The validity of the approximation is due to the great mass difference between electrons and nuclei. By carefully choosing the coordinate systems, one can minimize the coupling between motions and energies of electrons and nuclei. Under the Born-Oppenheimer approximation the coupling energy is neglected to express the energy of a molecular system by nuclear part and electronic part. The approximation

is particularly suited for systems with heavy nuclei as the coupling energy is very small. The detailed discussion of the Born-Oppenheimer approximation can be found elsewhere [22].

After separating the translation of the whole molecule using standard center-of-mass approach, the internal energy of the molecule can be expressed in the form of electronic and nuclear under the Born-Oppenheimer approximation with the corresponding Schrödinger equations for the electronic and the nuclear motions assuming, respectively, the forms

$$H_{el}\psi_{el}(r;R) = E_{el}(R)\psi_{el}(r;R) \tag{1.1}$$

and

$$H_N\psi_N(R) = E_N(R)\psi_N(R)\,, \tag{1.2}$$

where H_{el} and H_N are the electronic Hamiltonian and nuclear Hamiltonian respectively, ψ_{el} and ψ_N are the electronic wavefunction and nuclear wavefunction respectively. The total energy and the corresponding wavefunction expressed below

$$E = E_{el}(r;R) + E_N(R) \tag{1.3}$$

$$\psi(r;R) = \psi_{el}(r;R)\psi_N(R) \tag{1.4}$$

are required to satisfy the Schrödinger equation

$$H\Psi(r,R) = E\Psi(r,R) \tag{1.5}$$

by neglecting the coupling energy as discussed above.

Nuclear motion involves vibration and rotation. Once again, it can be shown that

the great difference between energies of vibration and rotation allows the separation of the two motions with minimized coupling energy [16]. The separation gives rise to two independent Schrödinger equations for vibration and rotation, respectively, leading to the energy expressions for diatomic molecules

$$E_v = (v + 1/2)\omega_e - (v + 1/2)^2 \omega_e \chi_e + \cdots \quad (1.6)$$

and

$$E_J = B_v J(J+1) - D_v J^2 (J+1)^2 + \cdots, \quad (1.7)$$

where ω_e and $\omega_e\chi_e$, are the harmonic frequency and anharmonic constant, respectively, for vibrational motion. B_v, and D_v are rotational constant and centrifugal distortion constant, respectively, for rotational motion. Quantum numbers v and J are used to label the vibrational and rotational energy levels, respectively, in the electronic state.

The multi-electron Schrödinger equation (Eq. 1.1) for electronic motion cannot be solved without making approximation as the motion of each electron is coupled to give the lowest total electronic energy. The common approach is to express the multi-electron wavefunction by products of single electron wavefunction (orbital). The energy for each one-electron wavefunction can then be determined based on the average field from the remaining electrons and nuclei. After consideration of the Pauli principle for the permutation property and the normalization property, the product wavefunction is often expressed in the form of Slater determinant. The correlation of the motion for each electron is then added using various models with different level of accuracy. The common correlation treatment includes MP3, MP4, density functional

theory, MCSCFCI, etc. The effect of electron correlation on the energy of an electronic state depends on the diffusive property and polarizability of the single-electron wavefunctions. For electronic states involving d orbitals, the electron correlation is expected to play an important role in the corresponding energies. Fig. 1.1 shows an experimentally determined energy level diagram of the low-lying electronic states of ScN, as an example to illustrate the rovibronic energy levels of a diatomic molecule [23].

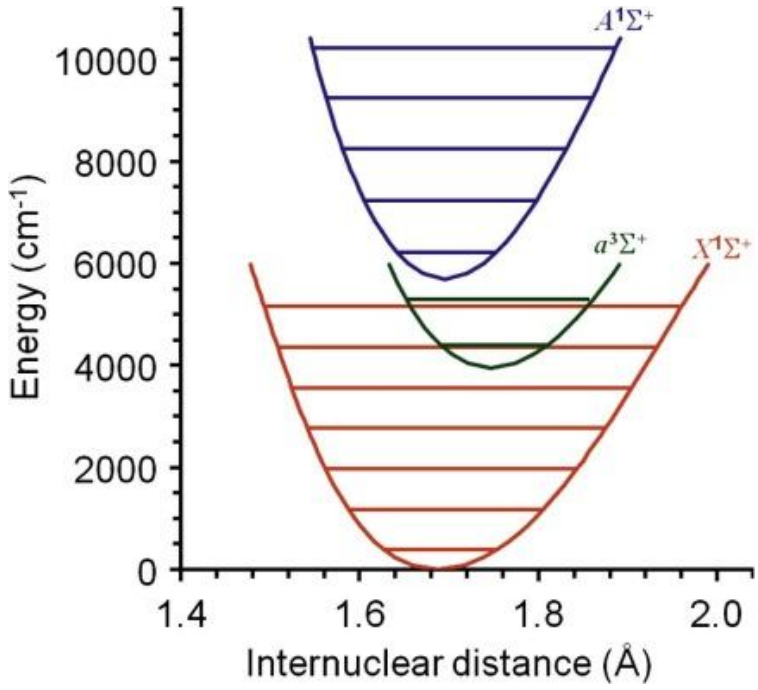

Fig. 1.1 Experimentally determined energy level diagram of the low-lying electronic states of ScN [22]

Electronic states are characterized by experimental parameters energy, total orbital angular momentum along molecular axis (Λ), and total spin angular momentum (S). In addition, rotational motion gives rise to rotational angular momentum (R). The magnetic moments associated with these angular momenta may interact to give rise to energy corrections to the rovibronic states of molecules [20, 21]. In addition, molecules with magnetic nuclei may have additional magnetic interaction due to nuclear spin. Common magnetic interactions in molecular systems are

R·S – Spin-rotation

L·S – Spin-orbit

S·S – Spin-spin

I·R – Nuclear spin-rotation

I·S – Nuclear spin-electron spin

I·L – Nuclear spin-orbit

I·I – Nuclear spin-nuclear spin

Depending on the relative magnitude of the magnetic interactions, various coupling scheme are known as the Hund's cases (a) to (e). The most common Hund's cases are (a), (b), and (c). The schematic vector diagrams of these three cases are shown in Fig. 1.2. The detailed discussion and the corresponding good angular momentum numbers for each case can be found in Herzberg's classic book [16]. It should be noted that the rotational invariance only requires the total angular momentum to be a conserved quantity that leads to rigorous quantum number.

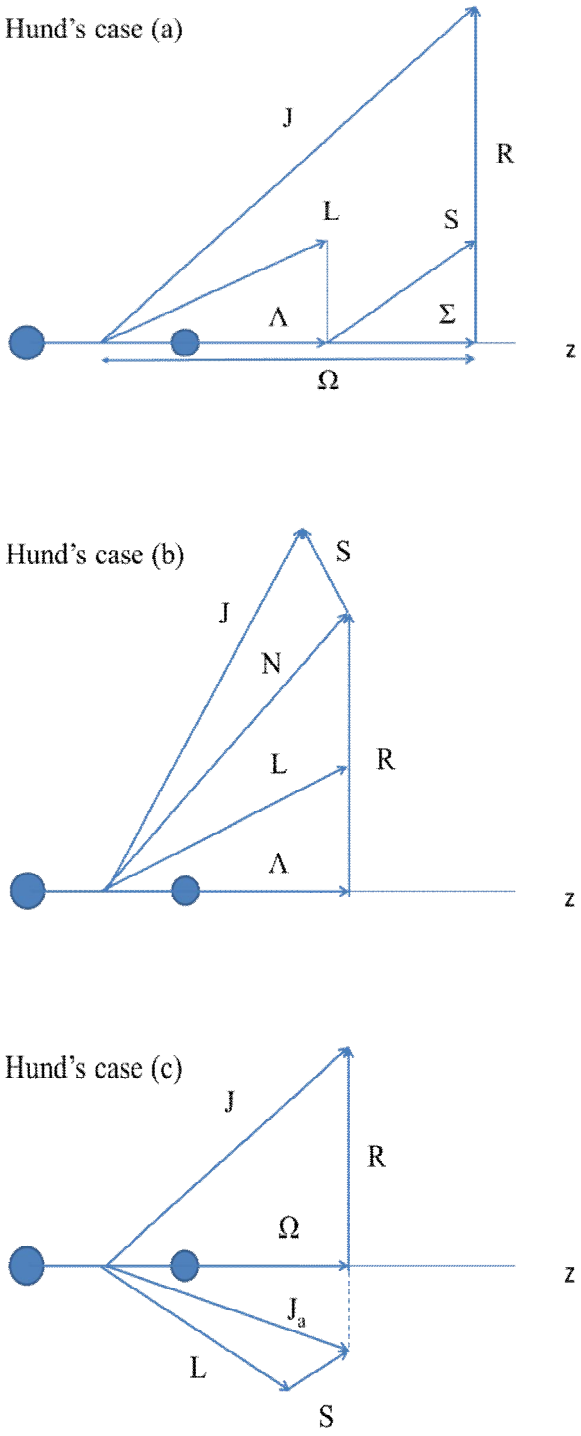

Fig. 1.2 Vector diagram for the Hund's coupling case (a), Hund's coupling case (b), and Hund's coupling case (c)

The rovibronic transitions between electronic states of diatomic molecules are governed by selection rules based on symmetry considerations. For transitions due to electric dipole moment mechanisms, these rules are well established and summarized below [16]:

1. Parity of rovibronic states

$+ \leftrightarrow -$;

2. Permutation symmetry (applied to molecules with identical nuclei)

$\mathrm{s} \leftrightarrow \mathrm{s},\ \mathrm{a} \leftrightarrow \mathrm{a}$;

3. Inversion with respect to molecule-fixed axis system

$\mathrm{g} \leftrightarrow u$;

4. Total angular momentum including nuclear spin and electronic spin

$\Delta F = 0, \pm 1$;

5. Total angular momentum excluding nuclear spin

$\Delta J = 0, \pm 1$.

6. Nuclear spin (applied to magnetic nuclei)

$\Delta I = 0$

These are rigorous selection rules based on symmetry of permutation-inversion and rotational invariance. In addition, various approximate selection rules can be derived depending on the Hund's cases that have different good quantum numbers:

7. Orbital angular momentum along molecular axis

$\Delta \Lambda = 0, \pm 1$;

for transitions between Σ electronic states, only $\Sigma^+ - \Sigma^+$ and $\Sigma^- - \Sigma^-$ are allowed.

8. Electronic spin

$\Delta S = 0$ (applied to molecules with light atoms as it breaks down by strong spin-orbit coupling for heavy atoms, transition);

9. Electronic spin along molecular axis

$\Delta\Sigma = 0$ (applied to Hund's case (a) only);

10. Total angular momentum (excluded nuclear spin) along molecular axis

$\Delta\Omega = 0, \pm 1$ (applied to Hund's case (a) only);

11. Total angular momentum (excluded electronic spin and nuclear spin)

$\Delta N = 0, \pm 1$ (applied to Hund's case (b) only.

The analysis of a spectrum involves (1) making the assignment of quantum numbers involved in the observed transitions based on selection rules and spectral pattern; and (2) deriving the corresponding structural constants for the quantum states involved using the correct energy expressions. These two procedures are often done repeatedly until no more new assignment can be made. The effective Hamiltonian used to express the energy of the rovibronic states can be expressed in a general form of

$$H_{eff} = H_{Rot} + H_{SR} + H_{SO} + H_{SS} + H_{\Lambda D} + H_{MF} + H_{eqQ} + H_{NSR} \quad (1.8)$$

The terms represent electronic, vibrational, rotational, electron spin-rotation, electron spin-orbit, electron spin-electron spin, Λ-doubling, magnetic hyperfine, electric quadrupole, and nuclear spin-rotation interactions. Detailed descriptions of these

components, including higher order terms and physical interpretations, can be found in Brown and Carrington [20]. Depending on the nature of the states, some terms in the above equation may vanish. Once the Hamiltonian is determined for the rovibronic states, the energy can be calculated by the diagonalization of the corresponding Hamiltonian matrix using appropriate basis functions for the states. With the energy of rovibronic states determined, one can then calculate transition energy in terms of quantum numbers (from assignment) and structural parameters. Since the number of transitions is often much greater than the number of parameters involved, a statistical approach is used to obtain the best set of parameters that give rise to the minimum root-mean-square residue, which is supposed to be on the same order of the measurement uncertainty barring no systematic error is involved. Therefore, by comparing the residue of the optimized fitting with the measurement uncertainty, once can judge the quality of the fit and structural parameters.

Chapter II

Experiments

Spectroscopic studies of metal-containing diatomic molecules in the gas phase require special techniques due to the short lifetime, high reactivity, and low abundance of these species in the environment. As a result, fast detections with high sensitivity is necessary. In order to obtain structural parameters at high accuracy, rotationally-resolved spectrum is more desirable. The experimental apparatus employed for this work is composed of a gas chamber for producing molecules of interest and near infrared laser spectrometer for detecting the molecules using laser induced fluorescence (LIF) spectroscopy, a sensitive "zero-background" technique. In this approach, a laser source was used to excite the molecules of interest. The total fluorescence from the excited state was then measured. To have the fluorescence emission, molecules must be excited by the laser radiation first. In other words, the fluorescence signals indicate the absorption of molecules. By plotting the fluorescence signals against the frequency of excitation radiation, it is possible to obtain a spectrum that deviates from the absorption spectrum by only the relative intensity of the spectral peaks.

Since the resolution of the LIF spectrum depends on the spectral purity of the excitation laser source, Doppler-limited spectrum can be obtained without much

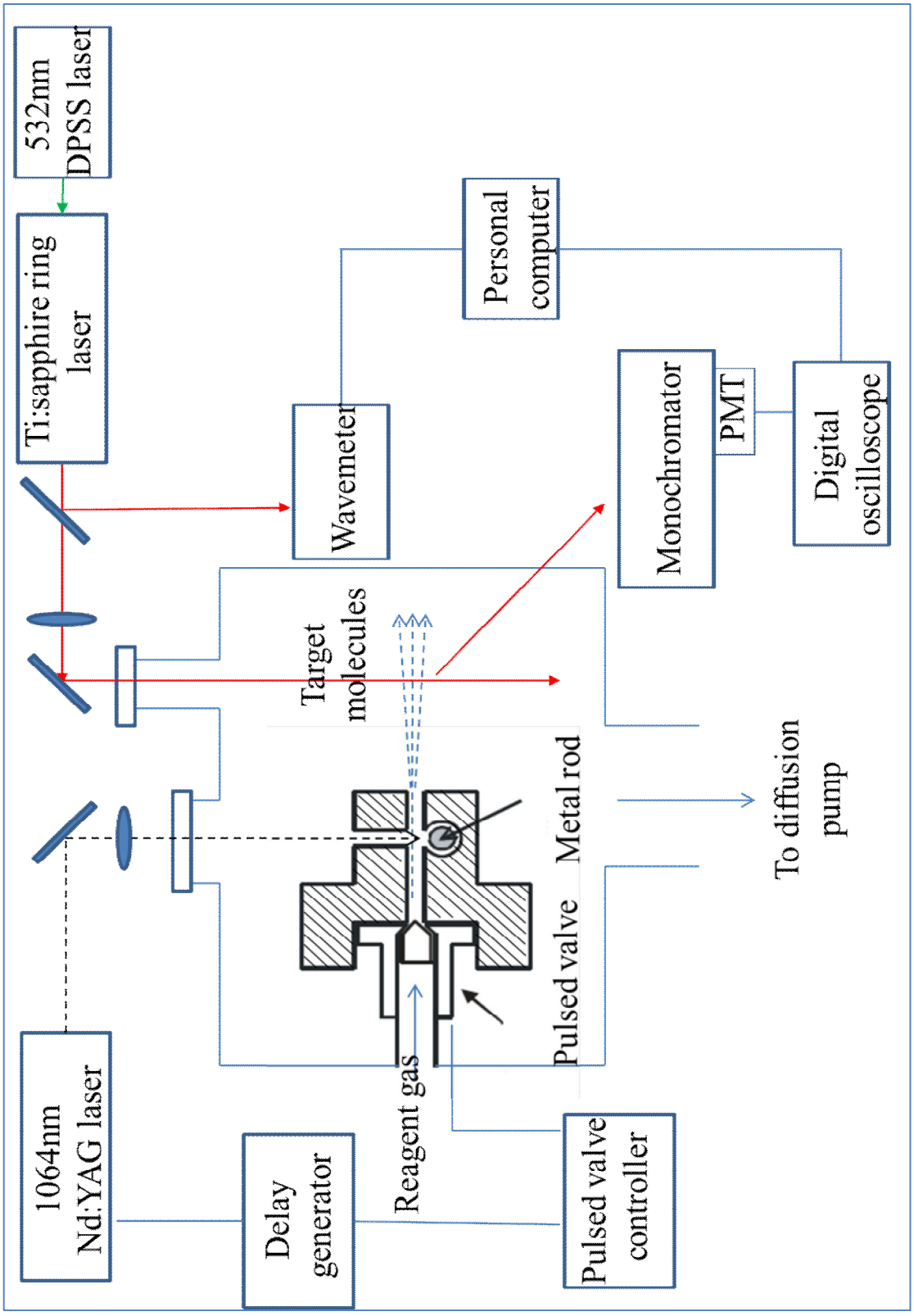

Fig. 2.1 Schematic diagram of laser ablation/reaction-free jet expansion-laser induced fluorescence (LARFE-LIF) experimental setup

difficulty. This approach has been widely used in the field. In this chapter we will describe the experimental setup in our laboratory. The apparatus as shown in Fig. 2.1 is composed of two parts, namely a vacuum chamber for the production of metal-containing molecules of interest and a high resolution LIF spectrometer, which will be discussed below.

II.1. Production of metal-containing molecules

The metal-containing molecules can be generated by reacting metal atoms with appropriate precursor gas. Laser ablation is a common approach to produce metal vapor by local heating of metal solids using high power pulse lasers. Fig. 2.2 shows the schematic diagram of the gas chamber used for this work. As shown in the figure, metal-containing molecules produced in the gas channel of the metal holder are expanded into a vacuum chamber so that the collisions between molecules were virtually ceased. The vacuum of the chamber was maintained at 10^{-5} Torr using a diffusion pump backed by a rotary pump. The details of various parts of the chamber as well as the production conditions are described below.

Fig. 2.3 shows the design of the metal holder made of aluminum. It was used for housing metal rods of up to 8 mm in diameter. A hole of 2 mm in diameter was opened on the surface of the holder to allow the ablation laser to irradiate on the metal surface. A gas channel of 2 mm in diameter and 20 mm in length was opened for

passing the precursor gas to react with the metal vapor produced by laser ablation. A pulse valve was installed at the entrance of the gas channel to control the gas flow. The exit of the gas channel was a hole of about 2 mm in diameter. By expanding the reaction mixture into vacuum, molecules were significantly cooled to about 100 K for spectroscopic study.

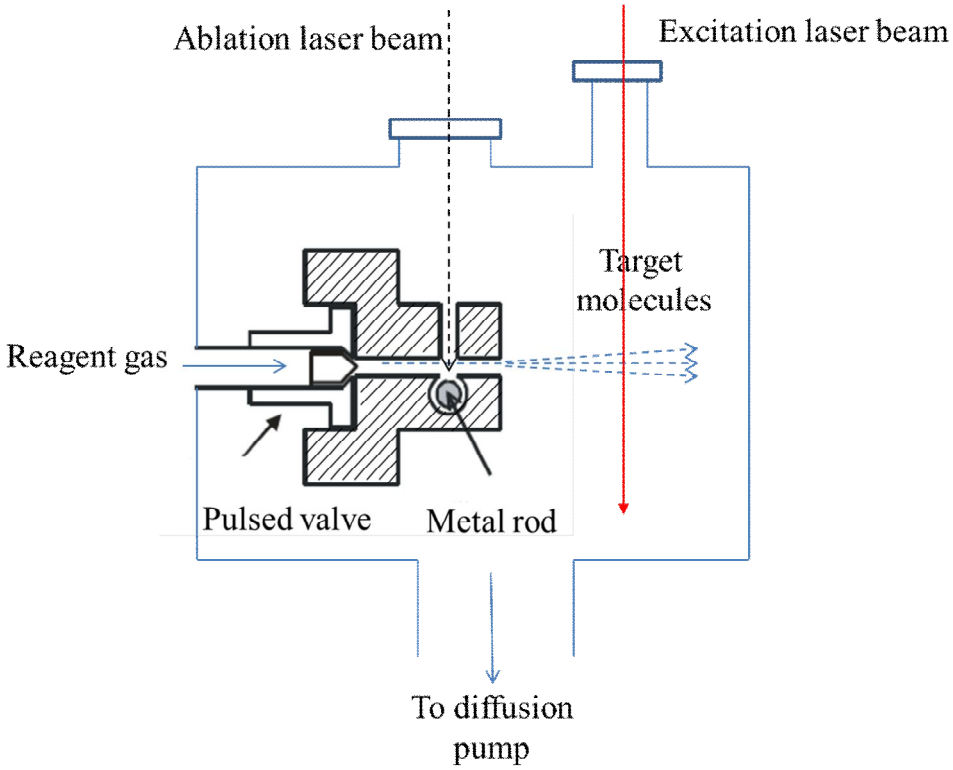

Fig. 2.2 Schematic diagram of the gas chamber

The ablation laser was a commercial pulsed Nd:YAG laser operated at 1064 nm and a repetition rate of 10 Hz. With a pulse width of 7 ns and an average energy output of 20 mJ, an average power of 2.86×10^{6} W was achieved during each pulse. The laser beam was defocused to a spot of ~2 mm in diameter to avoid overheating of

a small area. In addition, the metal rod was rotating at a constant speed so that the various parts of the metal surface are exposed to the laser radiation. As a result, reasonably good shot-to-shot stability was obtained for the production of metal vapor. The surface of the metal rod was cleaned after a few hours of operation to remove the soot so that the stability was maintained.

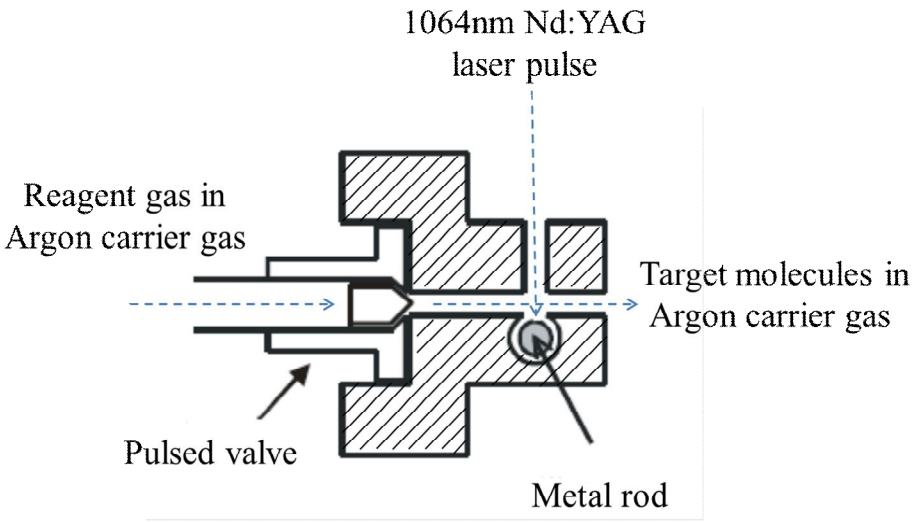

Fig. 2.3 Schematic diagram of laser ablation/reaction module

Adiabatic expansion of a high pressure gas through a nozzle (free jet expansion) has been commonly used to reduce the gas temperature. The technical details of the cooling effect of free jet expansion can be found in a number of textbooks [13, 19]. When the diameter d of the nozzle is much larger than the mean free path λ_0 of the expanding gas (i.e. $d >> \lambda_0$), the orifice will convert the random motions of the molecules in the gas into mass flow in the direction normal to the nozzle. As a result,

molecular motion has a preferential direction instead of random in all directions. This allows minimizing the Doppler broadening of spectral transitions by using a probe radiation orthogonal to the preferential direction. In addition, the cooling effect is particularly efficient on rotational motion that only a few rotational levels are significantly populated to exhibit much simpler pattern in the rotationally resolved spectrum.

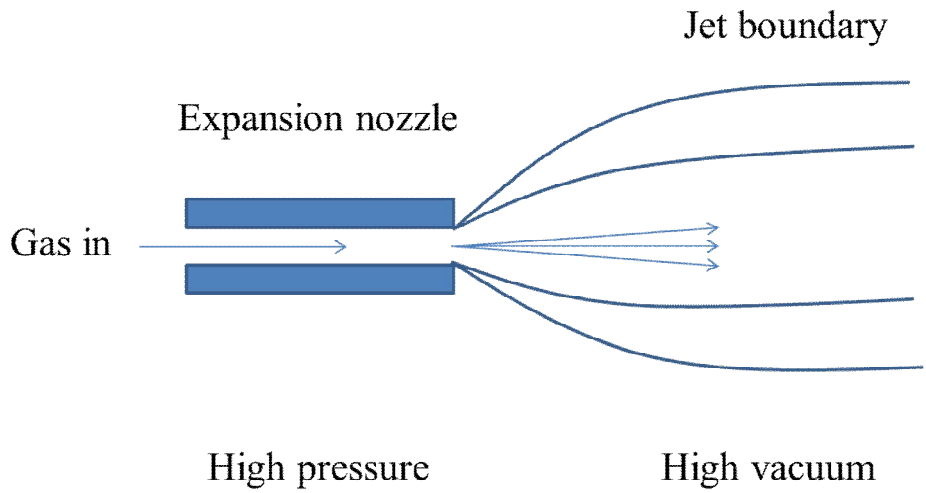

Fig. 2.4 Schematic diagram of free jet expansion using a nozzle

In our experiments, the carrier gas with the target molecules at a pressure of a few atm was expanded to a vacuum at a pressure of 10^{-5} Torr through a circular orifice of 2 mm in diameter. Since the precursor gas mixture was controlled by a pulsed valve operated at 10 Hz with a duration of 280 μs, the expansion was synchronous with pulsed laser repetition rate with some time delay depending on the dimension gas channel. The pulsed expansion not only allows lower pumping capacity but also

allows the LIF detection with less background noise.

Achieving the optimum conditions for production of target metal-containing molecules requires a bit of luck. While the choice of metal is of little doubt, the choice of precursor gas and its concentration often affects the efficiency of the production of target molecules. The overall efficiency of production depends on the ablation efficiency, precursor gas mixtures, and also the time sequence of processes involved. It often starts with the trial and error approach. Nevertheless, once fluorescence signals are obtained, signal optimization can be carried out systematically.

II.2. Laser induced fluorescence spectrometer

The laser induced fluorescence spectrometer used in our experiments consists a high resolution laser excitation source, a frequency calibration device and a fluorescence detector as described below.

A commercial ring Ti:sapphire laser source (899-21) from Coherent Inc. was used to excite the molecules for detection of LIF signals. It was optically pumped by a 7-W DPSS (diode-pumped solid state) laser at 532 nm. The output power of the ring laser was about 0.9 to 1.1 W with a spectral purity of ~500 kHz (RMS jittering). With three sets of cavity mirrors, the complete coverage of the ring laser was about 10000 - 14200 cm^{-1}. Most of the work reported here was done using the mid-wave (MW)

optics which covers the region 11000-13000 cm^{-1}. By electronically controlling the thick etalon assembly in the cavity, the Ti:sapphire laser can be continuously scanned for about 24 GHz (0.8 cm^{-1}). The starting frequency of each scan can be achieved by adjusting the positions of the birefringent filter (BRF) and the thin etalon assembly. The complete frequency coverage can thus be done by repeating these steps. The detailed discussion of the source can be found elsewhere [24].

The frequency of the ring laser output was calibrated using a wavelength meter (Burleigh Inc., WA1500) at a resolution of 0.001 cm^{-1}. The wavelength meter is based on the principle of Michelson interferometry that determines the absolute wavelength of the laser (600-1800 nm) by comparing its interference fringe pattern with that of a built-in thermally stabilized He-Ne laser. The frequency information from the wavelength meter was sent to a pc using an in-house data acquisition program written in Lab-View. It was found in a series of tests that the absolute accuracy of frequency measurement for the system was better than 0.003 cm^{-1} [24].

The fluorescence signals were collected using a lens system orthogonal to both directions of expansion and excitation axis. The signals were then sent to the input slit of a monochromator equipped with a photomultiplier tube (PMT) optimized for near infrared radiation. The monochromator also served as a primary filter for the excitation laser and background noise from production process. The fluorescence signals dispersed by the grating in the monochromator were detected by the PMT. The

signals from the PMT were digitized in a 300 MHz oscilloscope and then stored in a pc.

In the initial search of target molecules, the Ti:sapphire laser was manually scanned over a broad spectral region to collect the LIF signals. By removing the etalon assemblies of the ring laser to scan with the BRF, a spectral resolution of about 2 GHz was achieved for each scan of 50 cm^{-1} at a rate of round 0.2 cm^{-1}/s. After the identification of the observed vibronic bands, high resolution LIF spectrum was recorded with all the etalons installed. With a scanning range of 24 GHz for each scan and about 4 GHz overlap between adjacent scans, the whole vibronic band with rotationally resolved structure was measured for further analysis.

Chapter III

The first Observation of ScP Using Laser Induced Fluorescence Spectroscopy

Transition metals form a unique category of elements in chemistry. They play important roles in various disciplines such as organometallic chemistry, bioinorganic chemistry, and catalysis. The distinguished chemical properties of transition metals arise from the involvement of *d* electrons/orbitals in chemical bonding. It has been well known in the early days that energy of n*d* orbitals is very close to those of (n+1)*s* and (n+1)*p* orbitals. As a result, compounds containing transition metals usually possess a wealth of low-lying electronic states whose energies are sensitive to electron correlation. It is therefore a great challenge in computational chemistry to accurately predict the energies and structural parameters for these states. On the other hand, spectroscopic studies directly provide these information at high accuracy.

As the first transition metal with one d electron, scandium presents an ideal case for investigating the role of *d* electrons in chemical bonding [15]. Various scandium-containing diatomic molecules have been investigated experimentally and theoretically. Scandium monohalides including ScF [25-31], ScCl [31-39], ScBr [40-46], and ScI [47-53] have been most extensively studied using ab initio calculations as well as emission spectroscopy. Molecules involving group VI elements

ScO [54-61] and ScS [62-66] have also been known for years. By comparing properties of these isovalent species, insights of electronic structures of these species have been gained.

On the other hand, only a handful of work has been done on molecules formed with group V elements. From the studies of ScN [67-74], it was found that the agreement between theoretical calculations and experimental observations were not satisfactory indicating that even high level calculations are insufficient for predicting the properties of the system. The isovalent ScP has only been studied by theorists to date. DFT (density functional theory) methods at different levels of electron correlation have been used in characterizing the $X^1\Sigma^+$ ground electronic state of ScP since the 1990s [73, 75, 76]. It was only recently that the excited electronic states of ScP were extensively studied by Daodi *et al.* [73] using the multireference configuration CIPSI (configuration interaction by perturbation of multiconfiguration wavefunction selected iteratively) method as well as DFT calculations at B-P86 level. In these calculations the relative energies of four low-lying excited electronic states $^1\Sigma^+$, $^3\Sigma^+$, $^1\Pi$, and $^3\Pi$, have been determined together with the ground state. More recently, three more low-lying excited states, namely $^3\Phi$ (at 7486 cm^{-1}), $^5\Delta$ (at 8496 cm^{-1}), and $^5\Pi$ (at 11269 cm^{-1}) were predicted below the excited $^1\Sigma^+$ state by Tong *et al.* [76]

In order to investigate the accuracy of theoretical calculations for molecules

involving group V elements, we set out to study the electronic spectrum of ScP. Coupling the laser ablation with free jet expansion, ScP was produced and characterized using laser induced fluorescence. In the spectral region of ~11500 - 12900 cm^{-1}, ten rotationally resolved vibronic bands belonging to the $^1\Sigma^+$ - $^1\Sigma^+$ system have been observed and analyzed. In the chapter, the details of this work will be presented.

III.1. Experimental conditions

The general experimental setup has been described in chapter 2. The specific experimental conditions for ScP study will be given here. ScP molecules were produced from the reaction of scandium atoms with 1% PH_3 in argon buffer at a total pressure of about 8 atm. The Sc atoms were produced by laser ablation of a pure scandium rod using a pulsed Nd:YAG laser operated at 1064 nm and 10 Hz repetition rate with an average energy of ~20 mJ. The gas mixture reacting with Sc atoms was controlled by a pulsed valve synchronized with laser pulses with an appropriate delay. The reaction mixture was then expanded through a nozzle of 2 mm in diameter to form a free jet expansion.

The jet-cooled ScP molecules were excited by a ~1-W high resolution cw ring Ti:sapphire laser pumped by a 7-W DPSS laser at 532 nm. The LIF signals collected by a focusing lenses system were sent to a monochromator equipped with a near

infrared photomultiplier tube (PMT) detector. In addition to detecting the LIF signals, the monochromator also served as a primary optical filter in recording the LIF spectrum to remove the strong background radiation due to excitation laser, as well as a device for obtaining the wavelength-resolved fluorescence spectrum of ScP molecules. The output frequency of the ring laser, whose spectral purity was about 1 MHz, was calibrated using a wavelength meter with an accuracy of 0.001 cm^{-1}. The absolute accuracy of a measured line position was expected to be about 0.003 cm^{-1}.

III.2. Observation and Analysis

The overall LIF spectrum of ScP in the spectral region of 11500 - 12900 cm^{-1} is shown in Fig.3.1. A total of about 300 transitions from 10 rotationally resolved vibronic bands were observed with good signal-to-noise ratio. The typical linewidth (HWHM) of the transitions was observed to be about 280 MHz, consistent with the Doppler width at a temperature of about 90 K under our experimental conditions.

The observed bands are located at 11445, 11475, 11936, 11962, 11988, 12014, 12453, 12475, 12498, and 12518 cm^{-1}, respectively. These bands were assigned to the (0, 1), (1, 2), (0, 0), (1, 1), (2, 2), (3, 3), (1, 0), (2, 1), (3, 2), and (4, 3) bands, respectively, based on preliminary analysis of the wavelength resolved spectrum. As shown in Figs. 3.2 to 3.11, each vibronic band exhibits clear *P* and *R* branches with the absence of *Q* branch lines. This characteristic confirms the nature of the $\Delta\Lambda = 0$

type electronic transition. In addition, each band is violet-degraded with a characteristic *P* head, a characteristic resulting from the fact that the rotational constant of the upper state is greater than that in the lower state. The simple spectral pattern of the vibronic bands indicates a $\Sigma - \Sigma$ type band system. The lower state constants are consistent with those predicted for the ground $X^1\Sigma^+$ state [73], the observed band system is therefore assigned to the $[11.9]^1\Sigma^+ - X^1\Sigma^+$ electronic transition. Since the order of the excited electronic states of ScP is not known with certainty, we adopt the notation that uses a square bracket to indicate the frequency of the excited state instead of labeling the states by alphabetical order.

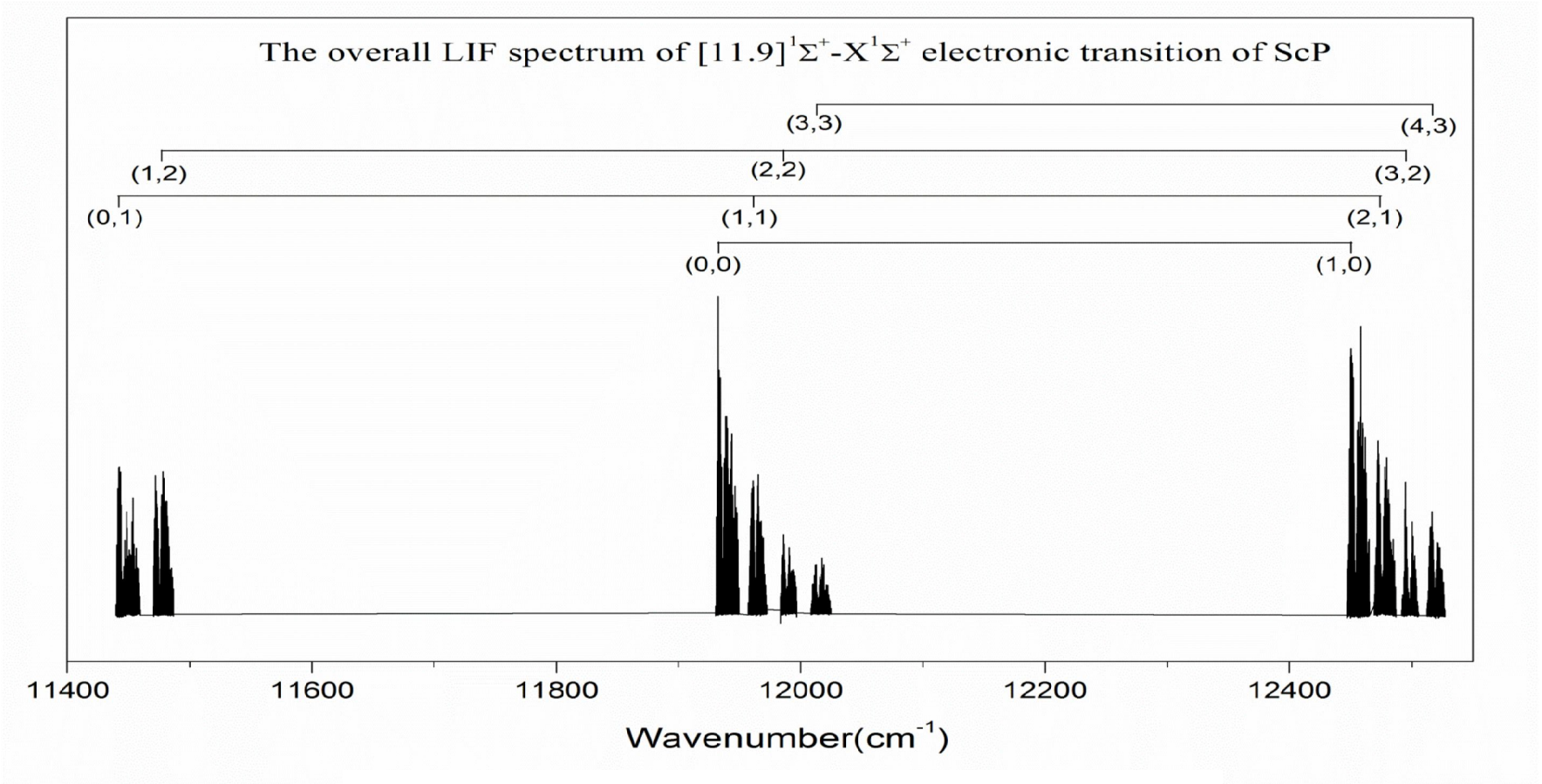

Fig. 3.1 The overall LIF spectrum of the [11.9]$^1\Sigma^+$- X$^1\Sigma^+$ transition of ScP

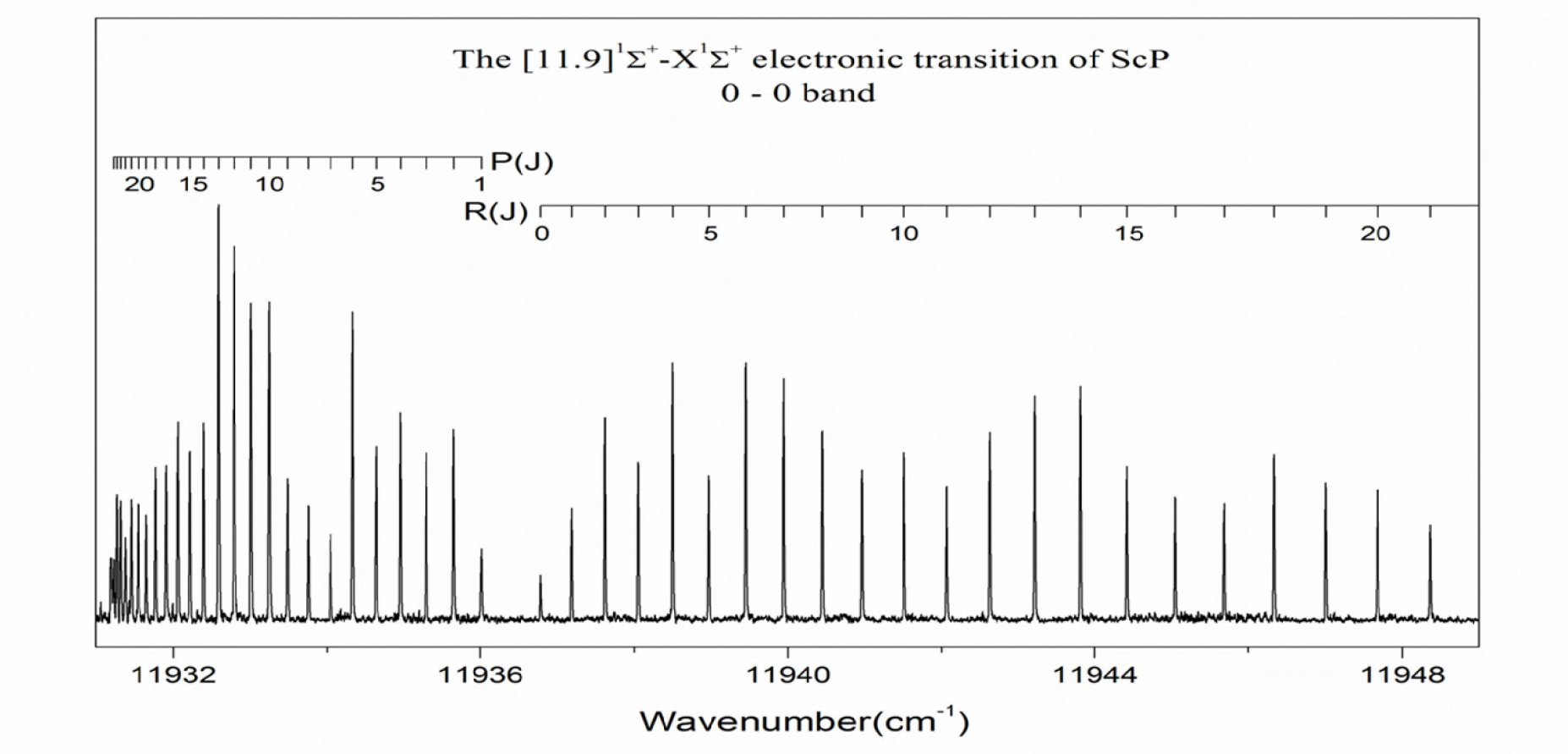

Fig. 3.2 The (0, 0) band of the [11.9]$^1\Sigma^+$- X$^1\Sigma^+$ transition of ScP

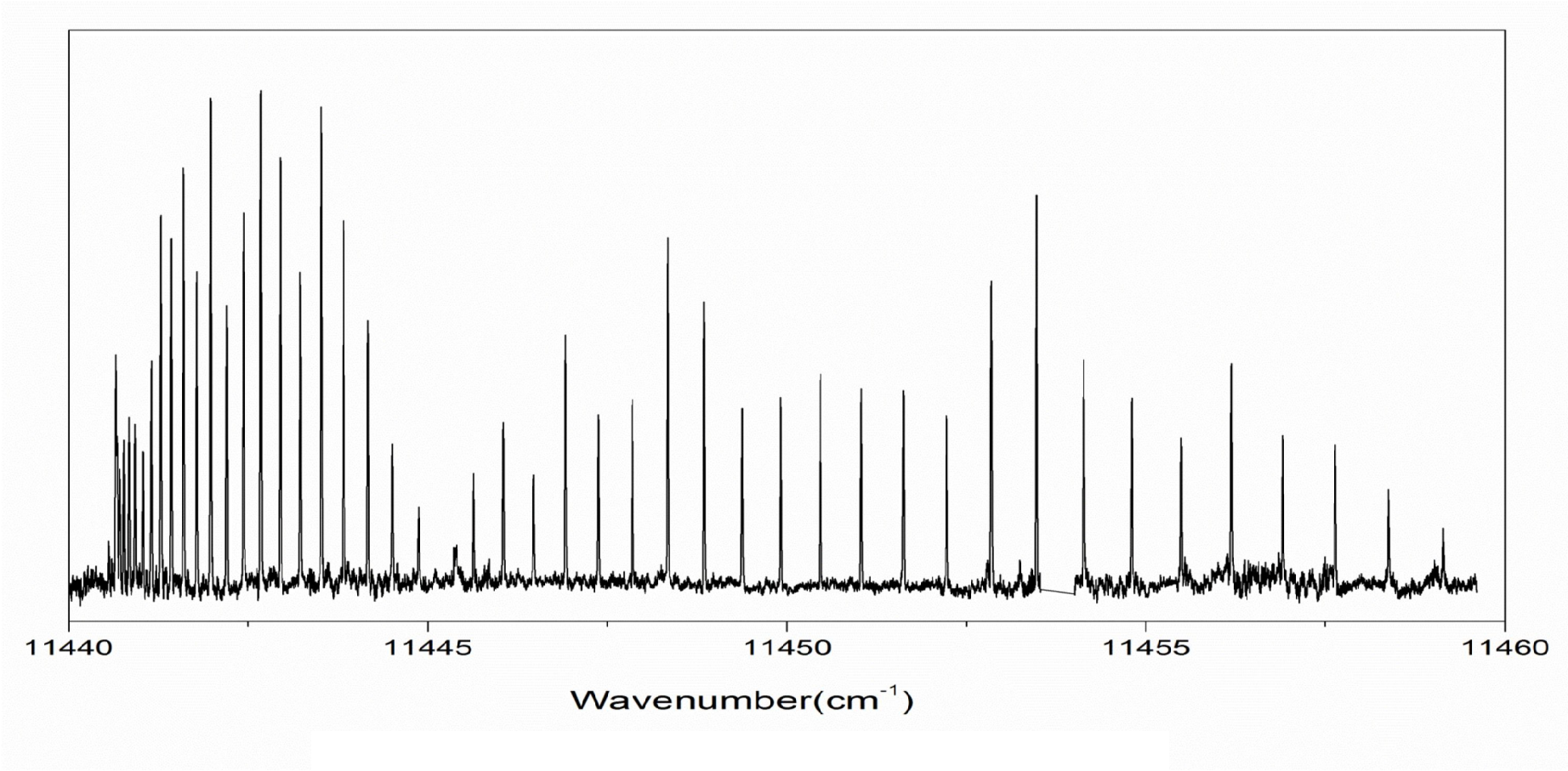

Fig. 3.3 The (0, 1) band of the $[11.9]^1\Sigma^+$- $X^1\Sigma^+$ transition of ScP

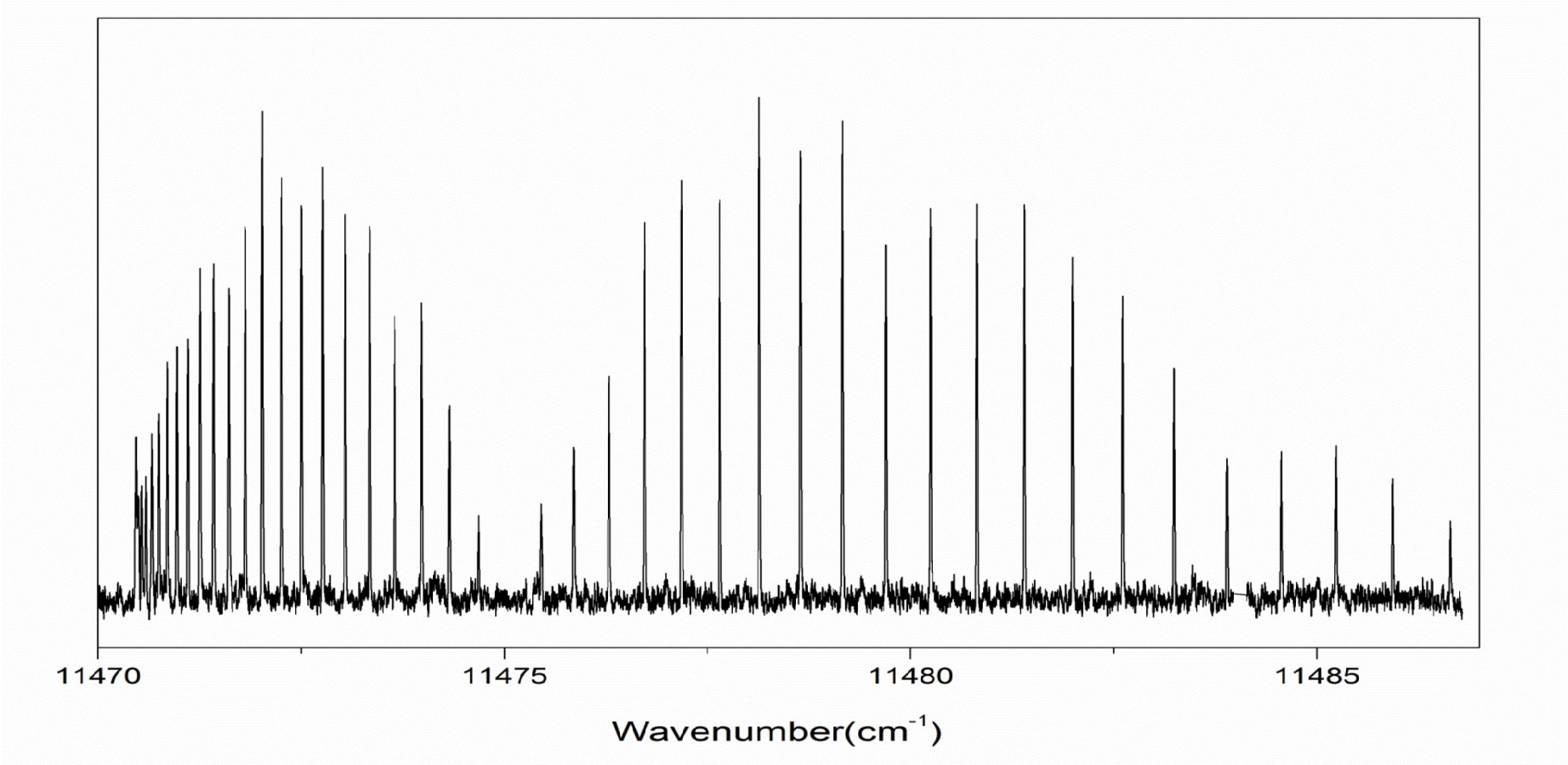

Fig. 3.4 The (1, 2) band of the $[11.9]^1\Sigma^+$- $X^1\Sigma^+$ transition of ScP

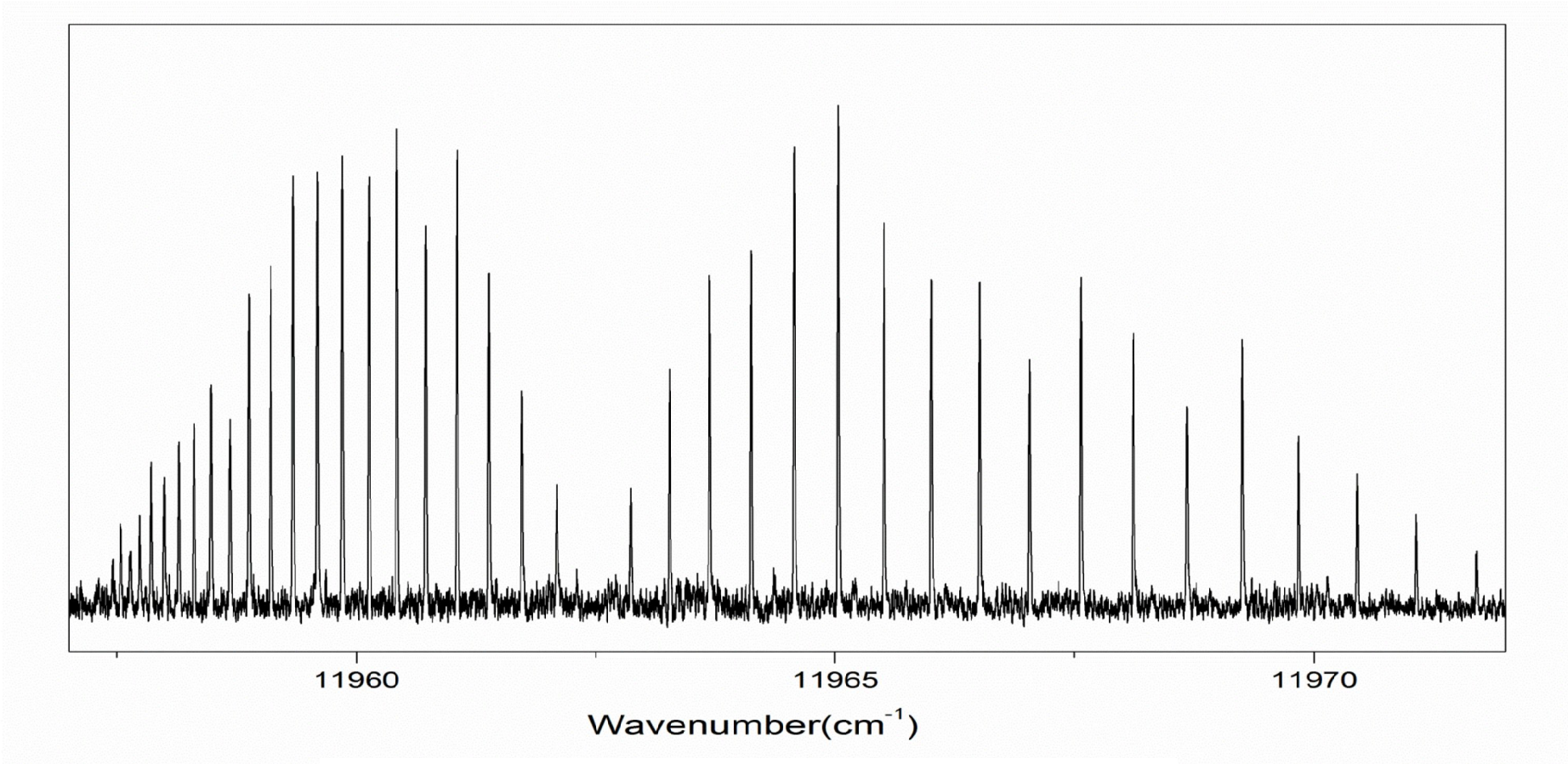

Fig. 3.5 The (1, 1) band of the $[11.9]^1\Sigma^+ - X^1\Sigma^+$ transition of ScP

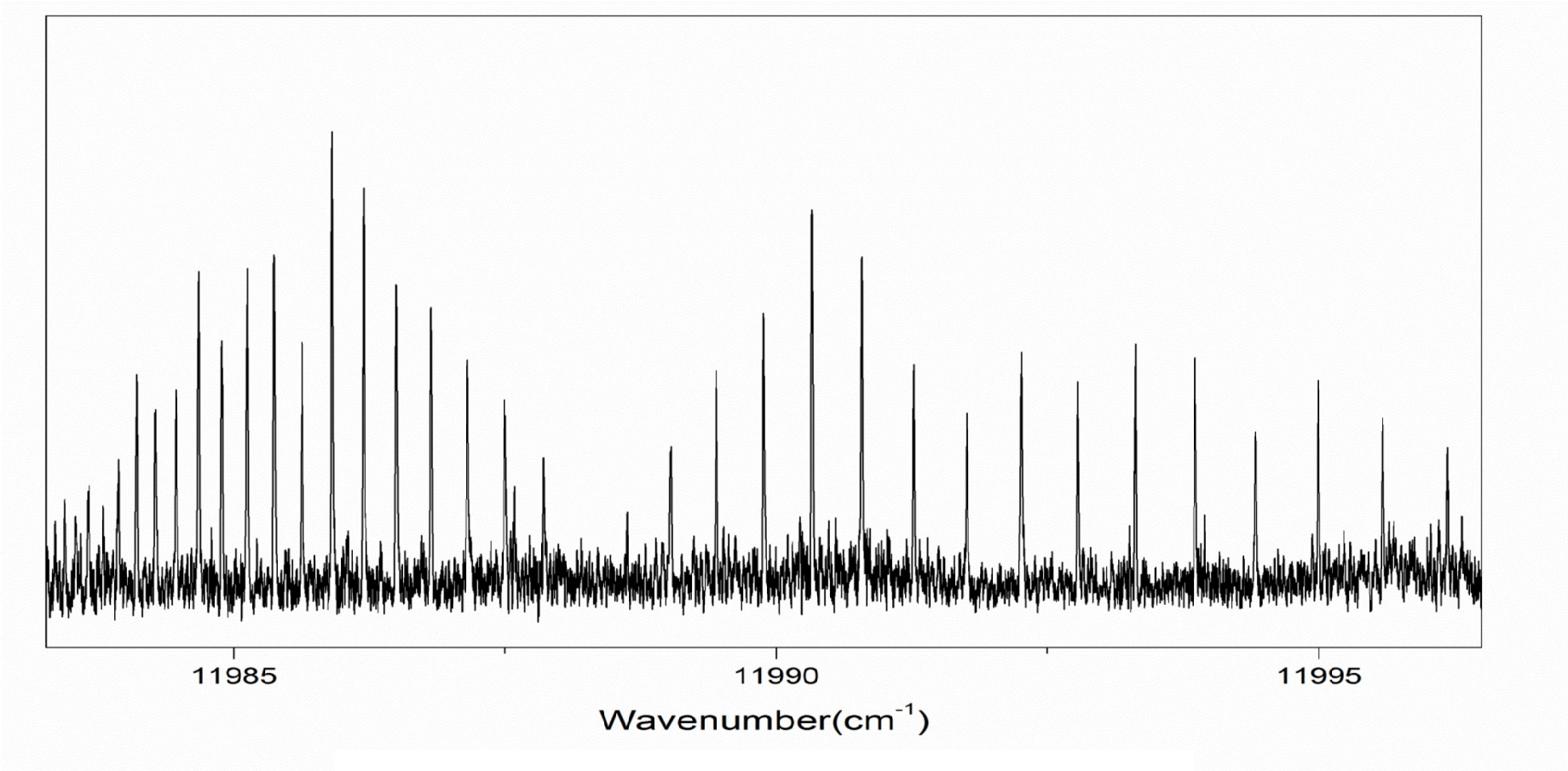

Fig. 3.6 The (2, 2) band of the $[11.9]^1\Sigma^+$- $X^1\Sigma^+$ transition of ScP

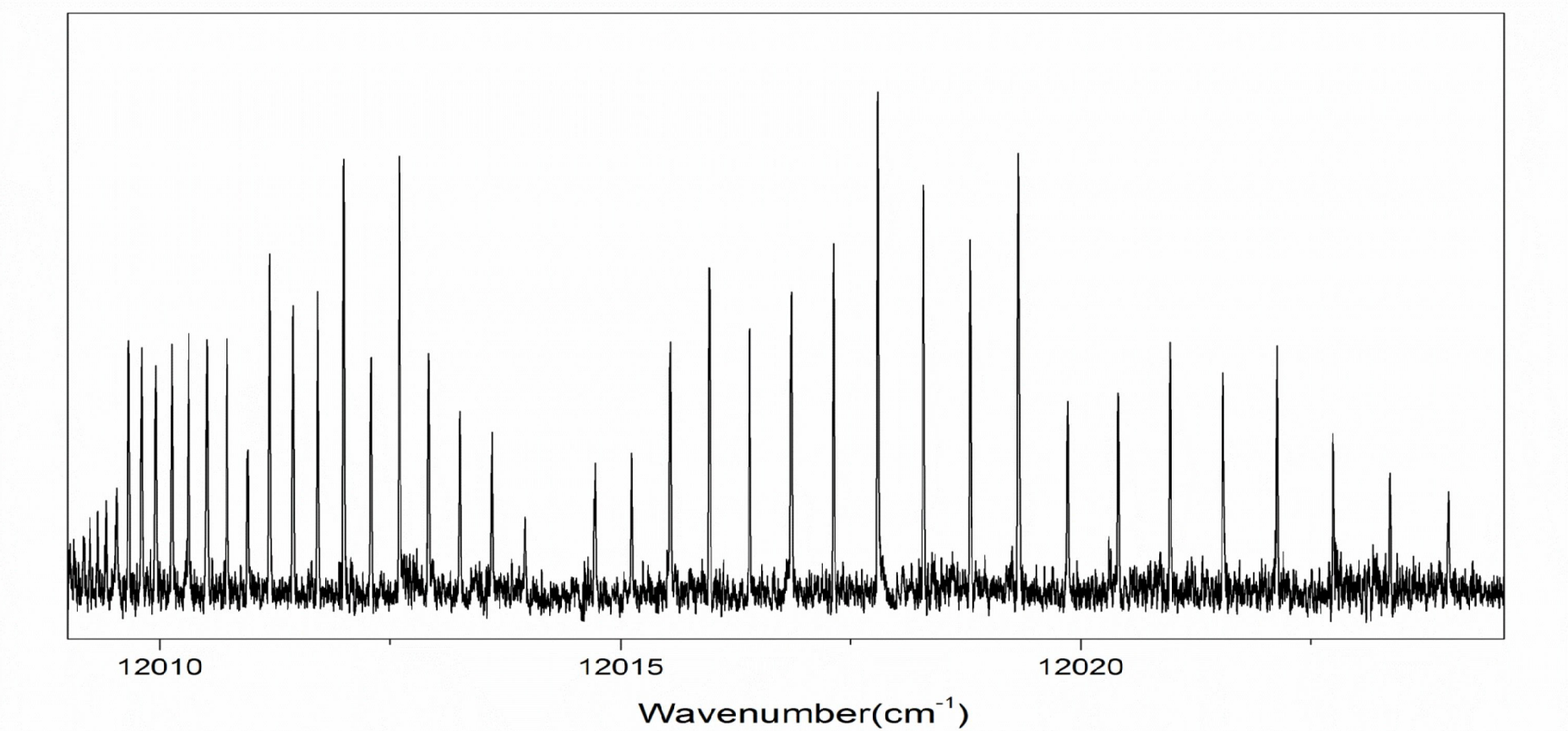

Fig. 3.7 The (3, 3) band of the $[11.9]^1\Sigma^+$- $X^1\Sigma^+$ transition of ScP

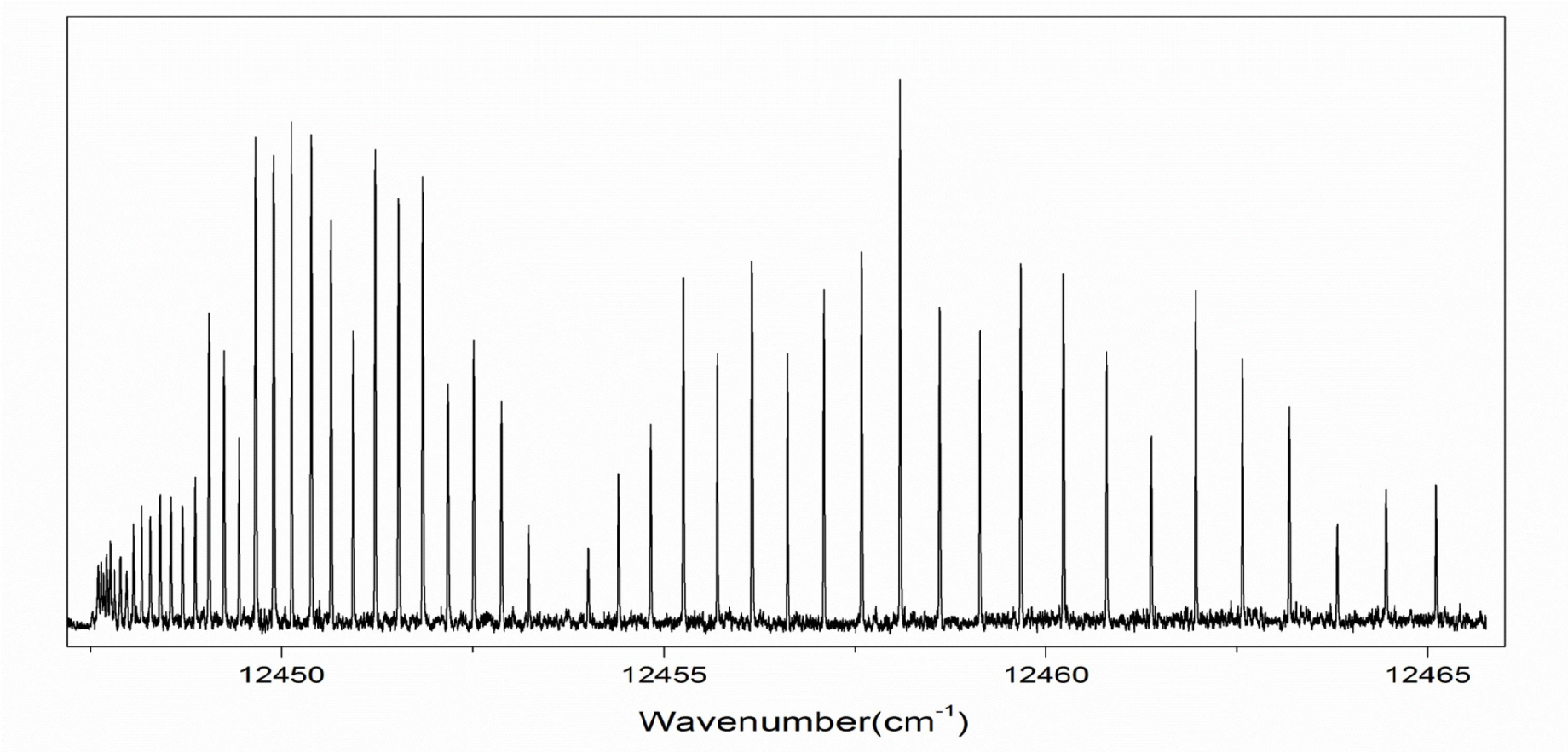

Fig. 3.8 The (1, 0) band of the $[11.9]^1\Sigma^+$- $X^1\Sigma^+$ transition of ScP

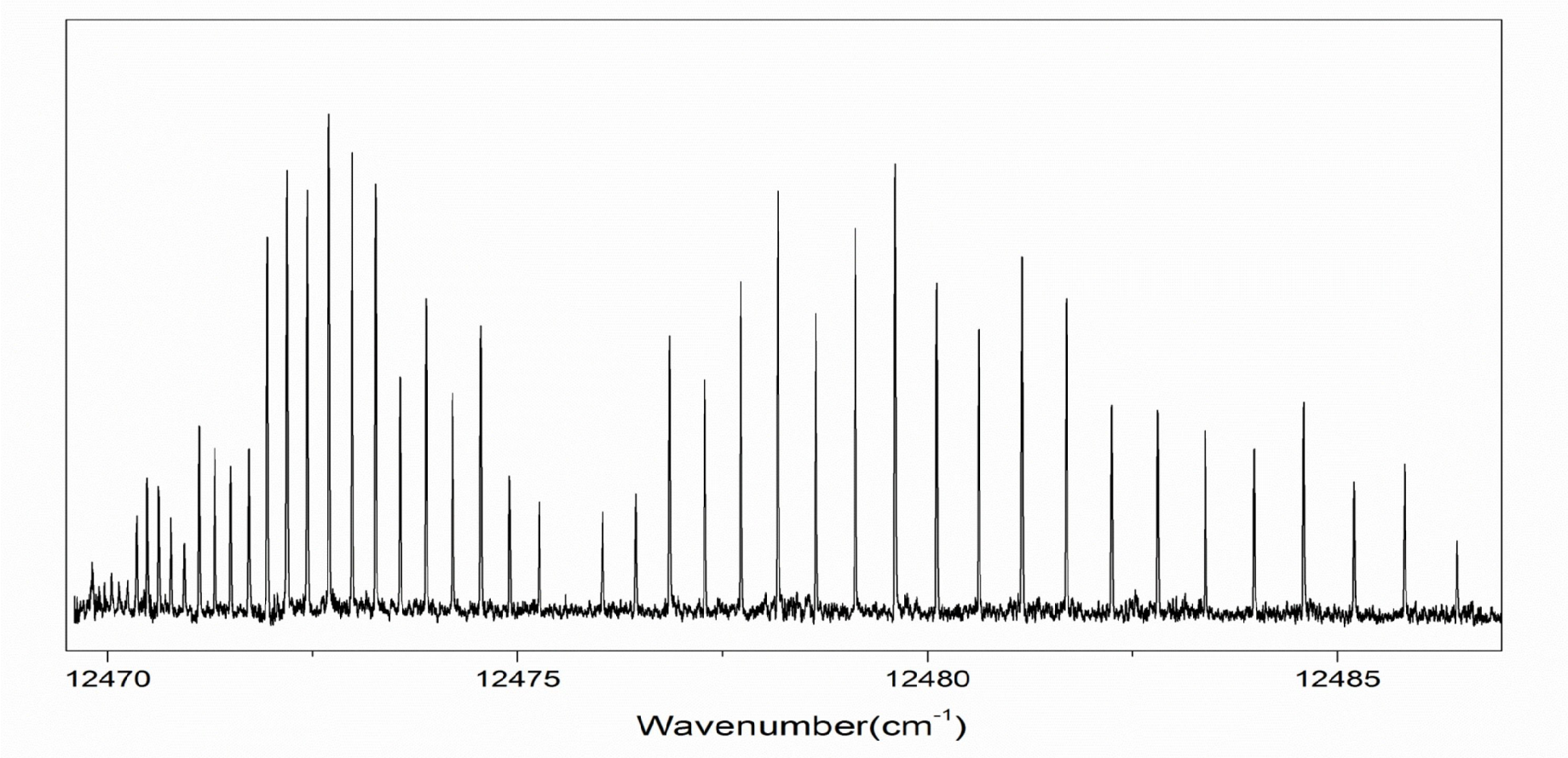

Fig. 3.9 The (2, 1) band of the $[11.9]^1\Sigma^+$- $X^1\Sigma^+$ transition of ScP

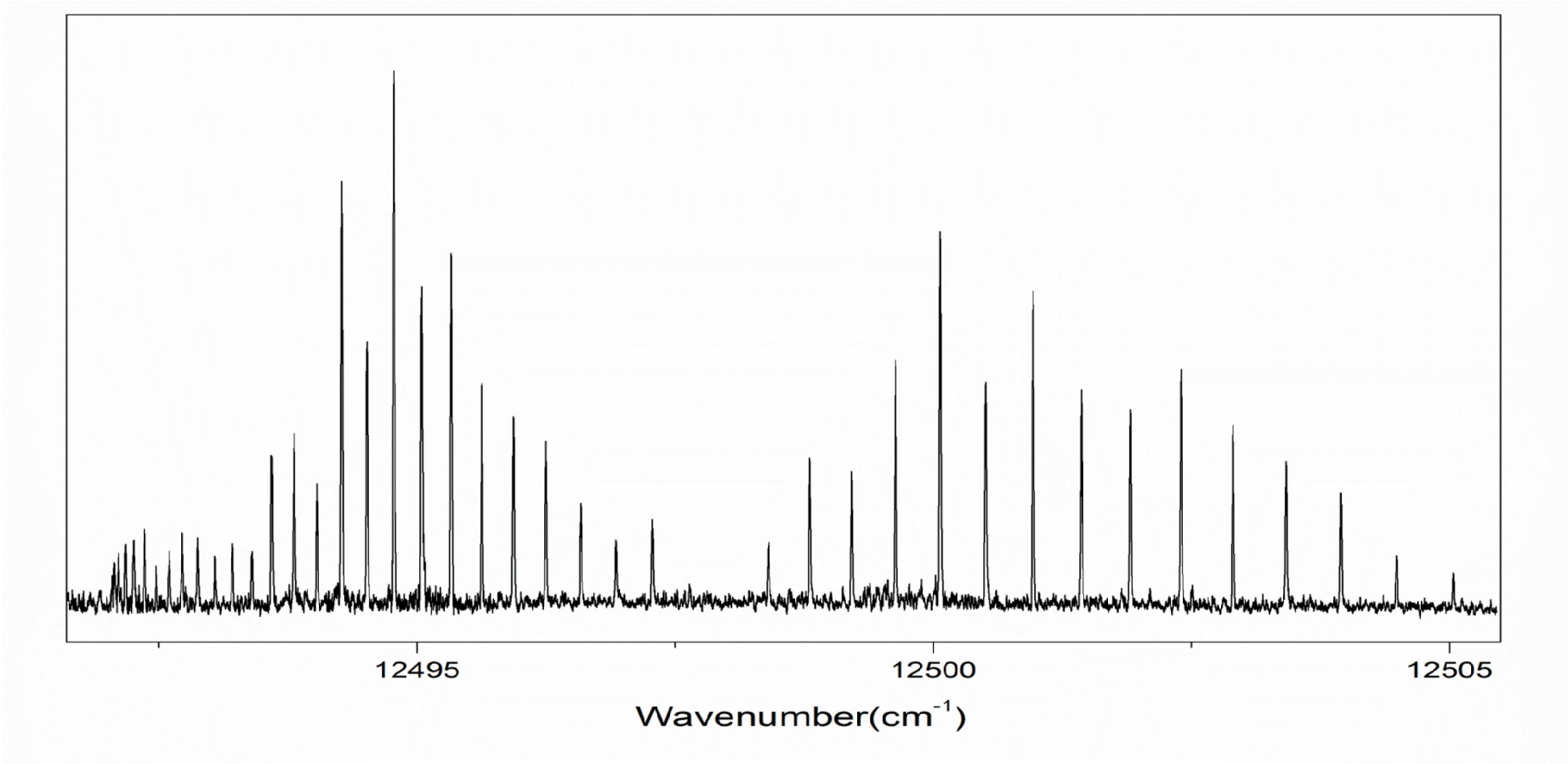

Fig. 3.10 The (3, 2) band of the $[11.9]^1\Sigma^+$- $X^1\Sigma^+$ transition of ScP

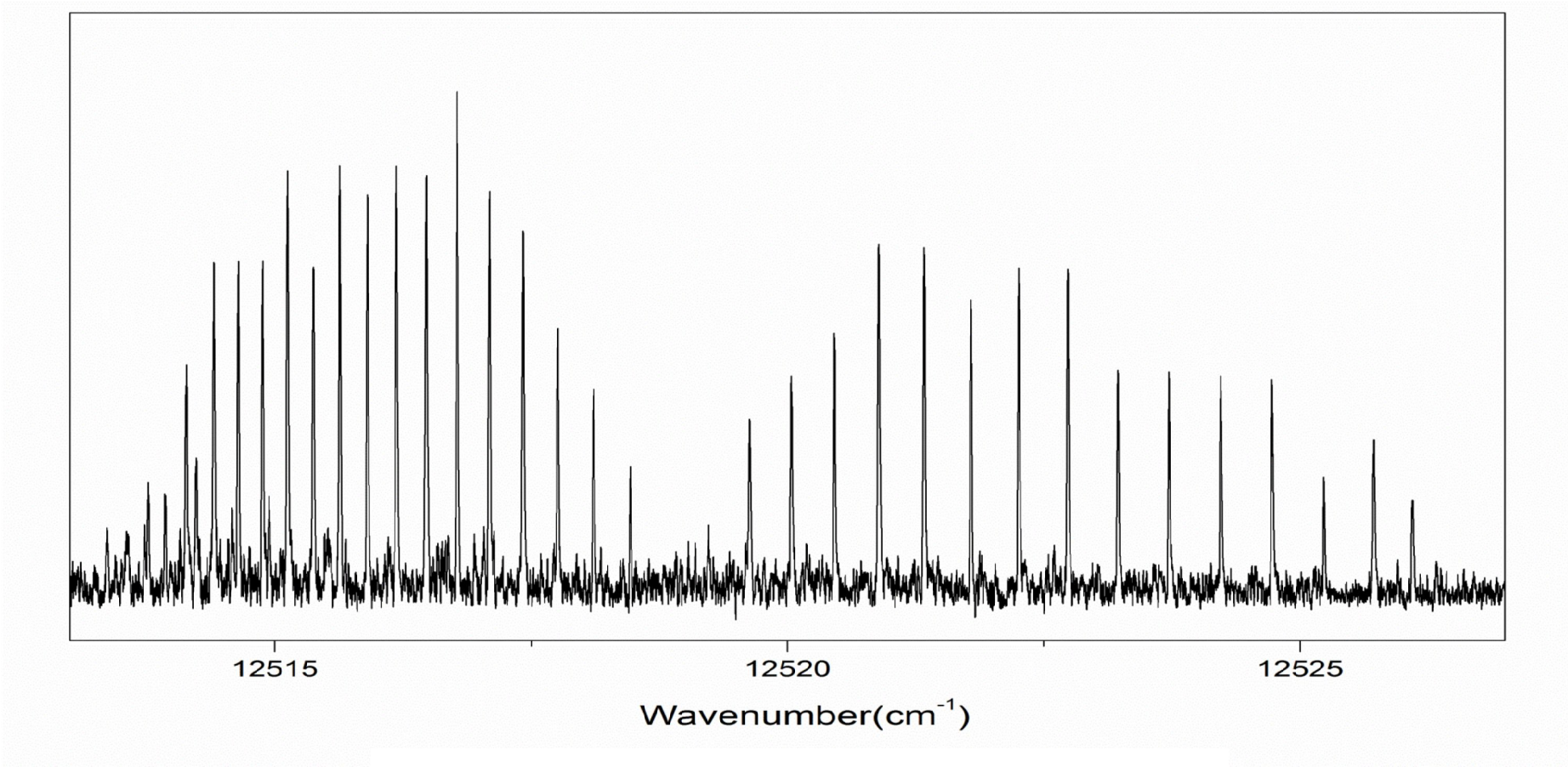

Fig. 3.11 The (4, 3) band of the $[11.9]^1\Sigma^+$- $X^1\Sigma^+$ transition of ScP

In the initial analysis, least-squares fittings were performed for each individual band using the standard formula

$$\nu = T_0 + B'_{v'}J'(J'+1) - D'_{v'}[J'(J'+1)]^2 - B''_{v''}J''(J''+1) + D''_{v''}[J''(J''+1)]^2$$

to obtain the corresponding vibronic energy ν, the rotational constant B' and centrifugal distortion constant D' in the upper state, and the rotational constant B'' and centrifugal distortion constant D'' in the lower state, respectively. Based on these initial fits and the wavelength-resolved fluorescence spectrum, the energies of vibronic states observed are shown schematically in Fig.3.12. Most bands with common levels exhibit constants within experimental error except that the fitting of (3, 2) and (3, 3) bands gave quite different B's for the v = 3 level in the upper Σ^+ state. This inconsistency may be due to possible perturbation in some rovibronic states. Furthermore, negative D' values were obtained for the (3, 3) and (4, 3) bands while a positive value was obtained for the (3, 2) band. Since D's are very small constants, they are easily affected by the fitting formula as well as the sets of transitions used in the fit. In order to remove these inconsistencies, we set $D_3 = D_4 = 0$ and included only transitions with J < 11 for the (4, 3), (3, 2) and (3, 3) bands in the fit so that the effect of centrifugation distortion on rotational energy was within the experimental uncertainty. A simultaneous fit of all observed bands in which common levels sharing the same set of constants was then performed to obtain a unique set of spectroscopic parameters for all observed vibronic levels. As shown in Table 3.1, these constants exhibited much better consistency with an overall uncertainty of 0.0014 cm^{-1} for the fit, which is on the order of the uncertainty in frequency calibration. The list of

measured transitions is given in Appendix.

The structural parameters at equilibrium configuration were then derived according to standard formula and listed in Table 3.2. The equilibrium bond length in the ground electronic state is found to be 2.1995 Å, which is slightly longer than the corresponding parameter of 2.1590 Å in the excited state, consistent with the preliminary analysis discussed above. Compared to the predictions by Daoudi *et al* [73], our values are also in qualitative agreement. Using the Kratzer relationship, the D_e constants were estimated to be ~ 1×10^{-7} cm^{-1}, which is on the same order as the experimental *D* values obtained in the fitting. Since the *D* constants are much smaller than the *B* constants, it is difficult to accurately determine their values in our experiments due to the absence of transitions with high J.

For heavy molecules such as ScP, the rotational constants in different vibrational states are expected to vary according to

$$B_v = B_e - \alpha_e(v + 1/2)$$

Nevertheless, it was found that *B* constants for different v levels in the upper electronic state decrease nonlinearly with increasing v, as shown in Table 3.1. These observations confirm the presence of perturbation in the v = 3 and 4 levels of the excited $^1\Sigma^+$ state to give rise to smaller *B* values. The nature of the perturbation is not clear from our observations but it appears to have the same effect on all rotational levels in each perturbed vibrational state to yield smaller rotational constants.

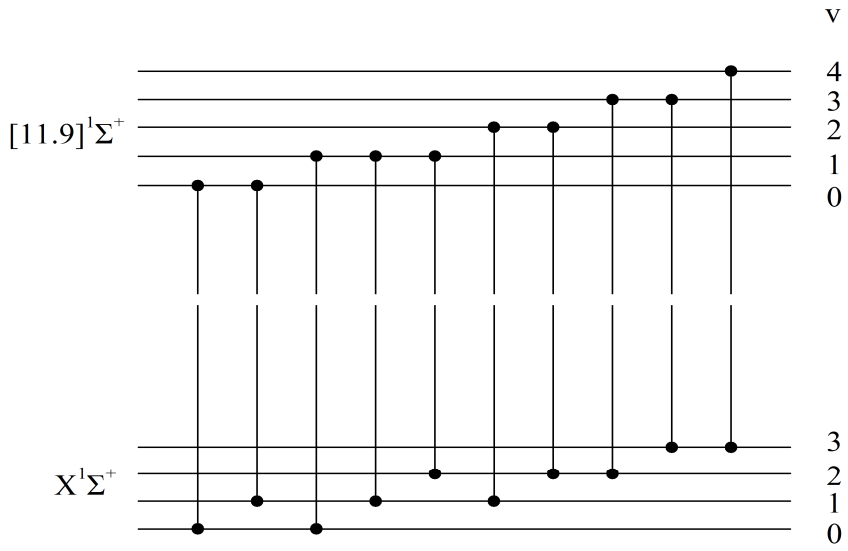

Fig. 3.12 The observed vibronic transitions of ScP

Table 3.1 Molecular constants for the $[11.9]^1\Sigma^+$ and $X^1\Sigma^+$ states of ScP (cm^{-1}).[a]

State	v	T_v	ΔT_v[c] (obs. –cal.)	B_v	ΔB_v[c] (obs. –cal.)
$[11.9]^1\Sigma^+$	4	13981.0764(8)	0.0314	0.19278(1)	-3.8E-4
	3	13476.5692(6)	0.6542	0.193510(9)	-5.5E-4
	2	12966.7891(4)	0.0321	0.194980(7)	2E-5
	1	12453.6151(3)	0.0441	0.195822(7)	-3.8E-5
	0	11936.3931(3)	0.0361	0.196783(7)	2.3E-5
$X^1\Sigma^+$	3	1462.2321(7)	0.0003	0.18691(1)	-1.3E-5
	2	978.5516(4)	0.0004	0.187826(7)	2.1E-5
	1	491.1415(3)	0.0003	0.188684(7)	-3E-6
	0	0	0	0.189565(7)	-4E-6
No. of lines			371		
RMS error			0.00141		

[a] Numbers in parentheses are one standard deviation (in unit of the last figure).
[b] Set to zero. Please refer to text for details.
[c] T_v(calc.) and B_v(calc.) values are calculated using equilibrium constants in Table 3.2.

Table 3.2 Equilibrium molecular constants for the $[11.9]^1\Sigma^+$ and $X^1\Sigma^+$ states of ScP (cm^{-1}).[a]

State	Parameter	This work	Theoretical[b]	
			DFT (B-P86)	CIPSI
$[11.9]^1\Sigma^+$	T_e	11923.209(7)	10581.9	13832.3
	ω_e	521.242(9)	542.4	503.1
	$\omega_e\chi_e$	2.014(2)	1.54	2.25
	B_e	0.19721(4)[c]	0.1966	0.1931
	$10^4\alpha_e$	0.00090(3)[c]	0.000769	0.001075
	r_e (Å)	2.1590	2.162	2.181
$X^1\Sigma^+$	ω_e	494.8716(6)	521.6	441.0
	$\omega_e\chi_e$	1.8652(2)	1.55	1.66
	B_e	0.19001(1)	0.1915	0.1806
	$10^4\alpha_e$	0.000882(7)	0.000777	0.000907
	r_e (Å)	2.1995	2.191	2.256

[a] Numbers in parentheses are one standard deviation (in unit of the last figure).
[b] Ref.[73].
[c] Derived from $v = 0$, 1, and 2 levels.

III.3. Discussion

This work provides, for the first time, accurate structural parameters of ScP that serve as ultimate tests for high level calculations. As shown in Table 3.2, the structural parameters of the two $^1\Sigma^+$ states predicted by Daoudi *et al.* [73] are only in qualitative agreement with those obtained in this work. The significant discrepancy between experimental and predicted values reflects inadequate accuracy of theoretical calculations in handling electron correlations in this system. Parameters predicted by B-P86 method appear to give a better quantitative agreement with our observations. In the case of ScN, however, the CIPSI gives better predictions overall [73]. Based on studies of these two systems, it is not conclusive which computation method will give

a more reliable prediction.

To date, a number of low-lying excited states including the $^3\Sigma^+$, $^1\Pi$, and $^3\Pi$ states by Daoudi *et al.* [73] and $^3\Phi$, $^5\Delta$, and $^5\Pi$ states have been predicted by Tong *et al.* [76]. As expected, theoretical calculations of the energies of these states are far from satisfactory because of the effect of electronic correlation. Any observation of the transitions between these states will provide the crucial information to determine their order in energy. According to Daoudi *et al.* [73], the $^1\Pi$ state is around 5000 cm^{-1} above the ground state and the $^1\Pi - {}^1\Sigma^+$ transition can be studied using infrared spectroscopy. On the other hand, the lowest state in the triplet manifold, $^3\Pi$, is about 4000 cm^{-1} above the ground state. It may need a much higher electronic temperature to significantly populate this state for LIF measurements. Experiments along this line are underway.

With the structural parameters of ScP determined for the first time, it is interesting to compare them with the extensively studied isovalent species ScN and YN [77-80]. Table 3.3 lists the parameters of these species obtained in experiments. It is seen that the parameters for ScN and YN are quite similar with YN appearing to have weaker binding due to greater metal atom. This is expected from the periodic properties down the group. On the other hand, ScP exhibits drastically different structural parameters compared to ScN. First of all, the energy difference between the two $^1\Sigma^+$ states of ScP is quite a bit higher compared to ScN. According to the

calculations by Daoudi *et al.* [73], this phenomenon was ascribed to more antibonding nature in the excited $^1\Sigma^+$ state of ScP. This proposition is further supported by the lower harmonic frequency of ScP in the excited $^1\Sigma^+$ state. Together with the bond length issue discussed earlier, it appears that changing from N to P atoms would have significant effect on the electronic structure and binding of the systems. In the case of scandium monohalides, in which the corresponding $^1\Sigma^+ - X^1\Sigma^+$ electronic transition reduces in energy smoothly from ScF to ScBr, and then increases again for ScI. This trend was interpreted by the ionic nature for Sc-F, Sc-Cl, and Sc-Br bonds but covalent nature for Sc-I band [81]. The great change of structural properties from ScN to ScP may also reflect the change from ionic to covalent nature going from ScN to ScP. Spectroscopic studies of other low-lying state will no doubt shed some light on understanding the bonding of these systems. It will also be interesting to compare the structrural properties with isovalent species YP, whose spectrum has recently been observed in our laboratory for the first time [82].

Table 3.3 Molecular constants for the low-lying singlet states of ScN, YN, and ScP (cm^{-1}).

State	Parameter	ScN[a]	YN[b]	ScP
Excited $^1\Sigma^+$	T_e	5695	3700	11923.20
	ω_e	1044.8	1007.4	521.242
	r_e (Å)	1.695	1.814	2.1590
$a^3\Sigma^+$	T_e	3961	2413	
	ω_e	888	805.12	
	r_e (Å)	1.747		
$X^1\Sigma^+$	ω_e	787.7	633.2	494.871
	r_e (Å)	1.687	1.804[d]	2.1995

[a] Ref. [70]
[b] Ref. [81]

It is a common practice to use molecular orbital approximation (based on products of single electron wavefunctions) to discuss the bonding, electronic structure, and spectroscopic constants of simple molecules. In the case of ScP, one may consider that the molecular orbitals are formally derived from the $3d_{Sc}$, $4s_{Sc}$, $3s_P$, and $3p_P$ atomic orbitals. The qualitative interaction scheme of these orbitals is shown in Fig. 3.13. In the figure we only label the molecular orbitals that are relevant to chemical bonding. As shown in the figure, the core-like 1σ orbital is primarily correlated to the $3s_P$ orbital. The bonding 2σ and degenerate 1π orbitals are primarily formed by the combinations of the $3d_{Sc}$, $4s_{Sc}$ and $3p_P$ orbitals. In addition, molecular orbitals 3σ, 1δ, 2π and 4σ are also formed. The 2π and 4σ orbitals are primarily antibonding with energies higher than the energies of its constituent orbitals. The 3σ and 1δ orbitals are often considered primarily nonbonding as their energies are close to one of the atomic

orbitals.

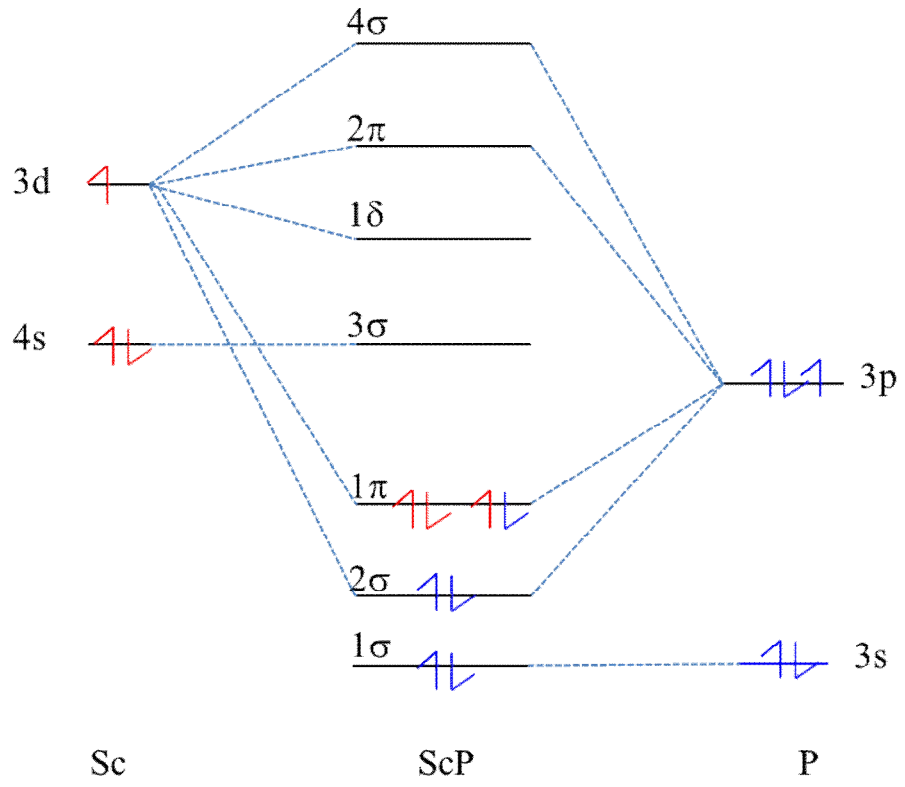

Fig. 3.13 Qualitative molecular orbital (MO) energy level diagram of ScP

Based on this scheme, the ground electronic state of ScP is predicted to have $^1\Sigma^+$ symmetry with the 1σ, 2σ and 1π orbitals full-filled with the configuration $1\sigma^2 1\pi^4 2\sigma^2$. By promoting an electron from 2σ to 3σ forming electronic configuration $1\sigma^2 1\pi^4 2\sigma^1 3\sigma^1$, either $^1\Sigma^+$ or $^3\Sigma^+$ low-lying state is formed depending on the two unpaired σ electrons being parallel spin or anti-parallel spin. Similarly, by promoting an electron from the 1π to 3σ, one obtains the $^1\Pi$ and $^3\Pi$ states. According to qualitative bonding theory, the close-shell $1\sigma^2 1\pi^4 2\sigma^2$ configuration with a bond order

of 3 is expected to be the ground $^1\Sigma^+$ state while the open-shell zero-spin $1\sigma^2 1\pi^4 2\sigma^1 3\sigma^1$ configuration (i.e. the $^1\Sigma^+$ state) with a bond order of 2.5 is expected to be the excited $^1\Sigma^+$ state with higher energy. In the case of ScN, the bonding theory was in qualitative agreement with the experimental observations. Based on the spectrum of the $A^1\Sigma^+ - X^1\Sigma^+$ transition in the 1.7 μm region, the bond length (derived from the observed rotational constant) in the upper state was found to be slightly longer than that in the ground state, in qualitative agreement with the bond order considerations. On the other hand, the two corresponding $^1\Sigma^+$ states of ScP exhibit structural properties that cannot be predicted using simple bonding theory. For instance, the ground state bond length was observed to be slightly longer by ~0.05 Å compared to the excited $^1\Sigma^+$ state. This observation undoubtedly implies a higher bond order in the excited state, opposite to the bonding theory. More importantly, both states exhibit similar harmonic vibrational frequencies. These phenomena imply that the electronic potential surfaces of these two states are remarkably similar but significantly different from neither formal electronic configuration that may not be a good description of the electronic states for ScP. As pointed out by Daoudi *et al.* [73] in their calculations, the dominant formal configuration contributes no more than 89% to the CI wave function and hence states of ScP cannot properly described by single determinant wavefunctions as shown above in simple MO theory. Several formal electronic configurations are therefore expected to contribute to each of the two $^1\Sigma^+$ states observed in this work.

In summary, spectrum of ScP has been observed for the first time using LIF in

the near infrared region. Based on the spectral pattern and theoretical prediction, it was assigned to the $[11.9]^1\Sigma^+ - X^1\Sigma^+$ electronic transition. The corresponding spectroscopic constants were determined using least-squares fitting. It was found that the bond length in the ground state is slightly longer than that in the excited state.

Chapter IV

Laser Induced Fluorescence Spectroscopy of ScBr and ScI

Scandium monohalides, like ScN and ScP, are ideal systems for investigating the effects of *d* electrons in chemical bonding. To date, numerous studies of scandium monohalides, including ScF [25-31], ScCl [31-39], ScBr [40-46], and ScI [47-53], have been reported because of the simplicity in their bonding scheme. According to simple molecular orbital approximation shown below, the bonding scheme of scandium monohalides is expected to be similar to ScN and ScP. As discussed in the previous chapter, the electron correlation among the valence electrons will greatly affect the energy of electronic state, the extra electrons in halide systems will undoubtedly make the situation more complex. In this chapter, our spectroscopic study of ScBr and ScI will be presented. The structural properties of these molecules will also be discussed.

IV.1. Laser induced fluorescence spectroscopy of ScBr

IV.1.1. Background

While most scandium monohalides have been extensively investigated, only a handful of spectroscopic studies of ScBr have been reported before our work. The first spectrum of ScBr was observed by Fischell *et al.* in 1980 using laser induced

fluorescence (LIF) spectroscopy in the visible region [40]. On the basis of the observed low resolution spectrum, the ground electronic state was determined to be $^1\Sigma^+$ symmetry while the excited states involved were undetermined. The pure rotational transitions of ScBr in the ground state were observed by Lin *et al.* using Fourier transform microwave spectroscopy [42]. The ground state molecular constants were thus determined with high accuracy based on the observed transitions. Electronic properties of ScBr have also been predicted using high-level ab initio calculations. Langhoff *et al.* was the first to predict the spectroscopic constants for the two lowest states, the $X^1\Sigma^+$ and $a^3\Delta$ states, using complete active space self-consistent field (CASSCF) method and multireference configuration interaction (MRCI) calculations [41]. Korek and Hamdan predicted properties of 23 low-lying electronic states of ScBr using similar level of computation theory [43]. Based on this prediction, we set out to study the electronic transitions of ScBr using laser induced fluorescence. This work was carried out with Dr. Y. Xia in a collaboration of our laboratory with the group of Professor Allan S.C. Cheung of The University of Hong Kong. Applying the same experimental technique as discussed in Chapter 2, three band systems, namely the $C^1\Sigma^+ - X^1\Sigma^+$ system, the $e^3\Delta - a^3\Delta$ system, and the $d^3\Phi - a^3\Delta$ system have been observed. Since the detail results and analysis of this study has been given elsewhere [44-46], we will only give a brief description here.

IV.1.2. Experimental conditions

The conditions for producing ScBr are very similar to ScP except that the precursor gas mixture used for reacting with the Sc atoms was different. Instead of using 0.5% PH_3 in Ar, we used a mixture of 2% of C_2H_5Br in Ar. As usual, the total stagnant pressure of 8 atm was used.

IV.1.3. Observations and Results

(a) The $C^1\Sigma^+ - X^1\Sigma^+$ system

The $C^1\Sigma^+ - X^1\Sigma^+$ system was observed in the region 11500 to 12800 cm^{-1}. Six vibronic bands observed at 11570, 11667, 11905, 11955, 12242 and 12527 cm^{-1} were assigned to the (2, 2), (0, 0), (2, 1), (1, 0), (2, 0) and (3, 0) bands, respectively. Both isotopic species $Sc^{79}Br$ and $Sc^{81}Br$ were observed for each band. Fig.4.1 shows the spectrum of the (3, 0) band, in which the presence of P and R branches with the absence of Q branch confirmed the $\Sigma - \Sigma$ type transition. These bands were fitted simultaneously using the typical diatomic Hamiltonian

$$\nu = T_0 + B'_{v'}J'(J'+1) - D'_{v'}[J'(J'+1)]^2 - B''_{v''}J''(J''+1) + D''_{v''}[J''(J''+1)]^2$$

to give a unique set of spectroscopic constants as listed in Table 4.1. The constants for the v = 0 and v = 1 levels in the $X^1\Sigma^+$ state were fixed to the much more accurate literature values from microwave studies. The corresponding constants at equilibrium configuration are listed in Table 4.2.

(b) The $e^3\Delta - a^3\Delta$ system

The $e^3\Delta - a^3\Delta$ system was observed in the region 11500 to 12800 cm^{-1}. Five vibronic bands with band heads at 12214, 12486, 12753, 12186 and 11887 cm^{-1} respectively have been assigned to the (0, 0), (1, 0), (2, 0), (1, 1) and (1, 2) bands. For the (0, 0) band, all three subbands corresponding to the $e^3\Delta_1 - a^3\Delta_1$, $e^3\Delta_2 - a^3\Delta_2$, $e^3\Delta_3 - a^3\Delta_3$ transitions were observed. For the other bands, however, only the $e^3\Delta_1 - a^3\Delta_1$, $e^3\Delta_2 - a^3\Delta_2$ transitions were observed. All the observed bands were shown schematically in Fig. 4.2. Similar to the case of the $C^1\Sigma^+ - X^1\Sigma^+$ system, both isotopomers due to bromine were observed as shown in Fig. 4.3. The observed transitions for each band were fitted simultaneously to the standard Hamiltonian

$$\nu = T_0 + B'_{v'}J'(J'+1) - D'_{v'}[J'(J'+1)]^2 - B''_{v''}J''(J''+1) + D''_{v''}[J''(J''+1)]^2$$

to obtain the unique set of molecular constants shown in Table 4.3. The structural parameters at equilibrium configuration were then derived according to standard formula and listed in Table 4.4. The effect of spin-orbit interactions on the three substates with different Ω was estimated. Using the Eq.

$$A = 2B^2/(B_{eff}(\Omega=3) - B_{eff}(\Omega=1))$$

the spin-orbit coupling constant A was estimated to be 28.5 cm^{-1} for the $a^3\Delta$ state, suggesting that a triplet appearance for the three substates. Using this estimated value, the spin-orbit coupling for the $e^3\Delta$ state was determined based on the parameters from the three (0, 0) subbands corresponding to different Ω and the Eq.

$$\hat{H}_{eff} = B\hat{R}^2 - D\hat{R}^4 + A\hat{L}_z\hat{S}_z + \frac{2}{3}\lambda\left(3\hat{S}_z^2 - \hat{S}^2\right) + \gamma\left(\hat{J} - \hat{S}\right)\cdot\hat{S}$$

where *B* and *D* are respectively the rotational constant and its centrifugal distortion; A is the spin-orbit constant, and λ is the spin-spin constant for the second-order spin-orbit interactions; γ is the spin-rotation constant. Matrix elements for the Hamiltonian can be found in Brown *et al* [83] and Balfour *et al* [84]. Table 4.5 lists the spin interactions parameters for both $e^3\Delta$ and $a^3\Delta$ states. The detailed analysis of this band can be found elsewhere [45, 46].

c. The $d^3\Phi - a^3\Delta$ system

Two vibronic bands corresponding to $d^3\Phi_2 - a^3\Delta_1$ transition have been observed at 11793 and 12063 cm^{-1}, respectively, as shown in Fig.4.5. Like the case of the $e^3\Delta - a^3\Delta$ system low J rotational lines were broadened by the unresolved hyperfine splitting. The observed transitions were fitted using the standard formula to obtain the spectroscopic parameters shown in Table 4.4. These constants are in excellent agreement with the predicted values [43].

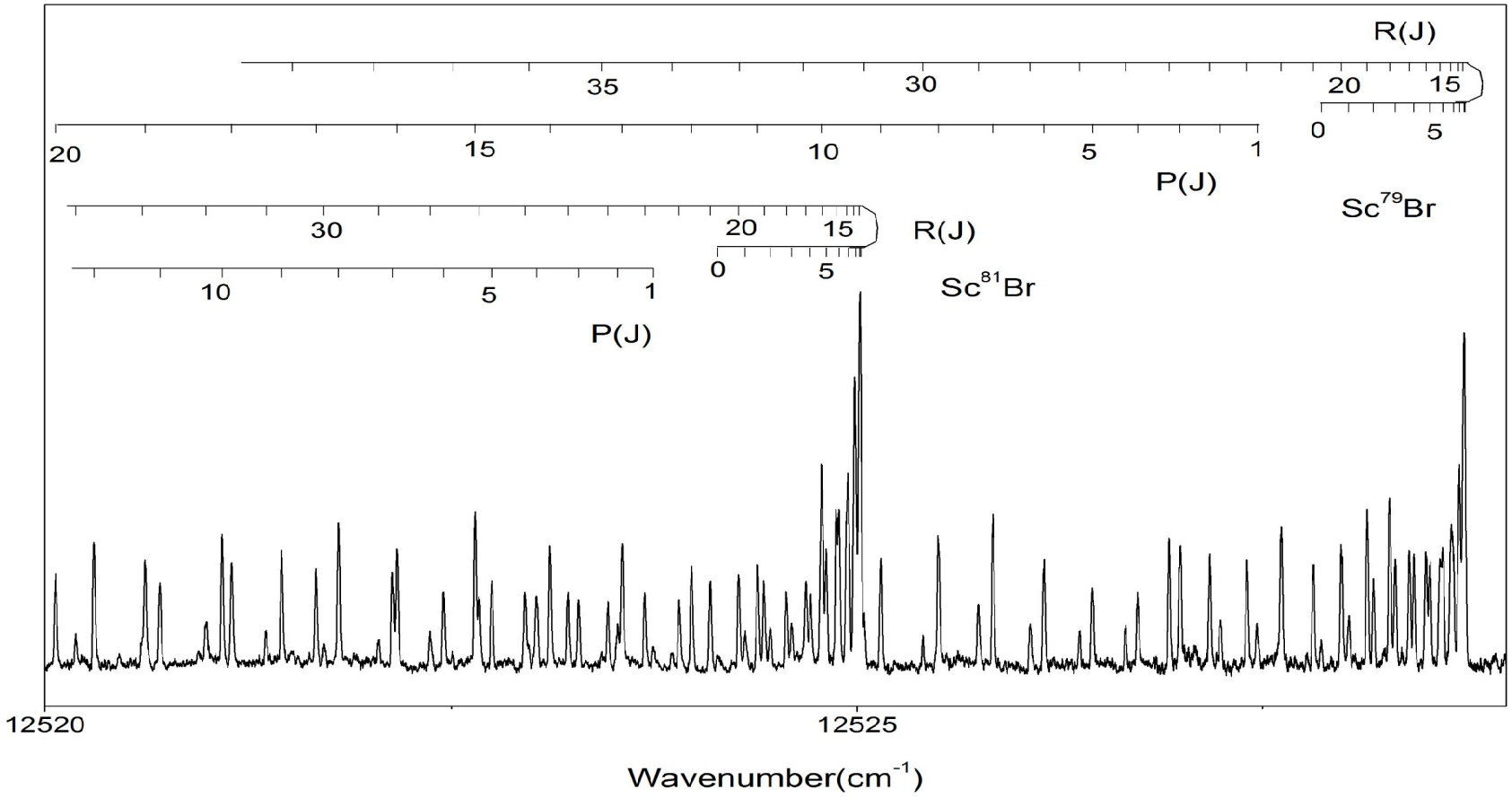

Fig. 4.1 The (3, 0) band of the $C^1\Sigma^+ - X^1\Sigma^+$ transition of ScBr

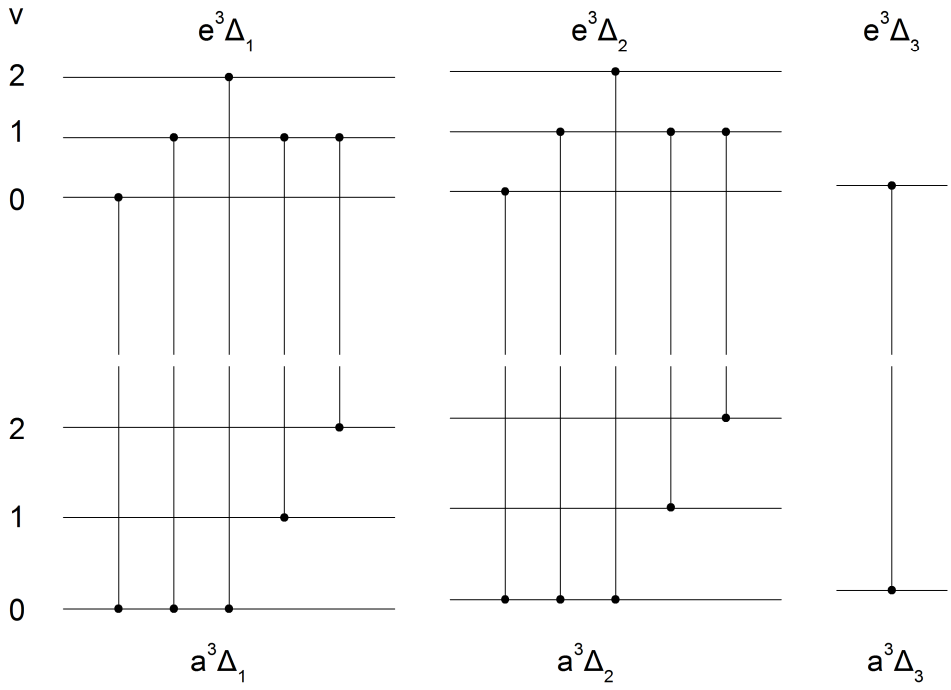

Fig. 4.2 Observed vibronic transitions of $e^3\Delta - a^3\Delta$ transition of ScBr

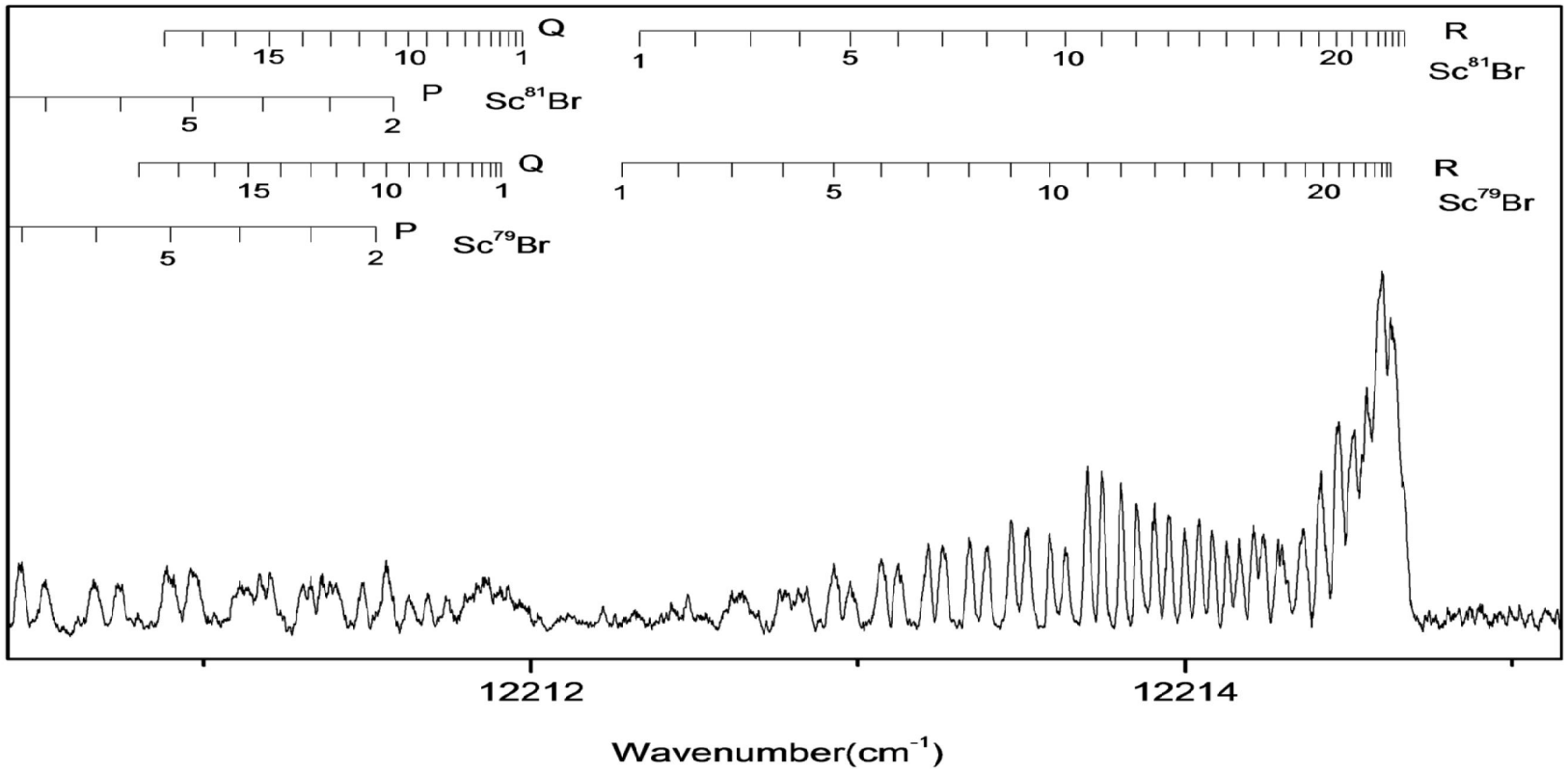

Fig. 4.3 The (0, 0) band of the $e^3\Delta_1$ - $a^3\Delta_1$ transition of ScBr

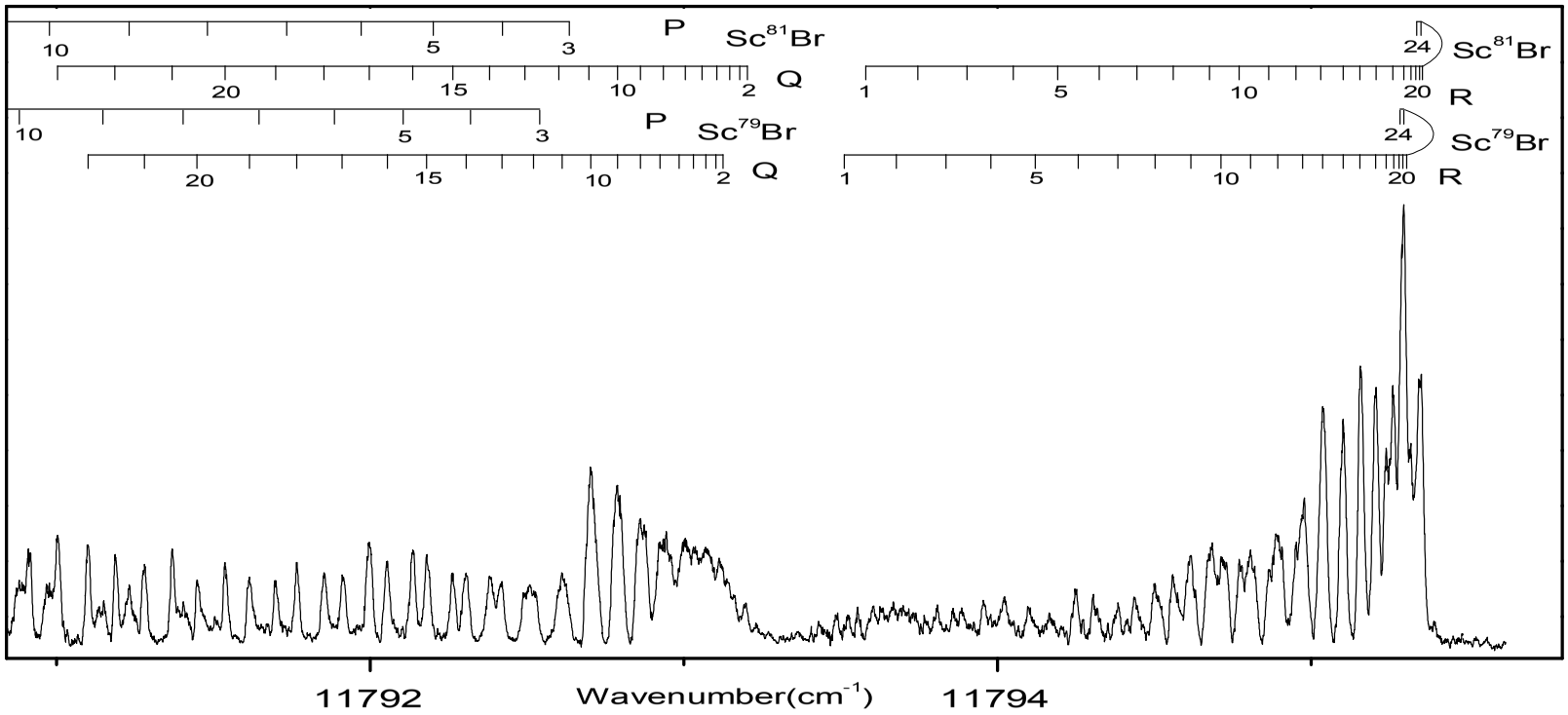

Fig. 4.4 The (0, 0) band of the $d^3\Phi_2$ - $a^3\Delta_1$ transition of ScBr

Table 4.1 Molecular constants for the $C^1\Sigma^+$ and $X^1\Sigma^+$ states of ScBr (cm^{-1}).[a]

State	Parameter	$Sc^{79}Br$	$Sc^{81}Br$
$C^1\Sigma^+$	T_3	12527.6710(3)	12523.9583(4)
	B_3	0.094509(1)	0.093668(2)
	10^7D_3	0.42(1)	0.41(2)
	T_2	12242.4269(3)	12239.9754(3)
	B_2	0.094900(1)	0.094055(1)
	10^7D_2	0.43(1)	0.44(1)
	T_1	11955.6839(2)	11954.5069(3)
	B_1	0.095296(1)	0.094441(2)
	10^7D_1	0.45(1)	0.42(3)
	T_0	11667.4421(3)	11667.5515(3)
	B_0	0.095678(1)	0.094825(1)
	10^7D_0	0.387(8)	0.414(9)
$X^1\Sigma^+$	T_2	672.196(4)	669.207(5)
	B_2	0.102767(3)	0. 101840(4)
	10^7D_2	0.49(6)	0.42(6)
	T_1	337.135(3)	335.631(3)
	B_1	0.10319109 [b]	0.10226940
	10^7D_1	0.381 [b]	0.389
	B_0	0.10362137 [b]	0.10269389
	10^7D_0	0.390 [b]	0.386

[a] Numbers in parentheses are one standard deviation (in unit of the last figure).

[b] Constants for the v= 0 and 1 levels of the $X^1\Sigma^+$ state from Ref.[42]

Table 4.2 Equilibrium molecular constants for the $C^1\Sigma^+$ and $X^1\Sigma^+$ states of ScBr (cm^{-1}).[a]

State	Parameter	$Sc^{79}Br$	$Sc^{81}Br$	Theoretical[b]	Experimental[c]
$X^1\Sigma^+$	T_e	0.0	0.0	0.0	0.0
	ω_e	339.209	337.686	343.7	338.8
	$\omega_e\chi_e$	1.037	1.028		1.099
	B_e	0.10385	0.10295	0.10186	0.10384
	$10^4\alpha_e$	4.50	4.48		4.30
	r_e (Å)	2.3806	2.3806	2.3985	2.3806
$C^1\Sigma^+$	T_e	11692.105(1)	11692.104(1)	12113	
	ω_e	289.740(1)	288.439(3)	297.7	
	$\omega_e\chi_e$	0.750(2)	0.743(1)		
	B_e	0.09588(1)	0.09502(1)	0.09392	
	$10^4\alpha_e$	3.91(2)	3.87(2)		
	r_e (Å)	2.4776	2.4776	2.4979	

[a] Numbers in parentheses are one standard deviation (in unit of the last figure).
[b] Ref.[43].
[c] Ref.[42].

Table 4.3 Band origins and B_{eff} values for the $a^3\Delta$, $d^3\Phi$ and $e^3\Delta$ states of ScBr (cm^{-1}).[a]

State	v	$Sc^{79}Br$		$Sc^{81}Br$	
		ν_o	B_{eff}	ν_o	B_{eff}
$e^3\Delta_3$	0	12204.156(2)	0.092647(9)	12204.232(2)	0.091958(9)
$e^3\Delta_2$	2	12749.448(1)	0.091463(8)	12747.111(1)	0.090657(9)
	1	12479.430(1)	0.091942(7)	12478.283(1)	0.091130(8)
	0	12207.640(1)	0.092410(8)	12207.702(1)	0.091578(9)
$e^3\Delta_1$	2	12753.838(1)	0.091390(7)	12751.512(1)	0.090522(8)
	1	12483.752(1)	0.091775(7)	12482.607(1)	0.090930(8)
	0	12211.915(1)	0.092184(7)	12211.975(1)	0.091334(8)
$d^3\Phi_2$	1	12063.733(1)	0.090957(2)	12062.599(1)	0.090109(1)
	0	11793.153(1)	0.091373(2)	11793.226(1)	0.090519(2)
$a^3\Delta_3$	0	0	0.096073(9)	0	0.095397(9)
$a^3\Delta_2$	2	600.940(1)	0.094976(8)	598.261(1)	0.094142(8)
	1	301.314(1)	0.095358(8)	299.968(1)	0.094515(9)
	0	0	0.095755(8)	0	0.094893(8)
$a^3\Delta_1$	2	600.752(1)	0.094653(8)	598.076(1)	0.093781(9)
	1	301.225(1)	0.095007(8)	299.859(1)	0.094260(9)
	0	0	0.095429(7)	0	0.094543(8)

[a] Numbers in parentheses are RMS deviation (in unit of the last digit)

Table 4.4 Equilibrium molecular constants for the $a^3\Delta_1$, $a^3\Delta_2$, $d^3\Phi_2$, $e^3\Delta_1$ and $e^3\Delta_2$ states of ScBr (cm^{-1}).[a]

State	Parameters	$Sc^{79}Br$	$Sc^{81}Br$	Theoretical[b]
$e^3\Delta_2$	T_e	12222.3705	12222.3662	13614
	ω_e	273.562	272.334	287.6
	$\omega_e\chi_e$	0.886	0.8765	
	B_e	0.092650(5)	0.09181(1)	0.09152
	$104\alpha_e$	4.73(3)	4.60(7)	
	r_e (Å)	2.5205	2.5208	2.5304
$e^3\Delta_1$	T_e	12226.5892	12226.5566	
	ω_e	273.588	272.359	
	$\omega_e\chi_e$	0.8755	0.8635	
	B_e	0.09238(1)	0.091540(1)	
	$104\alpha_e$	3.97(6)	4.06(1)	
	r_e (Å)	2.5242	2.5246	
	T_o	11793.153	11793.216	13840
	$\Delta G_{1/2}$	270.58	269.373	280.9
$d^3\Phi_2$	B_e	0.091581	0.09073	0.09029
	$104\alpha_e$	4.16	4.10	
	r_e (Å)	2.5351	2.5351	2.5477
$a^3\Delta_2$	T_e	0	0	733
	ω_e	303.002	301.643	305
	$\omega_e\chi_e$	0.844	0.8375	
	B_e	0.095950(7)	0.095080(2)	0.09320
	$104\alpha_e$	3.89(4)	3.75(1)	
	r_e (Å)	2.4767	2.4770	2.5076
$a^3\Delta_1$	T_e	0	0	
	ω_e	302.923	301.501	
	$\omega_e\chi_e$	0.849	0.821	
	B_e	0.09561(3)	0.09477(5)	
	$104\alpha_e$	3.8(1)	3.8(3)	
	r_e (Å)	2.4811	2.4811	

[a] Numbers in parentheses are RMS deviation (in unit of the last digit)
[b] Ref. [43]

Table 4.5 Molecular constants for the $a^3\Delta$ and $e^3\Delta$ states of $Sc^{79}Br$ (cm^{-1}).[a]

Parameter	$a^3\Delta$	$e^3\Delta$
ν_o	0.0	12207.467(9)
B	0.095778(3)	0.092428(2)
$10^{-7}D$	0.77(3)	0.54(3)
A	28.5*	26.9(1)
λ	1.59(5)	1.95(5)
γ	0.371(4)	0.041(6)
RMS	0.003	

[a] Numbers in parentheses are RMS deviation (in unit of the last digit)
*Value fixed in the least-squares fit.

IV.2. Laser induced fluorescence spectroscopy of ScI

IV.2.1. Background

Spectroscopic observation of ScI was first reported by Fischell *et al.* in 1980 using LIF spectroscopy in the visible region [40]. Based on the two low-resolution electronic transitions observed in blue region, it was concluded that the ground electronic state was $X^1\Sigma^+$ symmetry while the two observed upper states lying above the ground state by ~22000 cm^{-1} remained unassigned. Shenyavskaya and coworkers [47, 48] carried out high resolution dispersed fluorescence spectra by the excitation with individual laser lines of argon and krypton ion lasers to observe the $X^1\Sigma^+$, $A^1\Delta$, and $B^1\Pi$ singlet and the $a^3\Delta$, $b^3\Pi$, and $c^3\Sigma^+$ triplet low-lying electronic states. The equilibrium vibrational and rotational constants for the $X^1\Sigma^+$ ground state were reported. Taher *et al.* observed the $B^1\Pi$ – $X^1\Sigma^+$ transition using Fourier transform spectroscopy. Spectroscopic constants were retrieved from the rotationally resolved spectrum for eight vibronic bands [49]. A perturbation between the v = 1 level of the $X^1\Sigma^+$ state and the v = 0 level of the $a^3\Delta$ state at J = 70 was also reported in this work. Following these observations, Bencheikl reported the first computational work to predict many electronic states of ScI using ligand field theory [50]. Reddy *et al.* constructed RKR potential energy curves for the $B^1\Pi$ and $X^1\Sigma^+$ states and calculated the dissociation energy as well as the Franck-Condon factors for the $B^1\Pi$ – $X^1\Sigma^+$ transition [51]. Korek *et al*. predicted 18 low-lying electronic states of ScI using CASSCF and MRCI calculations [52]. Thirteen of these new electronic states were

expected to be in the range of 4500 to 21000 cm^{-1}. Rotationally resolved spectrum of the $D^1\Pi - X^1\Sigma^+$ system has recently been observed by Xia *et al*. using laser induced fluorescence in the visible region [53]. Molecular constants at high accuracy for both $D^1\Pi$ and $X^1\Sigma^+$ states were obtained. A perturbation resulting from the interaction between the v = 2 level of the $X^1\Sigma^+$ state and the v =1 level of the $a^3\Delta_1$ sub-state was observed. The low-lying state $C^1\Sigma^+$, while predicted by Korek *et al*., has yet to be observed. According to the calculation, the $C^1\Sigma^+ - X^1\Sigma^+$ system was expected to lie in the near infrared region that is accessible by our spectrometer. In this Chapter, spectroscopic study of the $C^1\Sigma^+ - X^1\Sigma^+$ system is discussed. In addition, two vibronic bands due to triplet states were also observed. Nevertheless, attempts at searching for other bands of the same system were not successful. Any definite assignment for these bands will no doubt require more experimental pursuits.

IV.2.2. Experimental conditions

The experimental setup for this study was discussed in Chapter II. ScI molecules were produced by reacting high pressure (~8 atm) gas mixture of 1% CH_3I in Ar with Sc atoms produced by laser ablation, followed by free jet expansion to a vacuum of 10^{-5} Torr. The gas jet was then excited by the high resolution Ti:sapphire laser for observing the LIF signals.

IV.2.3. Observations and Results

LIF spectrum of ScI was observed in the region 11500 to 12900 cm^{-1}, as shown in Fig. 4.5. A total of 10 vibronic bands were observed, respectively, at 11754, 11768, 11794, 12021, 12039, 12063, 12290, 12311, 12585 and 12859 cm^{-1}. These bands are illustrated in Fig. 4.6 to 4.15. The absence of *Q* branch in each band together with the observed *P(1)* and *R(0)* as the first lines confirmed the nature of a $^1\Sigma^+ - {}^1\Sigma^+$ transition. Comparing the spectral regions of the bands for other observed transitions of scandium monohalides with those observed in this work, the bands were assigned to the $C^1\Sigma^+ - X^1\Sigma^+$ system of ScI. The vibrational assignment of these bands was made based on the observed wavelength-resolved fluorescence spectrum. The assignment for the $X^1\Sigma^+$ state was straightforward and also confirmed by the rotational constants obtained from the least-squares fitting. The assignment for the $C^1\Sigma^+$ state, however, was not confirmed directly. It was found from the resolved fluorescence spectrum that the band at 12860 cm^{-1} was due to the lowest observed vibrational level in the $C^1\Sigma^+$ state. Attempts at searching for bands with lower v' were unsuccessful. The 12860 cm^{-1} transition band was therefore assigned to be the (0, 0) band of the $C^1\Sigma^+ - X^1\Sigma^+$ transition. Once this assignment was made, other bands were assigned, accordingly, to the (2, 6), (0, 4), (1, 5), (2, 5), (0, 3), (1, 4), (2, 4), (0, 2), (0, 1) and (0, 0) bands of the $C^1\Sigma^+ - X^1\Sigma^+$ system. The schematic energy diagram indicating the observed transitions is shown in Fig. 4.16. It is interesting to note that bands with v" as high as 6 were observed, suggesting that excess energy might be produced from the formation of ScI.

Except for the very weak (0, 0) band, the observed transitions of each band were fitted to the standard Hamiltonian

$$\nu = T_0 + B'_{v'}J'(J'+1) - D'_{v'}[J'(J'+1)]^2 - B''_{v''}J''(J''+1) + D''_{v''}[J''(J''+1)]^2$$

to confirm the assignment. A simultaneous fit with all bands was then performed to obtain a unique set of molecular constants. The constants for vibrational levels with v = 0, 1, and 2 for the $X^1\Sigma^+$ state were fixed to the accurate literature values [51, 53] in the least-squares fit. Table 4.7 lists the molecular constants obtained from the fit that gives an overall root-mean-squares (RMS) error of about 0.0034 cm^{-1}, and Table 4.8 lists the derived equilibrium molecular constants. For the $X^1\Sigma^+$ state, both the vibrational separations and the rotational constants are regular and determined up the v = 6 level. Equilibrium molecular constants determined are ω_e = 277.08(1), $\omega_e\chi_e$ = 0.784(4) and $\omega_e y_e$ = -0.0058(4) cm^{-1}. On the other hand, the molecular constants for the $C^1\Sigma^+$ state exhibit some irregularities as shown in Table 4.7. For instance, the vibrational separations $\Delta G_{1/2}$ and $\Delta G_{3/2}$ were measured to be 295.31 and 226.34 cm^{-1}, respectively, and the *B* value of the v = 0 level was found to be greater than those for neighboring vibrational levels. These irregularities indicate the presence of unseen perturbing state nearby. In addition, a small local perturbation was also observed for the (0, 2) band similar to that observed in the earlier study of the $D^1\Pi - X^1\Sigma^+$ system [53]. The perturbation was identified to be the crossing of the v = 2 level of the $X^1\Sigma^+$ state with the v = 0 level of the $a^3\Delta_1$ state at J = 8.

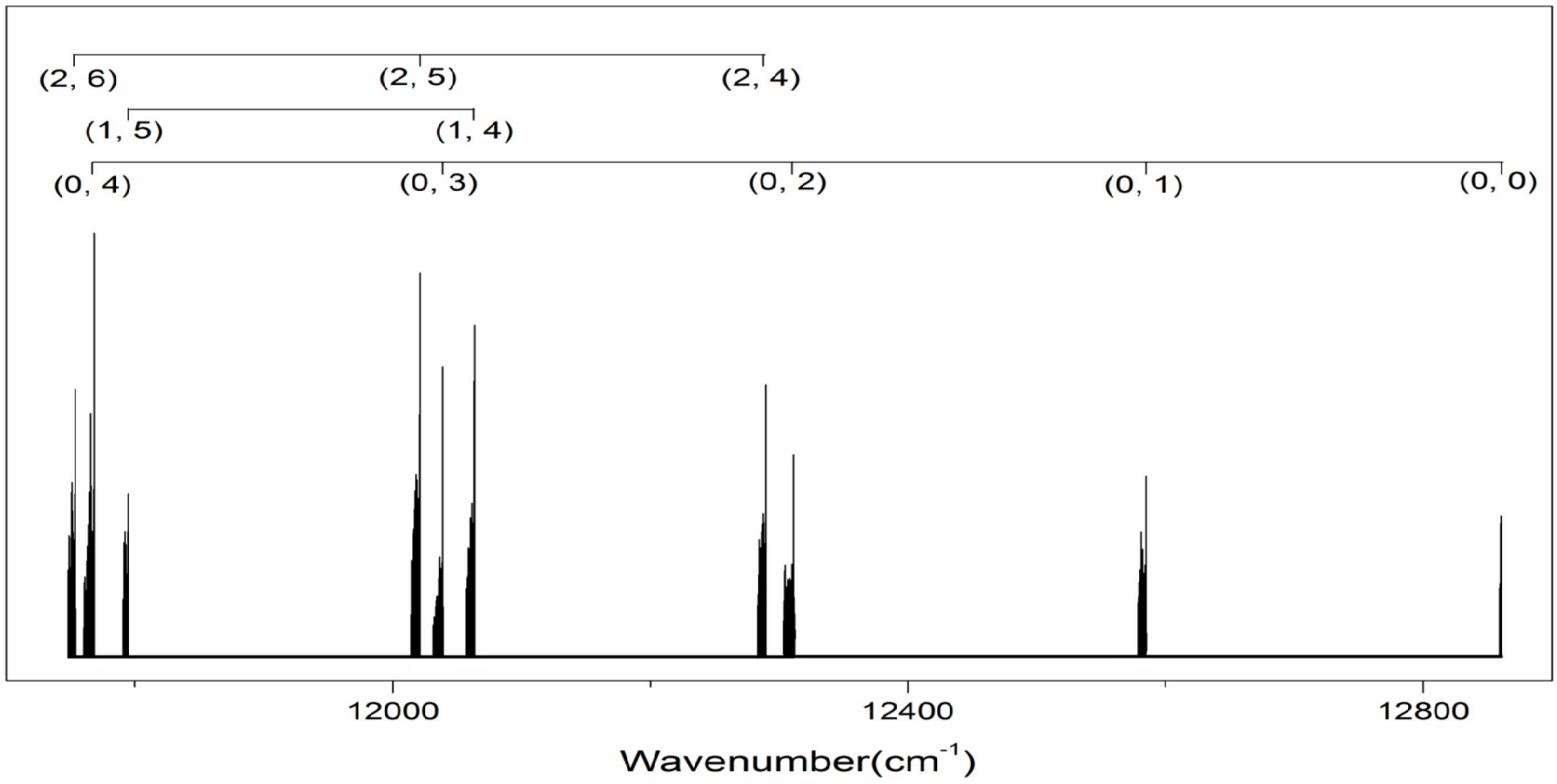

Fig. 4.5 The overall LIF spectrum of the $C^1\Sigma^+$- $X^1\Sigma^+$ transition of ScI

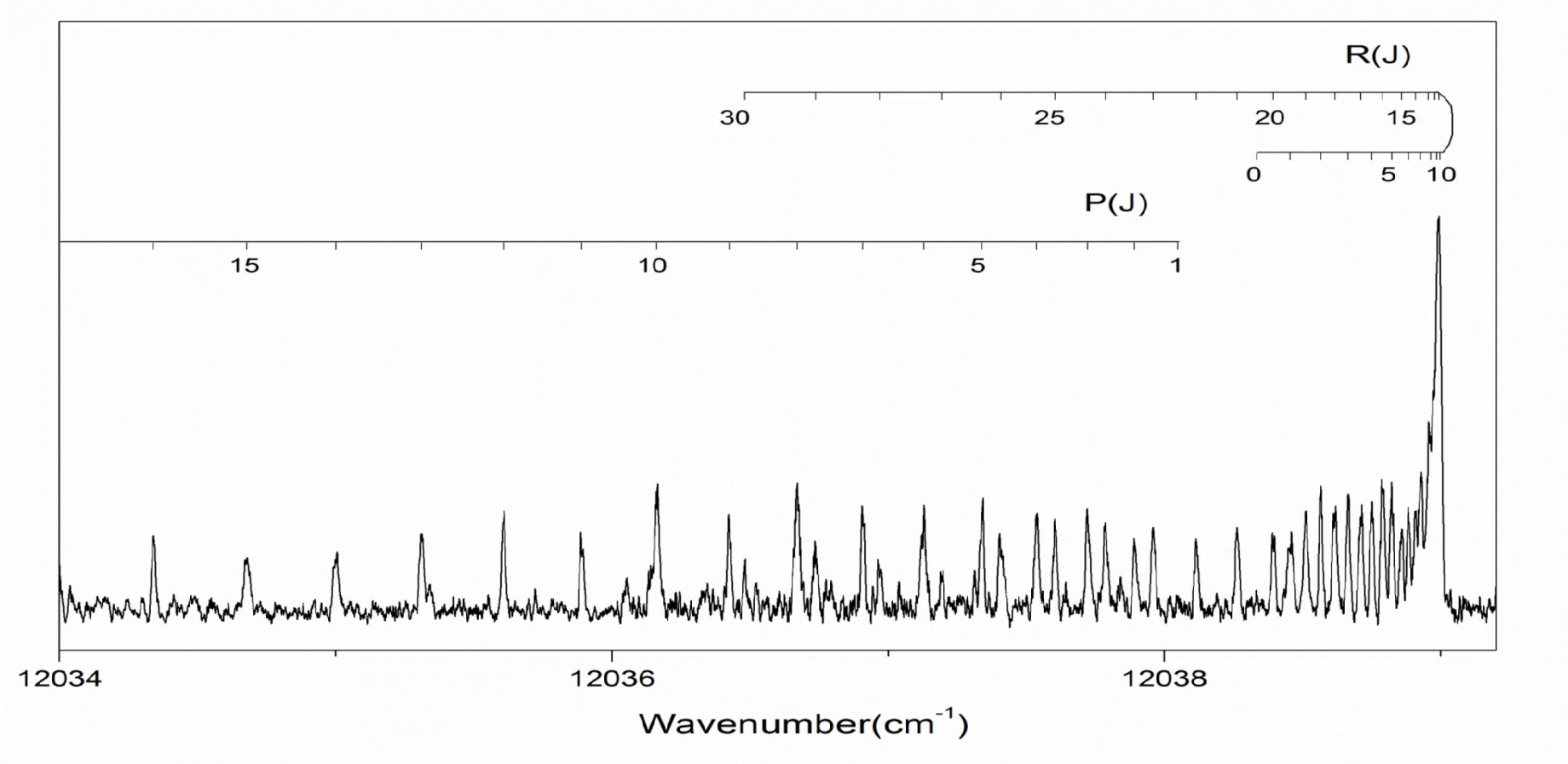

Fig. 4.6 The (0, 3) band of the $C^1\Sigma^+ - X^1\Sigma^+$ transition of ScI

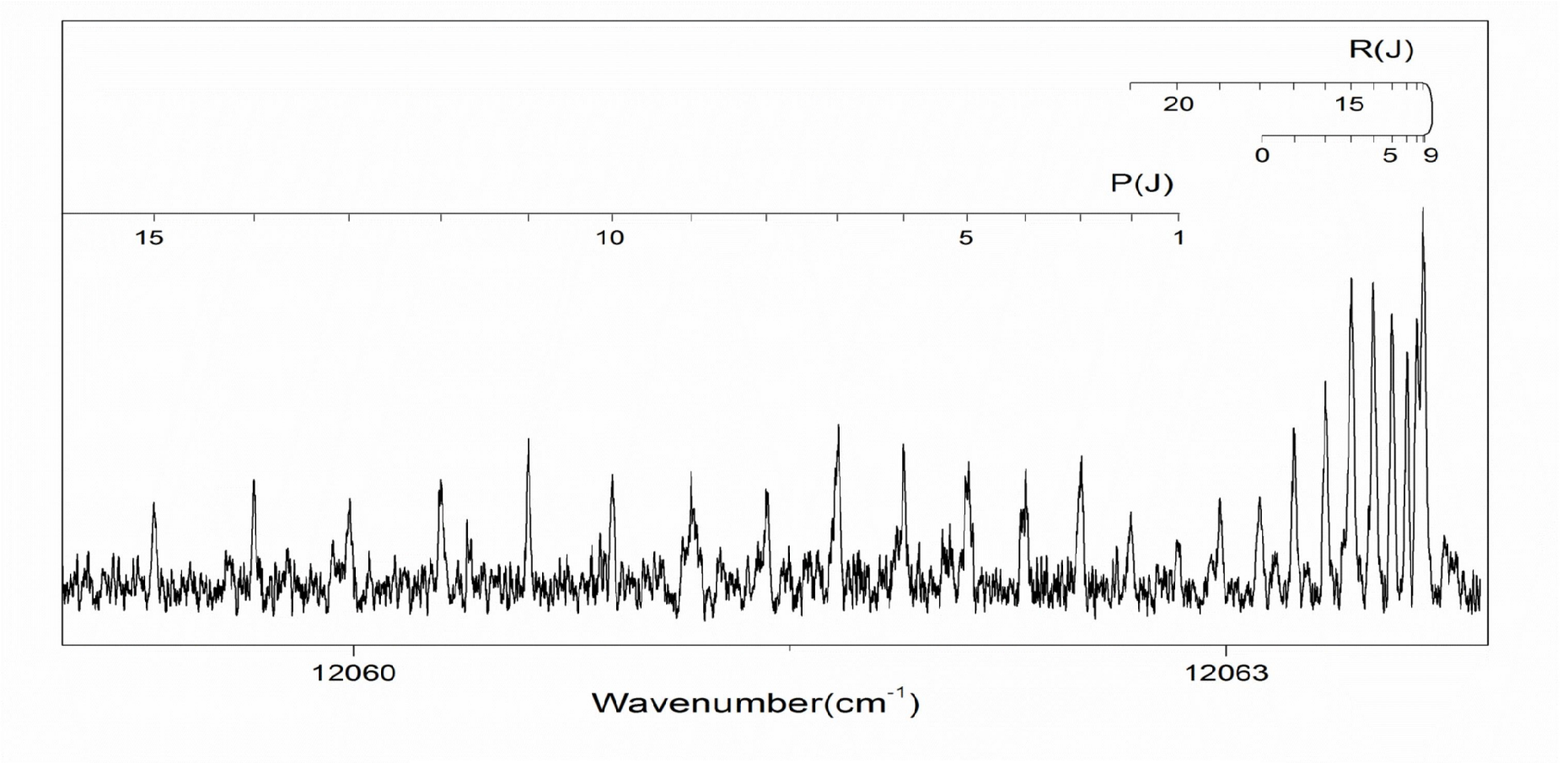

Fig. 4.7 The (1, 4) band of the $C^1\Sigma^+ - X^1\Sigma^+$ transition of ScI

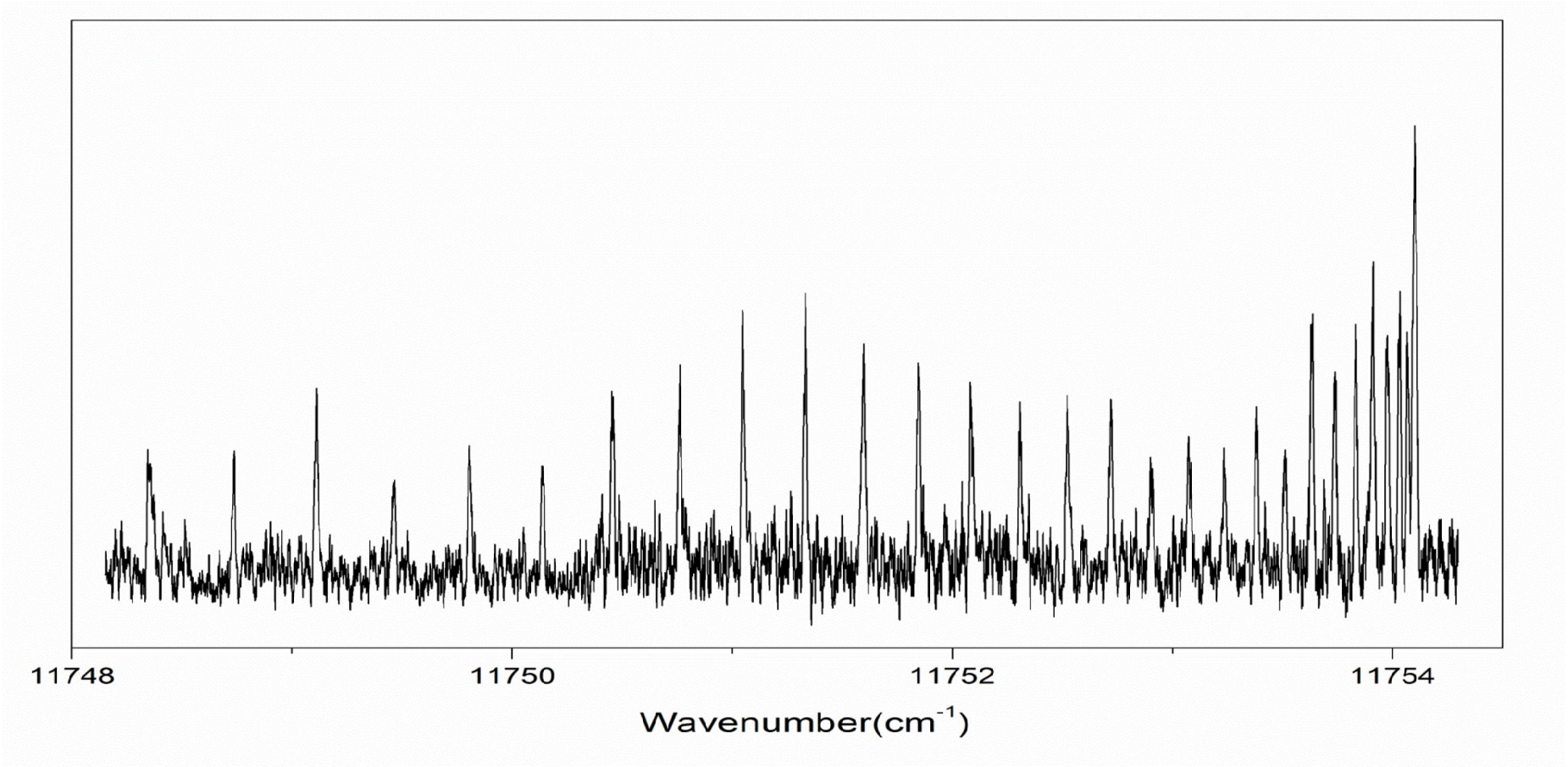

Fig. 4.8 The (2, 6) band of the $C^1\Sigma^+ - X^1\Sigma^+$ transition of ScI

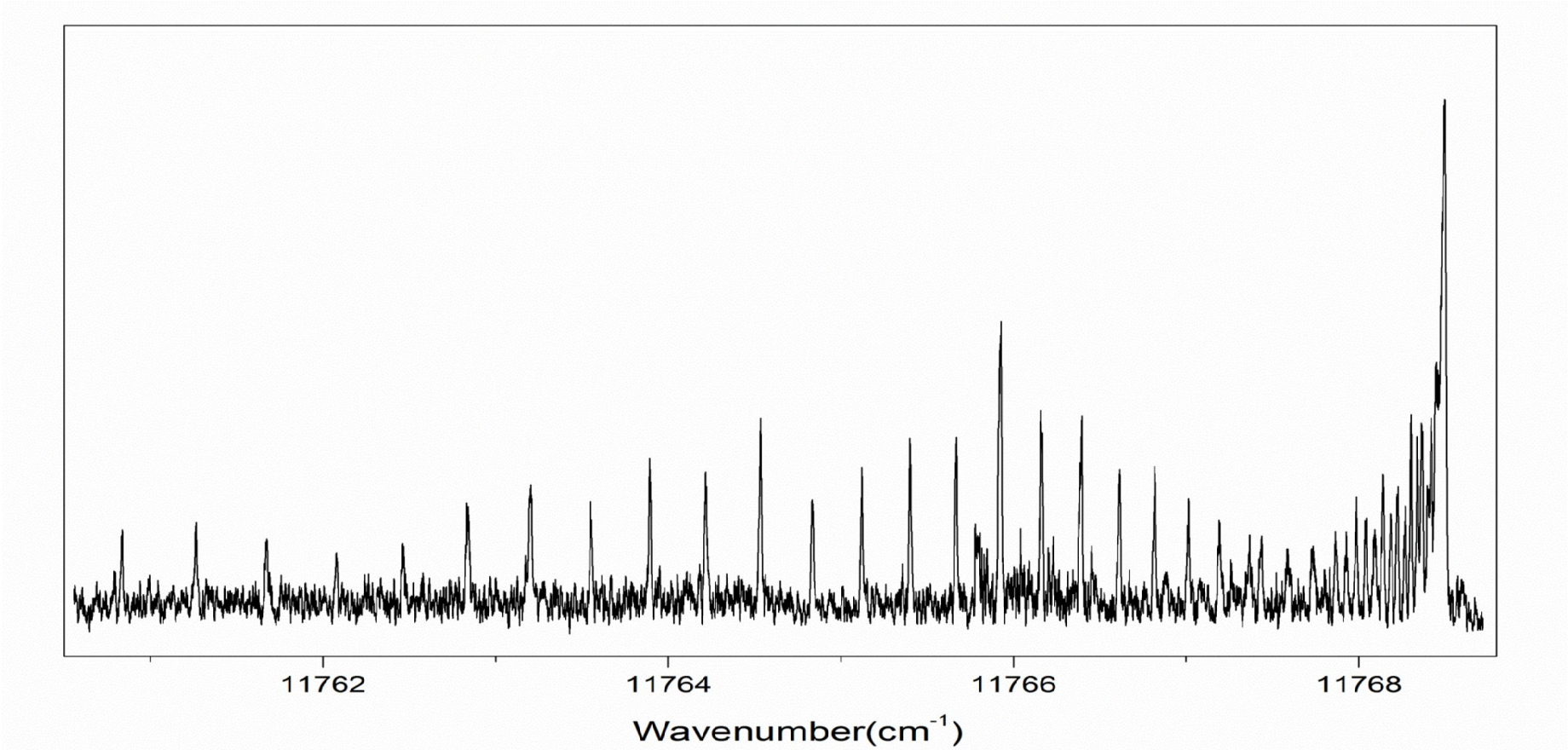

Fig. 4.9 The (0, 4) band of the $C^1\Sigma^+ - X^1\Sigma^+$ transition of ScI

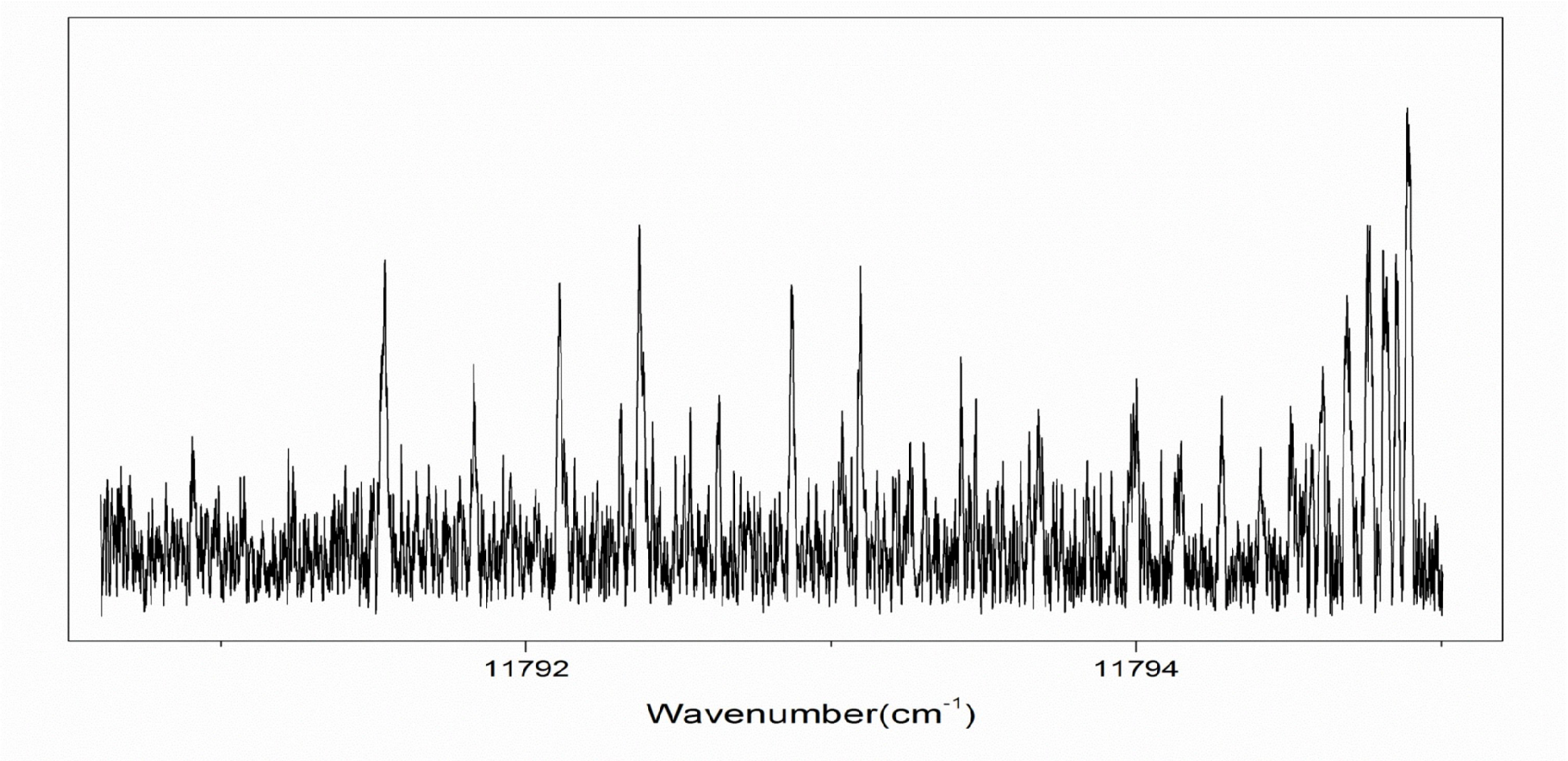

Fig. 4.10 The (1, 5) band of the $C^1\Sigma^+ - X^1\Sigma^+$ transition of ScI

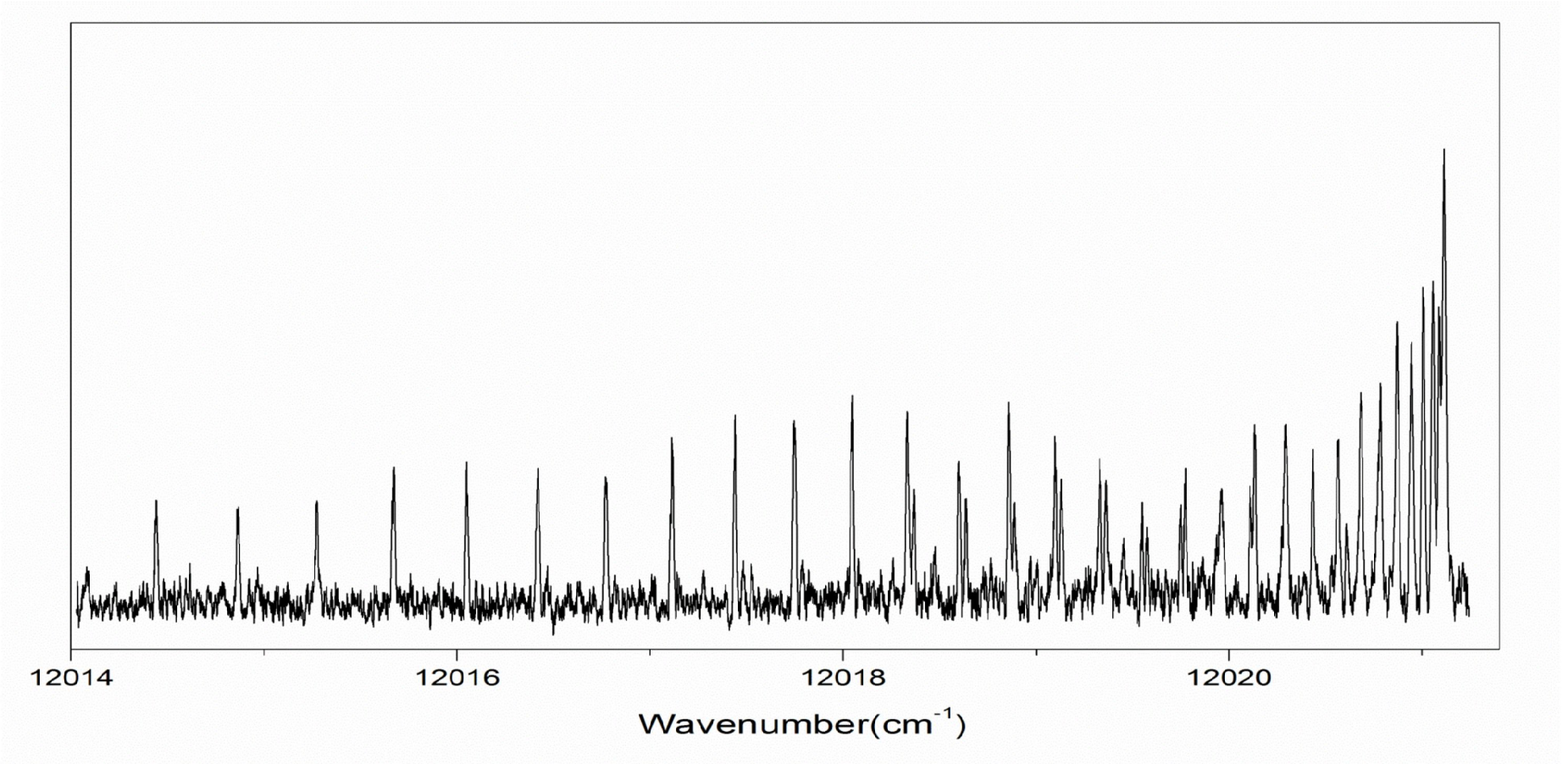

Fig. 4.11 The (2, 5) band of the $C^1\Sigma^+ - X^1\Sigma^+$ transition of ScI

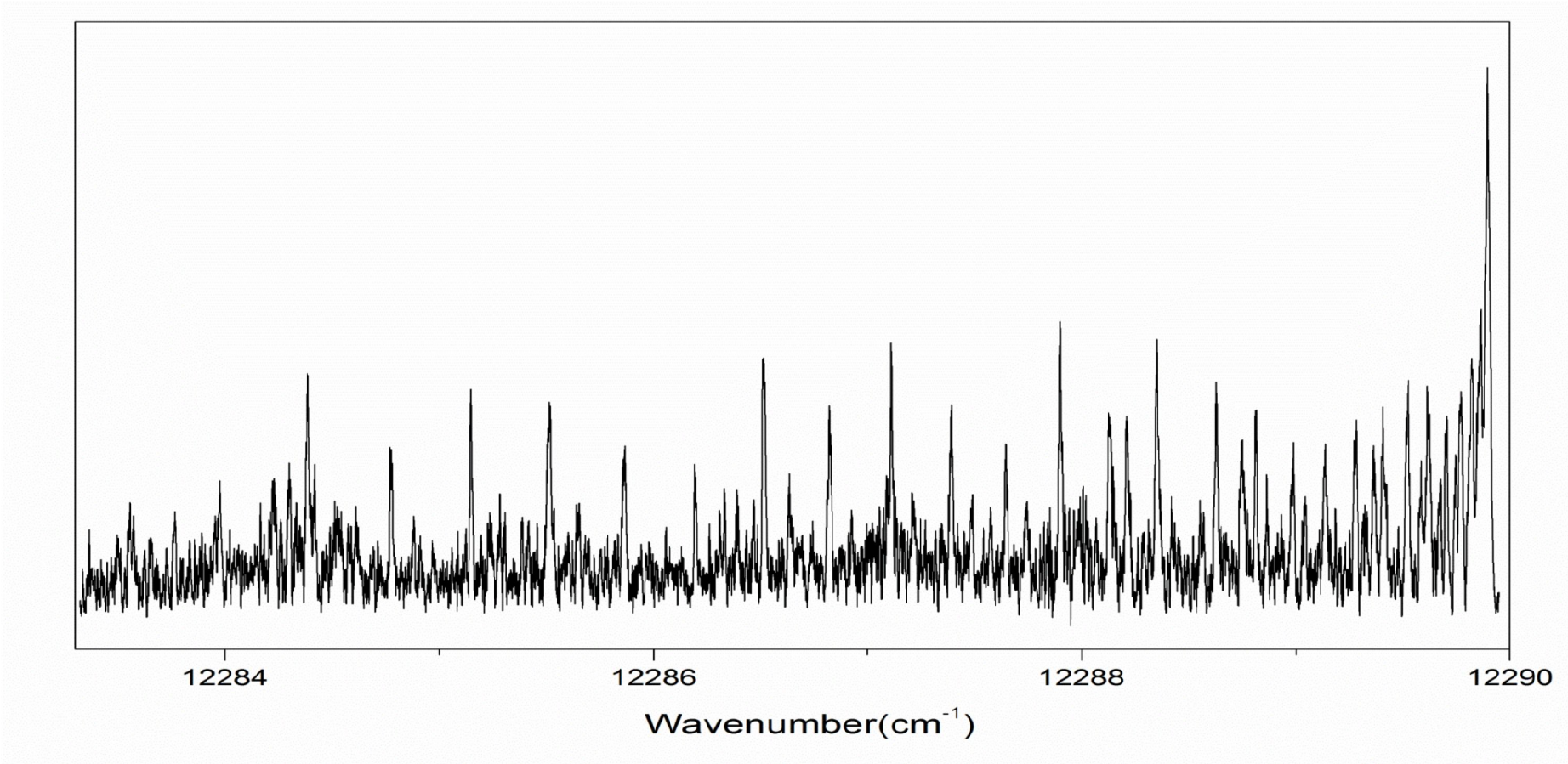

Fig. 4.12 The (2, 4) band of the $C^1\Sigma^+ - X^1\Sigma^+$ transition of ScI

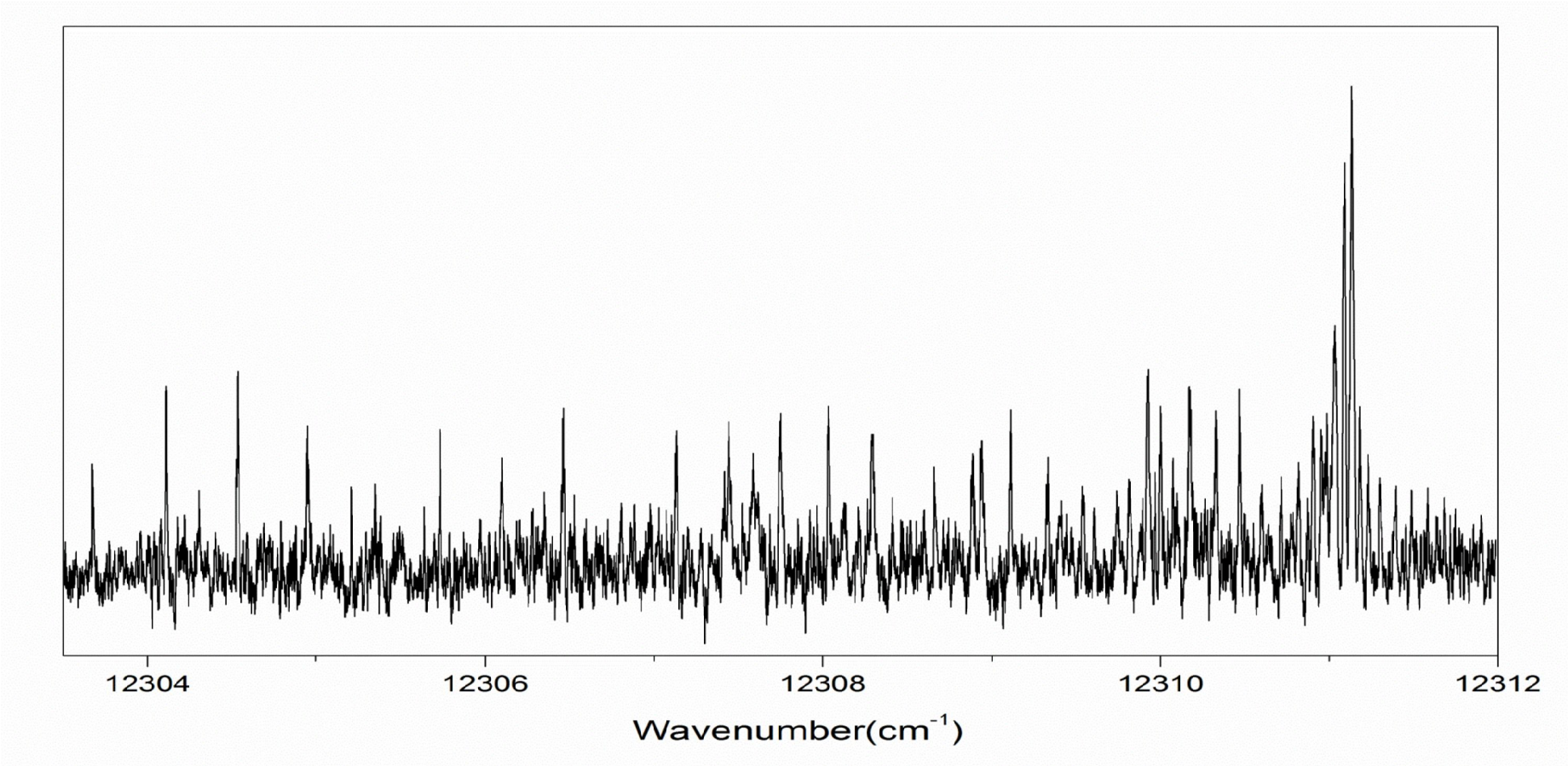

Fig. 4.13 The (0, 2) band of the $C^1\Sigma^+ - X^1\Sigma^+$ transition of ScI

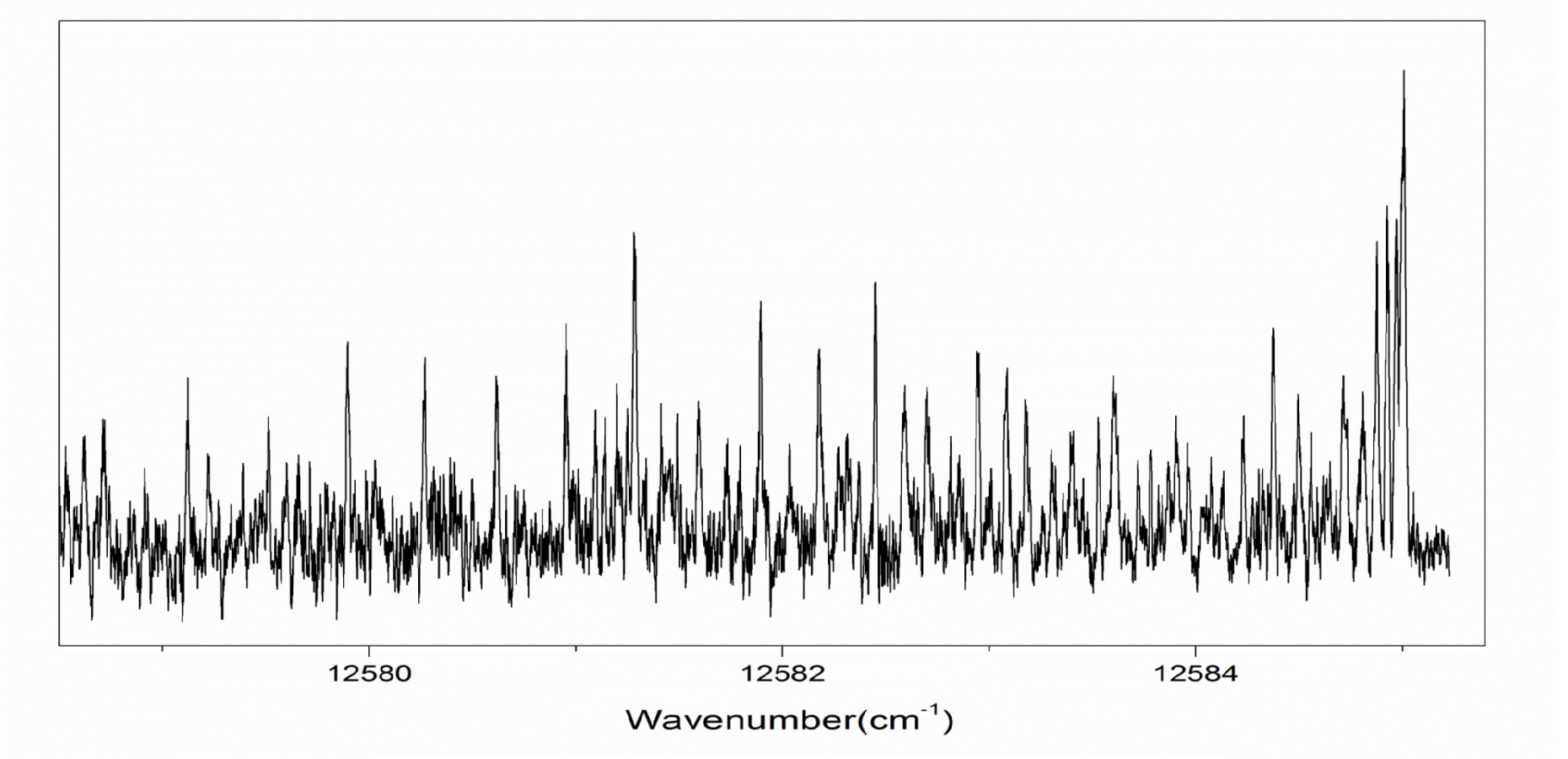

Fig. 4.14 The (0, 1) band of the $C^1\Sigma^+ - X^1\Sigma^+$ transition of ScI

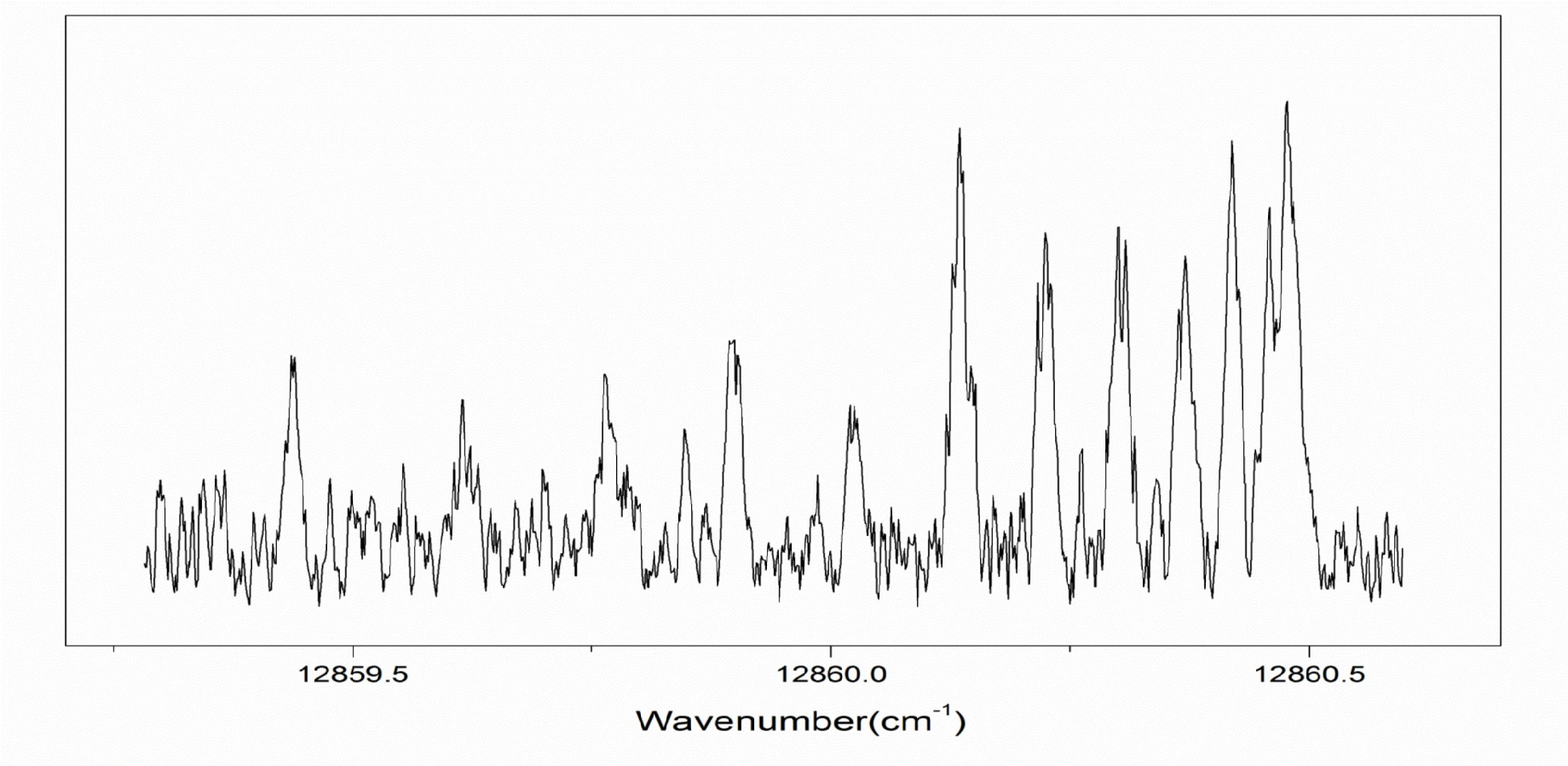

Fig. 4.15 The R branch of the (0, 0) band of the $C^1\Sigma^+ - X^1\Sigma^+$ transition of ScI

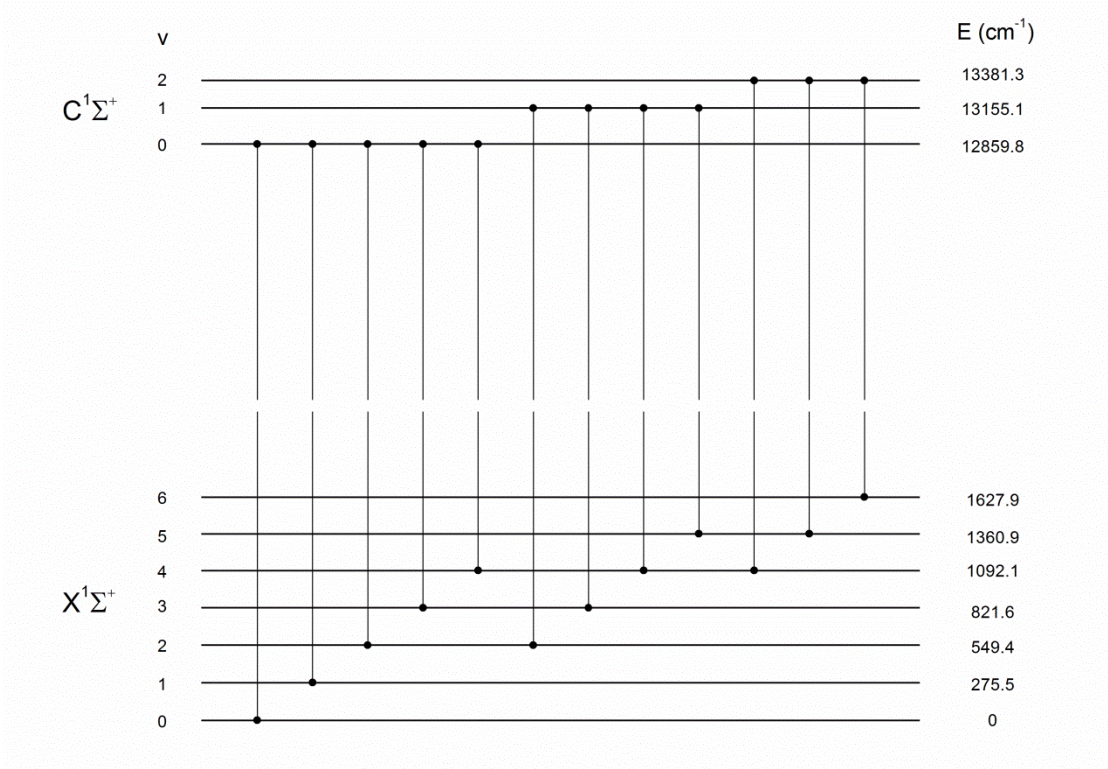

Fig. 4.16 Observed vibronic transitions of ScI

Table 4.7 Molecular constants for the $C^1\Sigma^+$ and $X^1\Sigma^+$ states of ScI (cm^{-1}).[a]

State	v	T_v	ΔT_v (obs. –cal.)	B_v	ΔB_v (obs. –cal.)
$C^1\Sigma^+$	2	13381.3287(7)	0[b]	0.066229(8)	0[b]
	1	13155.0836(7)	34.5346[b]	0.066468(8)	2.39 E-4[b]
	0	12859.7693(4)	0[b]	0.067521(1)	0[b]
$X^1\Sigma^+$	6	1627.9424(8)	-0.0496	0.07290(1)	6E-6
	5	1360.9085(8)	0.0285	0.07317(1)	-8E-6
	4	1092.0998(6)	0.0198	0.073457(7)	-5E-6
	3	821.571	-0.021	0.07374	-6E-6
	2	549.366	-0.05	0.07404	1E-5
+	1	275.491	-0.061	0.07439	7.6E-5
	0	0	0	0.07460	2E-6

[a] Numbers in parentheses are one standard deviation (in unit of the last figure).
[b] Calculated by assuming v = 1 level is perturbed. Please refer to text for details.

Table 4.8 Equilibrium molecular constants for the $C^1\Sigma^+$ and $X^1\Sigma^+$ states of ScI (cm^{-1}).[a]

State	Parameter	ScI	Theoretical[b]
$C^1\Sigma^+$	T_0	12859.7693	12483
	$\Delta G_{1/2}$	261	256.53
	B_e	0.06784	0.06793
	$10^4\alpha_e$	6.46	
	r_e (Å)	2.7359	2.733
$X^1\Sigma^+$	T_e	0	0
	ω_e	277.24(3)	273.29
	$\omega_e\chi_e$	0.844(4)	
	B_e	0.074740(7)	0.07435
	$10^4\alpha_e$	2.84(1)	
	r_e (Å)	2.6066	2.613

[a] Numbers in parentheses are one standard deviation (in unit of the last figure).
[b] Ref. [52]

IV.3. Discussion

The electronegativities of F, Cl, Br, I, and Sc are, respectively, 3.98, 3.16, 2.96, 2.66, and 1.36. It is therefore expected that these monohalides are mainly ionic compounds and the ionic character decreases from ScF to ScI. The ionic nature of the binding for these compounds can also be visualized in the MO energy level diagram shown below. The formation of the ScX involves essentially taking a 3*d* elecron to fill in the 1π orbital that has much 2*p* nature of halogen. Such a transfer of electron from the Sc atom to the halogen atom forms the expected $Sc^{+}X^{-}$ ionic compound.

As in the cases of ScN and ScP, the involvement of d electrons in bonding gives rise to a wealth of low-lying electronic states that are subjects of electronic spectroscopy in the near infrared and visible regions. For ScX (X =F, Cl, Br, or I), the electronic states can be reasonably approximated by single electronic configurations constructed using qualitative molecular orbital theory [41]. Fig. 4.17 shows the qualitative molecular orbital (MO) energy level diagram of scandium monohalides formed from the scandium 3*d* and 4*s* atomic orbitals (AOs) and the n*p* AO of halogen atoms. The lowest energy 1σ and 1π MOs are mainly n*p*σ and n*p*π AOs of the halogen atoms. The slightly anti-bonding 3σ MO is formed from the Sc 3*d*σ and X n*p*σ, and the 2π MO is formed from the Sc 3*d*π and X *p*π AOs. The 2σ MO is mainly the n*s* AO of the Sc atom. The 1δ MO is mainly the 3*d*δ AO as no other orbital of δ symmetry lying nearby.

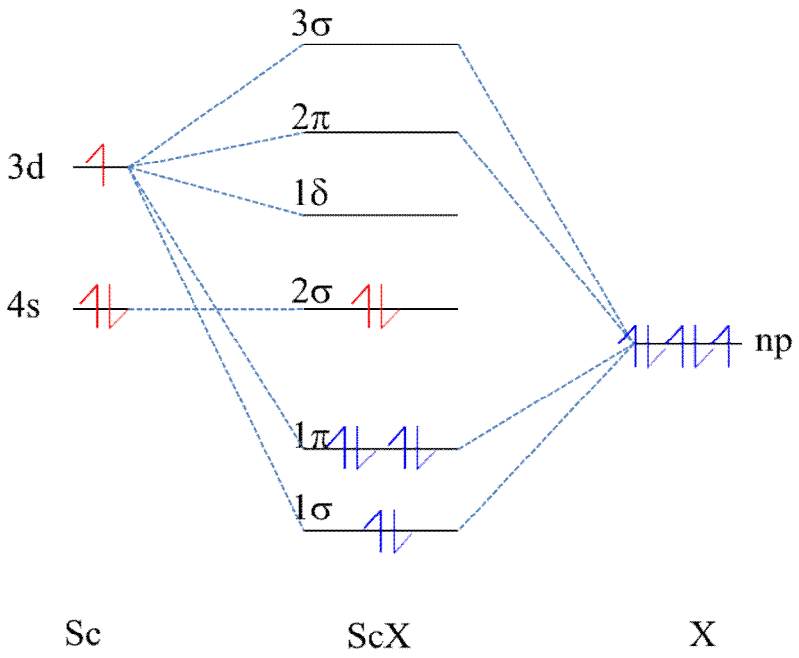

Fig.4.17 Qualitative molecular orbital (MO) energy level diagram of ScX

The first few low-lying electronic states can therefore correlate to the electronic configurations one by one as below:

$1\sigma^2\ 1\pi^4\ 2\sigma^2$	$X^1\Sigma^+$	(1)
$1\sigma^2\ 1\pi^4\ 2\sigma^1\ 1\delta^1$	$A^1\Delta$, $a^3\Delta$	(2)
$1\sigma^2\ 1\pi^4\ 2\sigma^1\ 2\pi^1$	$B^1\Pi$, $b^3\Pi$	(3)
$1\sigma^2\ 1\pi^4\ 2\sigma^1\ 3\sigma^1$	$C^1\Sigma^+$, $c^3\Sigma^+$	(4)
$1\sigma^2\ 1\pi^4\ 1\delta^1\ 2\pi^1$	$d^3\Phi$, $^3\Pi$, $^1\Phi$, $^1\Pi$	(5)
$1\sigma^2\ 1\pi^4\ 1\delta^1\ 3\sigma^1$	$e^3\Delta$, $^1\Delta$	(6)
$1\sigma^2\ 1\pi^4\ 2\sigma^1\ 3\pi^1$	$D^1\Pi$, $f^3\Pi$	(7)

The excitation to $C^1\Sigma^+$ state from the ground $X^1\Sigma^+$ state corresponds to promoting an electron from the non-bonding 2σ orbital to the antibonding 3σ orbital based on the correlation above. The $C^1\Sigma^+$ state is therefore expected to have a longer bond length and lower vibrational frequency compared to the ground state. The study of ScBr confirms this prediction. On the other hand, the results of ScI are somewhat unexpected. While the bond length in the $C^1\Sigma^+$ state is longer, the corresponding vibrational frequency is greater compared to the $X^1\Sigma^+$ state. This anomaly may be explained by the perturbation in the v = 1 level of the $C^1\Sigma^+$ state that pushes up the v = 1 level from its normal position. This is further confirmed by the exceptionally small $\Delta G_{3/2}$ (i.e. energy difference between the v = 2 and v =1 levels) value of 227 cm^{-1}. The true vibrational frequency can therefore be approximated by averaging the values of $\Delta G_{1/2}$ and $\Delta G_{3/2}$. A value of 266 cm^{-1} was therefore derived that is slightly smaller than vibrational frequency of 277 cm^{-1} in the $X^1\Sigma^+$ state as expected.

With the molecular parameters for the $C^1\Sigma^+$ and $X^1\Sigma^+$ states of ScBr and ScI, respectively, obtained from our studies, it is interesting to compare these constants for the series of scandium monohalides. The corresponding constants are listed in Table 4.9. It is seen that the equilibrium bond lengths of ScX (X =F, Cl, Br, or I) increase down the period as expected from the increasing size of halogen atoms. In the $X^1\Sigma^+$ state, the vibrational frequencies and bond length exhibit the same trend as discussed above. For the $C^1\Sigma^+$ state, however, the trend breaks going from ScBr to ScI. In fact, the $C^1\Sigma^+$ state of ScI has an energy comparable to ScCl. As a result, the transition

energy from $X^1\Sigma^+$ to $C^1\Sigma^+$ states for ScI is also much higher. Judging from the great amount of energy change, it is not likely a result of perturbation from nearby states. A plausible explanation may be attributed to the contribution of antibonding orbitals in the $C^1\Sigma^+$ state. According to CASSCF and MRCI calculations [52], the $C^1\Sigma^+ - X^1\Sigma^+$ transition is predicted to be at 12483 cm^{-1}, in reasonable agreement with our observed value of 12860 cm^{-1}.

Comparing the observed vibronic bands of the $C^1\Sigma^+ - X^1\Sigma^+$ system for both ScBr and ScI, it was found that ScI was produced with high vibrational and rotational energies. Rovibronic transitions with v" as high as 6 and J" as high as 33 were observed. This may be due to the high exothermicity of the reaction forming ScI. Similar observation has also been reported on YI [85].

In summary, the LIF spectra of the $C^1\Sigma^+ - X^1\Sigma^+$, $e^3\Delta - a^3\Delta$, and $d^3\Phi - a^3\Delta$ systems of ScBr, and the $C^1\Sigma^+ - X^1\Sigma^+$ system of ScI were recorded and analyzed in the near infrared region. Accurate molecular constants for the $C^1\Sigma^+$, $X^1\Sigma^+$, $e^3\Delta$, $d^3\Phi$, and $a^3\Delta$ states of ScBr, and $C^1\Sigma^+$ and $X^1\Sigma^+$ states of ScI were obtained using the least-squares fitting method. Molecular orbital energy diagrams of the two molecules have been constructed to explain the origins of the observed electronic states. A comparison of the molecular constants of the low-lying electronic states of scandium monohalides from similar electronic configurations indicates a weakening of chemical bonding between the scandium and the halogen atoms down the group.

Table 4.9 Molecular constants for the low-lying singlet states of scandium monohalides (cm^{-1}).

State	E.C.	Parameter	ScF[a]	$Sc^{35}Cl$[b]	$Sc^{79}Br$	ScI
		T_e	20383.378	[17390.06][†]		15630.1[c]
$D^1\Pi$	$2\sigma3\pi$	ω_e	622.506	374.3		237.9[c]
		r_e (Å)	1.864	2.348		2.715[c]
		T_e	[16091.9][†]	12427.4	11692.1	[12859.8][†]
$C^1\Sigma^+$	$2\sigma3\sigma$	ω_e		377	289.7	[261][†]
		r_e (Å)	1.907	2.3305	2.4776	2.736
		T_e	9555.6	6020.5		4409.7[d]
$B^1\Pi$	$2\sigma2\pi$	ω_e	593.0	381.0		243.4[d]
		r_e (Å)	1.907	2.351		2.722[d]
		T_e	4587.1	3555.7		2868.5[e]
$A^1\Delta$	$2\sigma1\delta$	ω_e	645.2	388.1		250.0[e]
		r_e (Å)	1.860	2.337		2.718[e]
$X^1\Sigma^+$	$2\sigma^2$	ω_e	735.3	447.5	339.2	277.1
		r_e (Å)	1.7874	2.3303	2.381	2.608

[†]Numbers in parenthesis are T_o or $\Delta G_{1/2}$ values

[a]Ref. [27]

[b]Ref. [38]

[c]Ref. [53]

[d]Ref. [47]

[e]Ref. [48]

Chapter V

Concluding Remarks

In this thesis, high resolution spectroscopic studies of diatomic scandium containing molecules ScP, ScBr, and ScI have been reported using laser induce fluorescence (LIF) spectroscopy. Our studies demonstrated that the combination of laser ablation, free jet expansion, and high resolution LIF spectroscopy provides a powerful means in obtaining structural parameters with high accuracy for reactive transition metal (TM) containing molecules. This approach has been widely used in the field in the past few decades. Considering the simplicity of experimental setup, it is still one of the most cost effective experimental approach.

We have observed the first spectrum of ScP. This work revealed the limitation of simple molecular orbital theory in understanding the electronic states of the molecule. In case of strong electron correlation, even the high level computation to date is insufficient in providing predictions that are in satisfactory quantitative agreement with observations [73]. This work provides a rigorous test modern computational chemistry.

The studies of ScBr and ScI provides new structural constants for several low-lying electronic states. By comparing the constants for the corresponding states of

various scandium monohalides, clear trends in chemical bonding was seen that can be rationalized using simple MO theory and periodic properties. The structural parameters obtained in our experiments exhibit very good agreements with those from computation [43, 52], indicating that the present level of theoretical calculations is far from satisfactory for ScP but sufficient in predicting properties of scandium monohalides. There is little doubt that more high quality experimental work will help establish a general computational algorithm for molecular systems containing transitions metals.

Reference

1. Veillard, A., *Chem. Rev.*, 91 (1991) 743.
2. Koga, N., Morokuma, K., *Chem. Rev.*, 91 (1991) 823.
3. Wojciechowska, M., Haber, J.; Lomnicki, S., Stoch, J., *J. Mol. Catal.* A, 141 (1999) 155.
4. C. Masters, "Homogeneous Transition-metal Catalysis", Chapman and Hall (1980).
5. Rao, C. N. R., *Annu. Rev. Phys. Chem.*, 40 (1989) 291.
6. Carlson, K. D., Claydon C. R., *Adv. High Temp. Chem.*, 1 (1967) 43 and other articles in this series.
7. "*High-Temperature Science: Future Needs and Anticipated Developments*", National Academy of Science: Washington, DC (1979).
8. Weltner, W., Jr., *Science* 155 (1967) 155.
9. White, N. M., Wing, R. F., *Astrophys. J.*, 222 (1978) 209.
10. C. W. Bauschlicber, Jr., S. P. Walch, and S. R. Langhoff, "*Quantum Chemistry; The Challenge of Transition Metals and Chemistry*", NATO Advanced Studies Institute, Series C: Mathematical and Physical Sciences (1986).
11. A. J. Merer, *Annu. Rev. Phys. Chem.*, 40 (1989) 407.
12. J.B. Hopkins, P.R.R. Langridgesmith, M.D. Morse, and R.E. Smalley, *J. Chem. Phys.*, 78 (1983) 1627.
13. J.M. Hollas and D. Phillips, "*Jet spectroscopy and molecular dynamics*". 1st ed, Blackie Academic & Professional, London, (1995).
14. T.G. Dietz, M.A. Duncan, D.E. Powers, and R.E. Smalley, J. Chem. Phys., 74

(1981) 6511.

15. S. R. Langhoff and C. W. Bauschlicher, Jr., Annu. Rev. Phys. Chem., 39 (1988) 181.
16. G. Herzberg, "*Spectra of Diatomic Molecules*", Van Nostran, New York (1950).
17. A. S.-C. Cheung, H. F. Pang, W. S. Tam, and J. W.-H. Leung *J. Chem. Phys.*, 131 (2009) 194301.
18. J.W.H. Leung, T.M. Ma, and A.S.C. Cheung, *J. Mol. Spectrosc.*, 229 (2005) 108.
19. Wolfgang Demtröder, *"Laser Spectroscopy"*, 4th ed, Springer, Verlag Berlin Heidelberg, (2008).
20. J. M. Brown and A. Carrington, "*Rotational Spectroscopy of Diatomic Molecules*", Cambridge University Press, London (2003).
21. H. Lefebvre-Brion and R. W. Field, *"The Spectra and Dynamics of Diatomic Molecules"*, Elsevier, New York (2004)
22. M. Born and Oppenheimer, *Ann. Phys.*, 84 (1927) 457.
23. S. Mukund and S. G. Nakhate, *Chem. Phys. Lett.*, 501 (2011) 221.
24. YEUNG, Shun Hin, *"Near infrared laser spectroscopy of carbon-containing plasmas"*, Ph.D Thesis (2010).
25. E. A. Shenyavskaya, A. J. Ross, A. Topouzkhanian, and G. Wannous, *J. Mol. Spectrosc.*, 162 (1993) 327.
26. M. A. Lebeault-Dorget, C. Effantin, A. Bernard, J. d'Incan, J. Chevaleyre, and E. A. Shenyavskaya, *J. Mol. Spectrosc.*, 163 (1994) 276.
27. E. A. Shenyavskaya, J. Verges, A. Topouzkhanian, M. A. Lebeault-Dorget, J.

d'Incan, C. Effantin, and A. Bernard, *J. Mol. Spectrosc.*, 164 (1994) 129.

28. M. A. Lebeault-Dorget, C. Effantin, J. d'Incan, A. Bernard, E. A. Shenyavskaya, and J. Verges, *J. Chem. Phys.*, 102 (1995) 708.
29. L. A. Kaledin, J. E. McCord, and M. C. Heaven, *J. Mol. Spectrosc.*, 171 (1995) 569.
30. E. A. Shenyavskaya, M. A. Lebeault-Dorget, C. Effantin, J. d'Incan, A. Bernard, and J. Verges, *J. Mol. Spectrosc.*, 171 (1995) 309.
31. W. Lin, S. A. Beaton, C. J. Evans, and M. C. L. Gerry, *J. Mol. Spectrosc.*, 199 (2000) 275.
32. F. Taher, C. Effantin, J. d'Incan, A. Bernard, J. Verges, and E. A. Shenyavskaya, *J. Mol. Spectrosc.*, 173 (1995) 62.
33. F. Taher, C. Effantin, J. d'Incan, A. Bernard, J. Verges, and E. A. Shenyavskaya, *J. Phy. B: At., Mol. Opt. Phys.*, 28 (1995) L181.
34. F. Taher, C. Effantin, A. Bernard, J. d'Incan, E. A. Shenyavskaya, and J. Verges, *J. Mol. Spectrosc.*, 179 (1996) 223.
35. F. Taher, A. Bernard, C. Effantin, J. d'Incan, E. A. Shenyavskaya, and J. Verges, *J. Mol. Spectrosc.*, 179 (1996) 229.
36. N. Boutassetta, A. R. Allouche, and M. Aubert-Frecon, *J. Phy. B: At., Mol. Opt. Phys.*, 29 (1996) 1637.
37. M. Bencheikh, *J. Phy. B: At., Mol. Opt. Phys.*, 30 (1997) L137.
38. F. Taher, C. Effantin, A. Bernard, J. d'Incan, J. Vergès, and E. A. Shenyavskaya, *J. Mol. Spectrosc.*, 184 (1997) 88.

39. A. G. Adam and J. R. D. Peers, *J. Mol. Spectrosc.*, 182 (1997) 215.

40. D.R. Fischell, H.C. Brayman and T.A. Cool, *J. Chem. Phys*. 73 (1980) 4260

41. S. R. Langhoff, C. W. Bauschlicher, and H. Partridge, *J. Chem. Phys.*, 89 (1988) 396.

42. W. Lin, C. J. Evans, and M. C. L. Gerry, *Phys. Chem. Chem. Phys.*, 2 (2000) 43.

43. M. Korek and A. Hamdan, *Int. J. Quant. Chem.*, 108 (2008) 456.

44. Y. Xia, Z. Liao, M. Yang, M.-C. Chan, and A. S-C. Cheung, *Chem. Phys. Lett.*, 527 (2012) 7.

45. Y. Xia, Z. Liao, M.-C. Chan, and A. S-C. Cheung, submitted to Chem. Phys.

46. Y. Xia, *"High resolution laser spectroscopy of scandium monohalides"*, Ph.D thesis, The University of Hong Kong (2012).

47. E. A. Shenyavskaya, C. Effantin, A. Bernard, J. Chevaleyre, J. d'Incan, A. Topouzkhanian, J. Vergès, and G. Wannous, *J. Phys. B: At., Mol. Opt. Phys.*, 29 (1996) L511.

48. C. Effantin, E. A. Shenyavskaya, J. d'Incan, A. Bernard, A. Topouzkhanian, and G. Wannous, *J. Mol. Spectrosc.*, 185 (1997) 249.

49. F. Taher, C. Effantin, A. Bernard, J. d'Incan, and J. Vergès, *J. Mol. Spectrosc.*, 189 (1998) 220.

50. M. Bencheikh, *J. Phys. B: At., Mol. Opt. Phys.*, 30, L137 (1997)

51. R. R. Reddy, Y. N. Ahammed, B. S. Devi, P. A. Azeem, K. R. Gopal, and T. V. R. Rao, *J Quant Spectrosc & Radia Tran.*, 74 (2002) 125.

52. M. Korek, S. Kontar, F. Taher-Mansour, and A.R. Allouche, *Int. J. Quant. Chem.*, 109 (2009) 236.

53. Z. H. Xia, Y. Xia, M-C. Chan, and A. S-C. Cheung, *J. Mol. Spectrosc.*, 268 (2011) 3.

54. Jeffrey Shirley, Chris Scurlock, and Timothy Steimle, *J. Chem. Phys.*, 93 (1990) 1568.

55. W. J. Childs and T. C. Steimle, *J. Chem. Phys.*, 88 (1988) 6168.

56. W. Weltner, D. McLeod, and P. H. Kasai, *J. Chem. Phys.*, 46 (1967) 3172.

57. C. W. Bauschlicher and S. R. Langhoff, *J. Chern. Phys.*, 85 (1986) 5936.

58. J. Andzelm, E. Radzio, Z. Barandianin, and L. Seijo, *J. Chern. Phys.*, 83 (1985) 4564.

59. S. Huzinaga, M. Klobukowski, and Y. Sakai, *J. Phys. Chem.*, 88 (1984) 4880.

60. L. Pettersson and U. Wahlgren, *Chem. Phys.*, 69 (1982) 185.

61. K. D. Carlson, E. Ludena, and C. Moser, *J. Chem. Phys.*, 43 (1965) 2408.

62. R. Stringat and B. Fenot, *Can. J. Phys.*, 54 (1976) 2293.

63. B. Fenot, J. L. Femenias, and R. Stringat, *J. Mol. Spectrosc.*, 78 (1979) 40.

64. C. W. Bauschlicher, Jr. and S. R. Langhoff, *J. Chem. Phys.*, 85 (1986) 5936.

65. T. C. Steimle, A. J. Marr, and D. M. Goodridge, *J. Chem. Phys.*, 107 (1997) 10406.

66. Jamie Gengler, Jinhai Chen, T.C. Steimle, R.S. Ram, P.F. Bernath, *J. Mol. Spectrosc.*, 237 (2006) 36.

67. R.S. Ram, P.F. Bernath, *J. Chem. Phys.*, 96 (1992) 6344.

68. S. G. Nakhate and S. Mukund, *Chem. Phys. Lett.*, 496 (2010) 243.

69. S. Mukund and S. G. Nakhate, *Chem. Phys. Lett.*, 501 (2011) 221.

70. G.H. Jeung, J. Koutecky, *J. Chem. Phys.*, 88 (1988) 3747.

71. K.L. Kunze, J.F. Harrison, *J. Am. Chem. Soc.*, 112 (1990) 3812.

72. A. Daoudi, S. Elkhattabi, G. Berthier, J.P. Flament, *Chem. Phys.*, 230 (1998) 31.

73. A. Daoudi, M. F. Baba, S. Elkhattabi, F. Rogemond, and H. Chermette, *Mol. Phys.*, 101 (2003) 2929.

74. F.J. Bai, C.L. Yang, Q. Qian, L. Zhang, *Chin. Phys.,* B 18 (2009) 549.

75. F. Tientega and J. F. Harrison, *Chem. Phys. Lett.*, 223 (1994) 202.

76. G. S. M. Tong, G. H. Jeung, A. S-C. Cheung, *J. Chem. Phys.*, 118 (2003) 9224.

77. R. Ram, P. Bernath, *J. Mol. Spectrosc.*, 165 (1994) 97.

78. I. Shim, K.A. Gingerich, *Int. J. Quantum Chem.*, 46 (1993) 145.

79. Z.J. Jakubek, S.G. Nakhate, B. Simard, *J. Mol. Spectrosc.*, 211 (2002) 86.

80. Z.J. Jakubek, S.G. Nakhate, B. Simard, *J. Mol. Spectrosc.*, 219 (2003) 145.

81. More details in *chapter 4*.

82. A total of 20 bands with clear rotational structures of YP have been recorded and the preliminary analysis has been done in our lab.

83. J.M. Brown, A. S.-C. Cheung, and A.J. Merer, *J. Mol. Spectrosc.*, 124 (1987) 464.

84. W.J Balfour, A.J. Merer, H. Nicki, B. Simard, P.A. Hackett, *J. Chem. Phys.*, 99 (1993) 3288.

85. J.W.-H. Leung, F.C.-Y. Hung, A.S-C. Cheung, *Chem. Phys. Lett.*, 363 (2002) 117

Appendix

Line list of ScP

Table 1a

Rotational Lines Assigned to the (0, 0) Band of the $A^1\Sigma^+ - X^1\Sigma^+$ Transition of ScP(cm^{-1})

J	ScP					
	P observed	**P calculated**	**ΔP**	**R observed**	**R calculated**	**ΔR**
0				**11936.7872**	11936.7866	.0006
1	**11936.0143**	11936.0139	.0004	**11937.1956**	11937.1946	.0010
2	**11935.6494**	11935.6493	.0001	**11937.6172**	11937.6171	.0001
3	**11935.2986**	11935.2990	-.0004	**11938.0537**	11938.0539	-.0002
4	**11934.9628**	11934.9632	-.0004	**11938.5059**	11938.5052	.0007
5	**11934.6416**	11934.6418	-.0002	**11938.9715**	11938.9709	.0006
6	**11934.3345**	11934.3349	-.0004	**11939.4507**	11939.4510	-.0003
7	**11934.0471**	11934.0424	.0047	**11939.9460**	11939.9455	.0005
8	**11933.7633**	11933.7643	-.0010	**11940.4538**	11940.4544	-.0006
9	**11933.4997**	11933.5007	-.0010	**11940.9767**	11940.9776	-.0009
10	**11933.2533**	11933.2514	.0019	**11941.5146**	11941.5152	-.0006
11	**11933.0164**	11933.0166	-.0002	**11942.0663**	11942.0672	-.0009
12	**11932.7962**	11932.7962	.0000	**11942.6328**	11942.6335	-.0007
13	**11932.5902**	11932.5902	.0000	**11943.2132**	11943.2142	-.0010
14	**11932.3976**	11932.3986	-.0010	**11943.8090**	11943.8091	-.0001
15	**11932.2200**	11932.2213	-.0013	**11944.4175**	11944.4184	-.0009
16	**11932.0587**	11932.0585	.0002	**11945.0412**	11945.0419	-.0007
17	**11931.9105**	11931.9099	.0006	**11945.6790**	11945.6797	-.0007
18	**11931.7756**	11931.7758	-.0002	**11946.3318**	11946.3317	.0001
19	**11931.6574**	11931.6559	.0015	**11946.9977**	11946.9979	-.0002
20	**11931.5512**	11931.5503	.0009	**11947.6784**	11947.6784	.0000
21	**11931.4598**	11931.4591	.0007	**11948.3729**	11948.3730	-.0001
22	**11931.3813**	11931.3821	-.0008	**11949.0823**	11949.0818	.0005
23	**11931.3208**	11931.3194	.0014			
24	**11931.2733**	11931.2709	.0024			
25	**11931.2327**	11931.2367	-.0040			

Table 1b

Rotational Lines Assigned to the (0, 1) Band of the $A^1\Sigma^+ - X^1\Sigma^+$ Transition of ScP(cm^{-1})

J	ScP					
	P observed	P calculated	ΔP	R observed	R calculated	ΔR
0				**11445.6436**	11445.6451	-.0015
1	**11444.8749**	11444.8741	.0008	**11446.0548**	11446.0548	.0000
2	**11444.5112**	11444.5130	-.0018	**11446.4820**	11446.4808	.0012
3	**11444.1676**	11444.1680	-.0004	**11446.9240**	11446.9229	.0011
4	**11443.8387**	11443.8392	-.0005	**11447.3820**	11447.3813	.0007
5	**11443.5256**	11443.5267	-.0011	**11447.8567**	11447.8557	.0010
6	**11443.2303**	11443.2303	.0000	**11448.3470**	11448.3464	.0006
7	**11442.9503**	11442.9501	.0002	**11448.8534**	11448.8532	.0002
8	**11442.6852**	11442.6861	-.0009	**11449.3765**	11449.3761	.0004
9	**11442.4376**	11442.4383	-.0007	**11449.9150**	11449.9152	-.0002
10	**11442.2063**	11442.2066	-.0003	**11450.4715**	11450.4704	.0011
11	**11441.9903**	11441.9911	-.0008	**11451.0427**	11451.0417	.0010
12	**11441.7919**	11441.7917	.0002	**11451.6289**	11451.6290	-.0001
13	**11441.6078**	11441.6085	-.0007	**11452.2320**	11452.2324	-.0004
14	**11441.4404**	11441.4414	-.0010	**11452.8518**	11452.8519	-.0001
15	**11441.2890**	11441.2904	-.0014	**11453.4858**	11453.4874	-.0016
16	**11441.1540**	11441.1554	-.0014	**11454.1402**	11454.1389	.0013
17	**11441.0374**	11441.0366	.0008	**11454.8060**	11454.8063	-.0003
18	**11440.9345**	11440.9338	.0007	**11455.4901**	11455.4897	.0004
19	**11440.8476**	11440.8470	.0006	**11456.1892**	11456.1891	.0001
20	**11440.7790**	11440.7763	.0027	**11456.9044**	11456.9043	.0001
21	**11440.7230**	11440.7215	.0015	**11457.6359**	11457.6354	.0005
22	**11440.6788**	11440.6827	-.0039	**11458.3822**	11458.3824	-.0002
23	**11440.6634**	11440.6599	.0035	**11459.1436**	11459.1451	-.0015

Table 1c

Rotational Lines Assigned to the (1, 0) Band of the $A^1\Sigma^+ - X^1\Sigma^+$ Transition of ScP(cm^{-1})

J	ScP					
	P observed	**P calculated**	**ΔP**	**R observed**	**R calculated**	**ΔR**
0				**12454.0069**	12454.0068	.0001
1	**12453.2356**	12453.2360	-.0004	**12454.4114**	12454.4109	.0005
2	**12452.8701**	12452.8694	.0007	**12454.8282**	12454.8276	.0006
3	**12452.5156**	12452.5153	.0003	**12455.2577**	12455.2568	.0009
4	**12452.1735**	12452.1737	-.0002	**12455.6994**	12455.6984	.0010
5	**12451.8446**	12451.8447	-.0001	**12456.1543**	12456.1526	.0017
6	**12451.5278**	12451.5281	-.0003	**12456.6192**	12456.6193	-.0001
7	**12451.2238**	12451.2241	-.0003	**12457.0968**	12457.0984	-.0016
8	**12450.9323**	12450.9326	-.0003	**12457.5894**	12457.5900	-.0006
9	**12450.6530**	12450.6536	-.0006	**12458.0938**	12458.0941	-.0003
10	**12450.3856**	12450.3871	-.0015	**12458.6106**	12458.6107	-.0001
11	**12450.1319**	12450.1331	-.0012	**12459.1394**	12459.1397	-.0003
12	**12449.8910**	12449.8916	-.0006	**12459.6806**	12459.6811	-.0005
13	**12449.6621**	12449.6627	-.0006	**12460.2351**	12460.2350	.0001
14	**12449.4440**	12449.4462	-.0022	**12460.8021**	12460.8013	.0008
15	**12449.2408**	12449.2422	-.0014	**12461.3806**	12461.3801	.0005
16	**12449.0499**	12449.0507	-.0008	**12461.9724**	12461.9712	.0012
17	**12448.8732**	12448.8716	.0016	**12462.5752**	12462.5747	.0005
18	**12448.7048**	12448.7051	-.0003	**12463.1913**	12463.1906	.0007
19	**12448.5505**	12448.5509	-.0004	**12463.8197**	12463.8189	.0008
20	**12448.4106**	12448.4093	.0013	**12464.4594**	12464.4596	-.0002
21	**12448.2807**	12448.2801	.0006	**12465.1123**	12465.1125	-.0002
22	**12448.1649**	12448.1633	.0016			
23	**12448.0595**	12448.0589	.0006			
24	12447.9676	12447.9670	.0006			
25	12447.8891	12447.8874	.0017			
26	12447.8170	12447.8203	-.0033			

Table 1d

Rotational Lines Assigned to the (1, 1) Band of the $A^1\Sigma^+ - X^1\Sigma^+$ Transition of ScP(cm^{-1})

J			ScP			
	P observed	**P calculated**	**ΔP**	**R observed**	**R calculated**	**ΔR**
0				**11962.8635**	11962.8652	-.0017
1	**11962.0968**	11962.0962	.0006	**11963.2712**	11963.2711	.0001
2	**11961.7345**	11961.7331	.0014	**11963.6906**	11963.6913	-.0007
3	**11961.3860**	11961.3843	.0017	**11964.1252**	11964.1258	-.0006
4	**11961.0510**	11961.0498	.0012	**11964.5738**	11964.5745	-.0007
5	**11960.7296**	11960.7295	.0001	**11965.0383**	11965.0374	.0009
6	**11960.4247**	11960.4235	.0012	**11965.5143**	11965.5147	-.0004
7	**11960.1315**	11960.1318	-.0003	**11966.0054**	11966.0061	-.0007
8	**11959.8553**	11959.8543	.0010	**11966.5107**	11966.5118	-.0011
9	**11959.5908**	11959.5912	-.0004	**11967.0315**	11967.0317	-.0002
10	**11959.3414**	11959.3422	-.0008	**11967.5669**	11967.5658	.0011
11	**11959.1072**	11959.1076	-.0004	**11968.1130**	11968.1141	-.0011
12	**11958.8856**	11958.8871	-.0015	**11968.6751**	11968.6766	-.0015
13	**11958.6796**	11958.6809	-.0013	**11969.2517**	11969.2533	-.0016
14	**11958.4875**	11958.4889	-.0014	**11969.8428**	11969.8441	-.0013
15	**11958.3109**	11958.3112	-.0003	**11970.4476**	11970.4491	-.0015
16	**11958.1467**	11958.1476	-.0009	**11971.0689**	11971.0682	.0007
17	**11957.9974**	11957.9983	-.0009	**11971.7007**	11971.7014	-.0007
18	**11957.8632**	11957.8631	.0001			
19	**11957.7436**	11957.7421	.0015			
20	**11957.6365**	11957.6352	.0013			
21	**11957.5448**	11957.5425	.0023			
22	**11957.4630**	11957.4639	-.0009			

Table 1e

Rotational Lines Assigned to the (1, 2) Band of the $A^1\Sigma^+ - X^1\Sigma^+$ Transition of ScP(cm^{-1})

J	ScP					
	P observed	**P calculated**	**ΔP**	**R observed**	**R calculated**	**ΔR**
0				**11475.4564**	11475.4552	.0012
1	**11474.6858**	11474.6879	-.0021	**11475.8629**	11475.8628	.0001
2	**11474.3293**	11474.3282	.0011	**11476.2875**	11476.2864	.0011
3	**11473.9845**	11473.9845	.0000	**11476.7267**	11476.7260	.0007
4	**11473.6566**	11473.6569	-.0003	**11477.1816**	11477.1816	.0000
5	**11473.3454**	11473.3452	.0002	**11477.6539**	11477.6532	.0007
6	**11473.0484**	11473.0496	-.0012	**11478.1418**	11478.1407	.0011
7	**11472.7697**	11472.7699	-.0002	**11478.6447**	11478.6443	.0004
8	**11472.5056**	11472.5063	-.0007	**11479.1642**	11479.1638	.0004
9	**11472.2594**	11472.2587	.0007	**11479.6997**	11479.6993	.0004
10	**11472.0274**	11472.0272	.0002	**11480.2511**	11480.2507	.0004
11	**11471.8117**	11471.8117	.0000	**11480.8191**	11480.8182	.0009
12	**11471.6123**	11471.6122	.0001	**11481.4026**	11481.4017	.0009
13	**11471.4290**	11471.4287	.0003	**11482.0029**	11482.0011	.0018
14	**11471.2604**	11471.2614	-.0010	**11482.6179**	11482.6165	.0014
15	**11471.1093**	11471.1100	-.0007	**11483.2484**	11483.2479	.0005
16	**11470.9753**	11470.9748	.0005	**11483.8963**	11483.8953	.0010
17	**11470.8549**	11470.8556	-.0007	**11484.5594**	11484.5587	.0007
18	**11470.7522**	11470.7526	-.0004	**11485.2370**	11485.2381	-.0011
19	**11470.6635**	11470.6656	-.0021	**11485.9328**	11485.9335	-.0007
20	**11470.5930**	11470.5947	-.0017	**11486.6485**	11486.6449	.0036
21	**11470.5382**	11470.5399	-.0017			
22	**11470.5006**	11470.5013	-.0007			
23	**11470.4732**	11470.4788	-.0056			

Table 1f

Rotational Lines Assigned to the (2, 1) Band of the $A^1\Sigma^+ - X^1\Sigma^+$ Transition of ScP(cm^{-1})

J	ScP					
	P observed	**P calculated**	**ΔP**	**R observed**	**R calculated**	**ΔR**
0				**12476.0381**	12476.0375	.0006
1	**12475.2697**	12475.2701	-.0004	**12476.4422**	12476.4400	.0022
2	**12474.9062**	12474.9054	.0008	**12476.8570**	12476.8552	.0018
3	**12474.5536**	12474.5532	.0004	**12477.2835**	12477.2829	.0006
4	**12474.2139**	12474.2136	.0003	**12477.7251**	12477.7231	.0020
5	**12473.8864**	12473.8866	-.0002	**12478.1780**	12478.1760	.0020
6	**12473.5722**	12473.5722	.0000	**12478.6426**	12478.6413	.0013
7	**12473.2704**	12473.2703	.0001	**12479.1198**	12479.1192	.0006
8	**12472.9803**	12472.9810	-.0007	**12479.6099**	12479.6097	.0002
9	**12472.7032**	12472.7043	-.0011	**12480.1120**	12480.1126	-.0006
10	**12472.4388**	12472.4401	-.0013	**12480.6270**	12480.6280	-.0010
11	**12472.1874**	12472.1885	-.0011	**12481.1556**	12481.1558	-.0002
12	**12471.9480**	12471.9493	-.0013	**12481.6954**	12481.6961	-.0007
13	**12471.7231**	12471.7226	.0005	**12482.2480**	12482.2488	-.0008
14	**12471.507**	12471.5085	-.0015	**12482.8125**	12482.8139	-.0014
15	**12471.3061**	12471.3067	-.0006	**12483.3896**	12483.3913	-.0017
16	**12471.1175**	12471.1174	.0001	**12483.9812**	12483.9811	.0001
17	**12470.9405**	12470.9405	.0000	**12484.5845**	12484.5831	.0014
18	**12470.7760**	12470.7760	.0000	**12485.198**	12485.1974	.0006
19	**12470.6246**	12470.6238	.0008	**12485.8240**	12485.8240	.0000
20	**12470.4852**	12470.4840	.0012	**12486.4642**	12486.4627	.0015
21	**12470.3566**	12470.3564	.0002			
22	**12470.2421**	12470.2411	.0010			
23	**12470.1380**	12470.1380	.0000			
24	**12470.0471**	12470.0471	.0000			
25	**12469.9666**	12469.9683	-.0017			
26	**12469.8973**	12469.9016	-.0043			

Table 1g

Rotational Lines Assigned to the (2, 2) Band of the $A^1\Sigma^+ - X^1\Sigma^+$ Transition of ScP(cm^{-1})

J	ScP					
	P observed	**P calculated**	**ΔP**	**R observed**	**R calculated**	**ΔR**
0				**11988.6266**	11988.6274	-.0008
1	**11987.8602**	11987.8618	-.0016	**11989.0301**	11989.0317	-.0016
2	**11987.5008**	11987.5005	.0003	**11989.4496**	11989.4502	-.0006
3	**11987.1543**	11987.1534	.0009	**11989.8857**	11989.8831	.0026
4	**11986.8205**	11986.8207	-.0002	**11990.3306**	11990.3302	.0004
5	**11986.5030**	11986.5023	.0007	**11990.7901**	11990.7917	-.0016
6	**11986.1989**	11986.1982	.0007	**11991.2673**	11991.2674	-.0001
7	**11985.9066**	11985.9085	-.0019	**11991.7565**	11991.7574	-.0009
8	**11985.6331**	11985.6330	.0001	**11992.2603**	11992.2617	-.0014
9	**11985.3740**	11985.3719	.0021	**11992.7789**	11992.7802	-.0013
10	**11985.1265**	11985.1251	.0014	**11993.312**	11993.3129	-.0009
11	**11984.8930**	11984.8926	.0004	**11993.8590**	11993.8599	-.0009
12	**11984.6741**	11984.6744	-.0003	**11994.4192**	11994.4212	-.0020
13	**11984.4725**	11984.4705	.0020	**11994.9955**	11994.9966	-.0011
14	**11984.2808**	11984.2809	-.0001	**11995.5860**	11995.5863	-.0003
15	**11984.1058**	11984.1056	.0002	**11996.1888**	11996.1902	-.0014
16	**11983.9445**	11983.9446	-.0001			
17	**11983.7985**	11983.7979	.0006			
18	**11983.6626**	11983.6655	-.0029			
19	**11983.5478**	11983.5473	.0005			
20	**11983.4435**	11983.4435	.0000			
21	**11983.3576**	11983.3538	.0038			

Table 1h

Rotational Lines Assigned to the (3, 2) Band of the $A^1\Sigma^+ - X^1\Sigma^+$ Transition of ScP(cm^{-1})

J	ScP					
	P observed	**P calculated**	**ΔP**	**R observed**	**R calculated**	**ΔR**
0				**12498.4052**	12498.40462	0.00058
1	**12497.6414**	12497.64195	-0.00055	**12498.8031**	12498.80301	0.00009
2	**12497.2784**	12497.27767	0.00073	**12499.2139**	12499.21277	0.00113
3	**12496.9248**	12496.92476	0.00004	**12499.6340**	12499.6339	0.00009
4	**12496.5825**	12496.58324	-0.00074	**12500.0655**	12500.06642	-0.00090
5	**12496.2517**	12496.25312	-0.00142	**12500.5108**	12500.51034	0.00046
6	**12495.9340**	12495.9344	-0.0004	**12500.9661**	12500.96566	0.00043
7	**12495.6255**	12495.62711	-0.00161	**12501.4322**	12501.43241	-0.00020
8	**12495.3302**	12495.33126	-0.00106	**12501.9113**	12501.9106	0.00070
9	**12495.0469**	12495.04687	0.00003	**12502.4033**	12502.40025	0.00305
10	**12494.7731**	12494.77397	-0.00087	**12502.9062**	12502.90139	0.00481
11	**12494.5144**	12494.51258	0.00182	**12503.4221**	12503.41404	0.00806
12	**12494.2668**	12494.26274	0.00406	**12503.9486**	12503.93824	0.01036
13	**12494.0315**	12494.02447	0.00703	**12504.4880**	12504.47401	0.01399
14	**12493.8077**	12493.79781	0.00989	**12505.0378**	12505.02139	0.01641
15	**12493.5976**	12493.5828	0.0148			
16	**12493.3978**	12493.37947	0.01833			
17	**12493.2127**	12493.18786	0.02484			
18	**12493.0401**	12493.00803	0.03207			
19	**12492.8762**	12492.84002	0.03618			
20	**12492.7286**	12492.68388	0.04472			
21	**12492.5966**	12492.53967	0.05693			
22	**12492.4722**	12492.40743	0.06477			
23	**12492.3616**	12492.28723	0.07437			
24	**12492.2608**	12492.17912	0.08168			
25	**12492.1765**	12492.08318	0.09332			
26	**12492.1044**	12491.99946	0.10494			
27	**12492.0653**	12491.92803	0.13727			

Table 1i

Rotational Lines Assigned to the (3, 3) Band of the $A^1\Sigma^+ - X^1\Sigma^+$ Transition of ScP(cm^{-1})

J	ScP					
	P observed	**P calculated**	**ΔP**	**R observed**	**R calculated**	**ΔR**
0				**12014.7243**	12014.7252	-0.0009
1	**12013.9645**	12013.96328	0.00122	**12015.1241**	12015.12758	-0.00348
2	**12013.6047**	12013.60374	0.00096	**12015.5379**	12015.54424	-0.00634
3	**12013.2574**	12013.25848	-0.00108	**12015.9649**	12015.97518	-0.01028
4	**12012.9206**	12012.9275	-0.0069	**12016.4034**	12016.4204	-0.017
5	**12012.5996**	12012.6108	-0.0112	**12016.8566**	12016.8799	-0.0233
6	**12012.2911**	12012.30838	-0.01728	**12017.3178**	12017.35368	-0.03588
7	**12011.9970**	12012.02024	-0.02324	**12017.8013**	12017.84174	-0.04044
8	**12011.7152**	12011.74638	-0.03118	**12018.2952**	12018.34408	-0.04888
9	**12011.4478**	12011.4868	-0.039	**12018.8023**	12018.8607	-0.0584
10	**12011.1931**	12011.2415	-0.0484	**12019.3241**	12019.3916	-0.0675
11	**12010.9517**	12011.01048	-0.05878	**12019.8575**	12019.93678	-0.07928
12	**12010.7257**	12010.79374	-0.06804	**12020.4052**	12020.49624	-0.09104
13	**12010.5114**	12010.59128	-0.07988	**12020.9679**	12021.06998	-0.10208
14	**12010.3142**	12010.4031	-0.0889	**12021.5445**	12021.658	-0.1135
15	**12010.1287**	12010.2292	-0.1005	**12022.1362**	12022.2603	-0.1241
16	**12009.9575**	12010.06958	-0.11208	**12022.7429**	12022.87688	-0.13398
17	**12009.8022**	12009.92424	-0.12204	**12023.3574**	12023.50774	-0.15034
18	**12009.6599**	12009.79318	-0.13328	**12023.9949**	12024.15288	-0.15798
19	**12009.5330**	12009.6764	-0.1434			

Table 1j

Rotational Lines Assigned to the (4, 3) Band of the $A^1\Sigma^+ - X^1\Sigma^+$ Transition of ScP(cm^{-1})

J	ScP					
	P observed	**P calculated**	**ΔP**	**R observed**	**R calculated**	**ΔR**
0				**12519.2291**	12519.22986	-0.00076
1	**12518.4695**	12518.47048	-0.00098	**12519.6300**	12519.62716	0.00284
2	**12518.1095**	12518.1084	0.0011	**12520.0373**	12520.0362	0.0011
3	**12517.7590**	12517.75806	0.00094	**12520.4596**	12520.45698	0.00262
4	**12517.4202**	12517.41946	0.00074	**12520.8923**	12520.8895	0.0028
5	**12517.0935**	12517.0926	0.0009	**12521.3360**	12521.33376	0.00224
6	**12516.7787**	12516.77748	0.00122	**12521.7915**	12521.78976	0.00174
7	**12516.4760**	12516.4741	0.0019	**12522.2586**	12522.2575	0.0011
8	**12516.1843**	12516.18246	0.00184	**12522.7358**	12522.73698	-0.00118
9	**12515.9028**	12515.90256	0.00024	**12523.2233**	12523.2282	-0.0049
10	**12515.6318**	12515.6344	-0.0026	**12523.7206**	12523.73116	-0.01056
11	**12515.3744**	12515.37798	-0.00358	**12524.2255**	12524.24586	-0.02036
12	**12515.1227**	12515.1333	-0.0106	**12524.7340**	12524.7723	-0.0383
13	**12514.8800**	12514.90036	-0.02036	**12525.2394**	12525.31048	-0.07108
14	**12514.6421**	12514.67916	-0.03706	**12525.7238**	12525.8604	-0.1366
15	**12514.4008**	12514.4697	-0.0689	**12526.1025**	12526.42206	-0.31956
16	**12514.1404**	12514.27198	-0.13158			
17	**12513.7651**	12514.086	-0.3209			

Line list of ScI

Table 2a

Assigned Rotational Lines of the (0, 0) Band of the $C^1\Sigma^+ - X^1\Sigma^+$ Transition of ScI (cm^{-1})

J	ScI	
	P	R
0		12859.8942
1	12859.6143	12860.0252
2	12859.4357	12860.1288
3	12859.2553	12860.2245
4	12859.0605	12860.3029
5	12858.8846	12860.3671
6	12858.6617	12860.4172
7	12858.4275	12860.4747
8		12860.4825

Table 2b

Assigned Rotational Lines of the (0, 1) Band of the $C^1\Sigma^+ - X^1\Sigma^+$ Transition of ScI (cm^{-1})

J	ScI	
	P	R
0		
1		
2	12583.9600	
3	12583.7831	12584.7290
4	12583.6023	12584.8100
5	12583.4083	12584.8840
6	12583.1762	12584.9332
7	12582.9423	12584.9760
8	12582.7009	12585.0000
9	12582.4466	12585.0120
10	12582.1774	12585.0077
11	12581.8958	12584.9920
12	12581.5944	12584.9661
13	12581.2812	12584.9170
14	12580.9544	12584.8670
15	12580.6162	12584.7900
16	12580.2707	12584.7080
17	12579.8980	
18	12579.5120	
19	12579.1216	
20	12578.7181	

Table 2c

Assigned Rotational Lines of the (0, 2) Band of the $C^1\Sigma^+ - X^1\Sigma^+$ Transition of ScI (cm^{-1})

J	ScI	
	P*	R*
0		
1		
2		
3	12309.9280	
4	12309.7445	12310.9565
5	12309.5433	12311.0260
6	12309.3374	12311.0892
7	12309.1146	12311.1310
8	12308.9429	
9	12308.6592	
10	12308.2918	
11	12308.0330	
12	12307.7538	
13	12307.4442	
14	12307.1330	12311.0460
15	12306.4631	12310.9869
16	12306.1000	12310.9055
17	12305.7305	12310.8190
18	12304.9469	12310.7150
19	12304.5345	12310.6000
20	12304.1126	12310.4679
21	12303.6764	12310.3273
22	12309.9280	12310.1714
23	12309.7445	12310.0019

*line positions in the empty boxes cannot be assigned with certainty due to the present experimental condition.

Table 2d

Assigned Rotational Lines of the (0, 3) Band of the $C^1\Sigma^+ - X^1\Sigma^+$ Transition of ScI (cm^{-1})

J	ScI	
	P	R
0		12038.3345
1	12038.0480	12038.4567
2	12037.8918	12038.5652
3	12037.7218	12038.6650
4	12037.5375	12038.7495
5	12037.3399	12038.8227
6	12037.1307	12038.8832
7	12036.9073	12038.9286
8	12036.6707	12038.9640
9	12036.4235	12038.9860
10	12036.1633	12038.9975
11	12035.8901	12038.9942
12	12035.6063	12038.9795
13	12035.3108	12038.9555
14	12035.0014	12038.9095
15	12034.6789	12038.8574
16	12034.3409	12038.7904
17	12033.9938	12038.7107
18	12033.6328	12038.6187
19	12033.2611	12038.5115
20	12032.8734	12038.3945
21	12032.4726	12038.2639
22	12032.0634	12038.1166
23	12031.6383	12037.9597
24		12037.7884
25		12037.6057
26		12037.4071
27		12037.1942
28		12036.9708
29		12036.7351
30		12036.4809

Table 2e

Assigned Rotational Lines of the (0, 4) Band of the $C^1\Sigma^+ - X^1\Sigma^+$ Transition of ScI (cm^{-1})

J	ScI	
	P	R
0		11767.8040
1	11767.5222	11767.9268
2	11767.3666	11768.0401
3	11767.1942	11768.1405
4	11767.0112	11768.2250
5	11766.8167	11768.3025
6	11766.6123	11768.3648
7	11766.3915	11768.4117
8	11766.1628	11768.4575
9	11765.9224	11768.4825
10	11765.6680	11768.5005
11	11765.4028	11768.5030
12	11765.1218	11768.4949
13	11764.8348	11768.4750
14	11764.5336	11768.4450
15	11764.2161	11768.3942
16	11763.8913	11768.3385
17	11763.5531	11768.2682
18	11763.2033	11768.1863
19	11762.8378	11768.0915
20	11762.4634	11767.9862
21	11762.0741	11767.8658
22	11761.6732	11767.7347
23	11761.2622	11767.5886
24	11760.8344	11767.4344

Table 2f

Assigned Rotational Lines of the (1, 4) Band of the $C^1\Sigma^+ - X^1\Sigma^+$ Transition of ScI (cm^{-1})

J	ScI	
	P	R
0		12063.1225
1	12062.8360	12063.2358
2	12062.6760	12063.3402
3	12062.5003	12063.4296
4	12062.3110	12063.5075
5	12062.1105	12063.5705
6	12061.8926	12063.6199
7	12061.6648	12063.6558
8	12061.4205	12063.6768
9	12061.1604	12063.6832
10	12060.8897	12063.6768
11	12060.6020	12063.6558
12	12060.3015	12063.6199
13	12059.9864	12063.5705
14	12059.6587	12063.5075
15	12059.3171	12063.4296
16	12058.9608	12063.3402
17	12058.5869	12063.2334
18		12063.1148
19		12062.9783
20		12062.8320
21		12062.6714

Table 2g

Assigned Rotational Lines of the (1, 5) Band of the $C^1\Sigma^+ - X^1\Sigma^+$ Transition of ScI (cm^{-1})

J	ScI	
	P	R
0		11794.3110
1		11794.4224
2		11794.5352
3		11794.6209
4		11794.7037
5	11793.3036	11794.7614
6	11793.0934	11794.8188
7	11792.871	11794.8563
8	11792.6328	11794.8901
9	11792.3712	11794.8991
10	11792.1079	11794.8991
11	11791.8326	11794.8901
12	11791.5372	11794.8602
13	11791.2205	11794.8217
14	11790.9056	11794.7666
15		11794.6911
16		11794.6164
17		11794.5168
18		11794.4086
19		11794.2818

Table 2h

Assigned Rotational Lines of the (2, 4) Band of the $C^1\Sigma^+ - X^1\Sigma^+$ Transition of ScI (cm^{-1})

J	ScI	
	P	R
0		12289.3645
1	12289.0800	12289.4800
2	12288.9190	12289.5860
3	12288.7488	12289.6730
4	12288.5543	12289.7465
5	12288.3516	12289.8090
6	12288.1310	12289.8510
7	12287.9015	12289.8855
8	12287.6483	12289.8995
9	12287.3922	12289.9025
10	12287.1105	12289.8898
11	12286.8222	12289.8618
12	12286.5167	12289.8226
13	12286.1964	12289.7710
14	12285.8638	12289.7018
15	12285.5144	12289.6181
16	12285.1495	12289.5223
17	12284.7742	12289.4082
18		12289.2802
19		12289.1385
20		12288.9851
21		12288.8120
22		12288.6276

Table 2i

Assigned Rotational Lines of the (2, 5) Band of the $C^1\Sigma^+ - X^1\Sigma^+$ Transition of ScI (cm^{-1})

J	ScI	
	P	R
0		12020.5506
1	12020.2766	12020.6721
2	12020.1109	12020.7755
3	12019.9372	12020.8690
4	12019.7506	12020.9445
5	12019.5497	12021.0061
6	12019.3325	12021.0558
7	12019.1024	12021.0890
8	12018.8611	12021.1103
9	12018.6033	12021.1175
10	12018.3363	12021.1123
11	12018.0476	12021.0926
12	12017.7488	12021.0586
13	12017.4399	12021.0106
14	12017.1130	12020.9511
15	12016.7734	12020.8725
16	12016.4183	12020.7863
17	12016.0528	12020.6835
18	12015.6712	12020.5663
19	12015.2731	12020.4346
20	12014.8663	12020.2959
21	12014.4430	12020.1347
22		12019.9576
23		12019.7758
24		12019.5766
25		12019.3648
26		12019.1337
27		12018.8917
28		12018.6403
29		12018.3714

Table 2i

Assigned Rotational Lines of the (2, 6) Band of the $C^1\Sigma^+ - X^1\Sigma^+$ Transition of ScI (cm^{-1})

J	ScI	
	P	R
0		11753.5200
1	11753.2415	11753.6350
2	11753.0828	11753.7425
3	11752.9094	11753.8341
4	11752.7242	11753.9126
5	11752.5233	11753.9805
6	11752.3093	11754.0326
7	11752.0882	11754.0720
8	11751.8480	11754.0965
9	11751.5946	11754.1095
10	11751.3307	11754.1038
11	11751.0490	11754.0915
12	11750.7594	11754.0650
13	11750.4564	11754.0251
14	11750.1375	11753.9755
15	11749.8080	11753.9088
16	11749.4620	11753.8300
17	11749.1090	11753.7355
18	11748.7341	11753.6284
19	11748.3476	11753.5119
20		11753.3812
21		11753.2354
22		11753.0720
23		11752.9010
24		11752.7210